

**Ocean & Sea Ice SAF**  
**Report on Algorithm Development**  
**and Prototyping Activities**

**Version 1.0**

---

*March 2000*

prepared by DMI, DNMI, Ifremer, KNMI, Météo-France and SMHI

<b>DOCUMENT SIGNATURE TABLE</b>
---------------------------------

	<b>Name</b>	<b>Date</b>	<b>Signature</b>
<b>Prepared by :</b>	O&SI SAF Project Team	13/03/00	
<b>Approved by :</b>	O&SI SAF Project Manager	13/03/00	

<b>DOCUMENTATION CHANGE RECORD</b>
------------------------------------

<b>Issue / Revision</b>	<b>Date :</b>	<b>Description :</b>
Version 1.0	13/03/00	First version prepared for the O&SI SAF Mid Term Review

<b>1. INTRODUCTION</b>	<b>6</b>
<b>1.1 Document Purpose</b>	<b>6</b>
<b>1.2 Definitions, acronyms and abbreviations</b>	<b>7</b>
<b>1.3 Applicable and Reference Documents</b>	<b>8</b>
1.3.1 Applicable Documents	8
1.3.2 Reference Documents	8
<b>1.4 Document Overview</b>	<b>8</b>
<b>2. ATLANTIC LOW AND MID LATITUDE PRODUCTS WP21100</b>	<b>9</b>
<b>2.1 SST WP21121</b>	<b>9</b>
2.1.1 General Product Specification	9
2.1.2 Scientific Approach for Algorithm Development	10
2.1.3 Selected Algorithm Specification and Tests Results	12
2.1.4 Processing Chain and Resources Requirements	14
2.1.5 Product Validation Plan and First Results	16
2.1.6 References	21
<b>2.2 Surface Solar Irradiance (SSI) WP21131</b>	<b>22</b>
2.2.1 General Product Specification	22
2.2.2 Scientific Approach for Algorithm Development	24
2.2.3 Selected Algorithm Specification and Tests Results	25
2.2.4 Processing Chain and Resources Requirements	27
2.2.5 Product Validation Plan	29
2.2.6 References	29
<b>2.3 Downward Long wave Irradiance (DLI) WP21132</b>	<b>30</b>
2.3.1 General Product Specification	30
2.3.2 Scientific Approach for Algorithm Development	30
2.3.3 Selected Algorithm Specification and Tests Results	33
2.3.4 Resources Requirements	36
2.3.5 Product Validation Plan	36
2.3.6 References	36
<b>3. ATLANTIC HIGH LATITUDE PRODUCTS WP21200</b>	<b>38</b>
<b>3.1 SST WP21221</b>	<b>38</b>
3.1.1 General Product Specification	38
3.1.2 Scientific Approach for Algorithm Development	39
3.1.3 Selected Algorithm Specification and Tests Results	39
3.1.4 Processing Chain and Resources Requirements	40
3.1.5 Product Validation Plan and First Results	41
3.1.6 References	42
<b>3.2 Surface Solar (SSI) and Downward Long wave Irradiance (DLI) WP21231</b>	<b>43</b>
3.2.1 General Product Specification	43
3.2.2 Scientific Approach for Algorithm Development	43
3.2.3 Selected Algorithm Specification and Tests Results	43
3.2.4 Resources Requirements	45

3.2.5 Product Validation Plan	46
3.2.6 References	47
<b>4. REGIONAL SEA SURFACE TEMPERAURES &amp; STRUCTURES WP22000</b>	<b>48</b>
<b>4.1 General Product Specification</b>	<b>48</b>
<b>4.2 Scientific Approach for Algorithm Development</b>	<b>50</b>
<b>4.3 Selected Algorithm Specification and Tests Results</b>	<b>50</b>
4.3.1 Cloud Mask	50
4.3.2 SST Algorithm	50
<b>4.4 Processing Chain and Resources Requirements</b>	<b>51</b>
<b>4.5 Product Validation Plan and First Results</b>	<b>53</b>
4.5.1 Control and monitoring tool	54
4.5.2 Control operating mode	56
4.5.3 Statistical results	57
<b>4.6 References</b>	<b>58</b>
<b>5. SEA ICE PRODUCTS WP23000</b>	<b>59</b>
<b>5.1 Introduction</b>	<b>59</b>
<b>5.2 General Products Specification</b>	<b>59</b>
<b>5.3 Multi-sensor Sea Ice Analysis WP23410</b>	<b>61</b>
5.3.1 Multi-sensor Scientific Approach	61
5.3.2 The Analysis System	62
5.3.3 Sea Ice edge detection	63
5.3.4 Sea Ice type	71
5.3.5 Resources Requirements	73
5.3.6 Validation Plan	73
<b>5.4 Passive Microwave Sea Ice concentration WP23110</b>	<b>74</b>
5.4.1 Scientific Approach for Algorithm Development	74
5.4.2 Selected Algorithm Specification and Tests Results	77
5.4.3 Resources Requirements	78
5.4.4 Validation Plan	80
<b>5.5 References</b>	<b>81</b>
<b>6. SCATTEROMETER WIND WP24000</b>	<b>84</b>
<b>6.1 General Product Specification</b>	<b>84</b>
<b>6.2 Scientific Approach for Algorithm Development</b>	<b>84</b>
6.2.1 Ice Screening WP24200	84
6.2.2 Ambiguity Removal WP24300	85
6.2.3 Quality Control and Monitoring WP24400	86
6.2.4 ASCAT study WP24600	87
6.2.5 Geophysical Model Function WP24700	87
6.2.6 Measurement Space visualisation WP24800	87

<b>6.3 Selected Algorithm Specification and Tests Results</b>	<b>88</b>
<b>6.4 Processing Chain and Resources Requirements</b>	<b>90</b>
<b>6.5 Product Validation Plan and First Results</b>	<b>92</b>
<b>6.6 References</b>	<b>92</b>

## 1. Introduction

### 1.1 Document Purpose

The Ocean & Sea Ice Satellite Application Facility (O&SI SAF) will be part of the ground segment for the future EUMETSAT missions Meteosat Second Generation (MSG) and European Polar System (EPS). Its development started in April 1997, in co-operation between EUMETSAT and a Consortium of European Meteorological Services and Institutes (M-F, DNMI, DMI, SMHI, KNMI and Ifremer).

The objective of the current phase is to develop algorithms and pre-operational software, allowing the processing of level 1.5 or equivalently level 1b data, to elaborate near real-time products relevant to the ocean/atmosphere interface and useful for meteorological and oceanographic applications. These products, described in detail in the O&SI SAF Science Plan [RD-1] are :

PRODUCT	COVERAGE	HOR. RESOLUTION	TIME FREQUENCY	INSTRUMENT
SURFACE WIND VECTOR	Regional and Global	50 km (possibly 25 km)		SCAT then ASCAT
ATLANTIC SST	100 W - 40 E	10 km	every 3 and 12 hour	GOES-E, SEVIRI and AVHRR
ATLANTIC RADIATIVE FLUXES	100 W - 40 E	10 km	every 3 and 12 hour	GOES-E, SEVIRI and AVHRR
SST AND STRUCTURES	Regional	2 km	every 6 hour	AVHRR
SEA ICE EDGE, COVER AND TYPE	Atlantic polar regions	10 km	daily	AVHRR, SSM/I, AMI then ASCAT, ATOVS

The scope of this document, prepared for the O&SI SAF Mid Term Review (MTR), is to report on the algorithm development and prototyping activities, which have been carried out since the start of the project. Since the scope of the project is clearly product oriented, the development activities have been organised among the Consortium on a product basis. Some of the products (ex : Regional SST) have already reached a pre-operational stage, and other products, because of their more innovative aspect, are still in the algorithm development stage (ex : radiative fluxes at high latitudes from AVHRR). From the examination of this document, the reviewers should be able to assess the level of progress in the algorithm development and software prototyping, and to address recommendations to the O&SI SAF Steering Group for a following integration and validation phase.

In the framework of these prototyping activities, a web server has been developed (<http://www.meteorologie.eu.org/safo>), where the project is described, and where quick-looks of some near real-time products already available are displayed.

## 1.2 Definitions, acronyms and abbreviations

AR	Ambiguity Removal
ASCAT	Advanced SCATterometer
AVHRR	Advanced Very High Resolution Radiometer
BUFR	Binary Universal Format Representation
Cmod4	C-band model, or geophysical transfer function of basckscatter versus wind
CMS	Centre de Météorologie Spatiale
CLW	Cloud Liquid Water
DADF	Data Acquisition And Dissemination facility
DLI	Downward Long wave Irradiance
DMI	Danish Meteorological Institute
DNMI	Norwegian Meteorological Institute
EPS	European Polar System
ERS	European Remote Sensing Satellite
GLB	Global oceans
GOES	Geostationary Operational Environmental Satellite
GRIB	GRIdded Binary format
GTS	Global Transmission System
HIRLAM	High Resolution Limited Area Model
HL	High Latitude
HRIT	High Rate Information Transmission
LML	Low and Mid Latitude
LUT	Look-Up Table
MAP	Merged Atlantic Product
METOP	METeorological OPERational Satellite
MODTRAN	MODèle de TRANSfert radiatif
MSG	Meteosat Second Generation
NESDIS	National Environmental Satellite, Data and Information Service
NAR	Northern Atlantic and Regional seas
NL	Non Linear
NMS	National Meteorological Service
NOAA	National Oceanic and Atmospheric Administration
NWC SAF	NowCasting and very short range forecasting SAF
NWP	Numerical Weather Prediction
O&SI	Ocean and Sea Ice
QC	Quality Control
RADR	Requirement analysis and Architectural Design Review
RMS	Root-Mean-Squared
SADT	Structured Analysis and Design Technique
SAF	Satellite Application Facility
SCAT	ERS scatterometer
SEVIRI	Spinning Enhanced Visible and Infra-Red Imager
SMHI	Swedish Meteorological and Hydrological Institute
SRD	Software Requirement Document
SSI	Surface Solar Irradiance

SST	Sea Surface Temperature
TBC	To Be Confirmed
TBD	To Be Defined
TIGR	Tovs Initial Guess Retrieval data base
TPW	Total Precipitable Water
UMARF	Unified Meteorological Archive & Retrieval Facility
WMO	World Meteorological Organisation

### **1.3 Applicable and Reference Documents**

#### 1.3.1 Applicable Documents

- [AD-1] MSG End-User Requirements Document, Issue 2.1, 3 April 1998, doc. no EUM/MSG/SPE/013
- [AD-2] EPS End-User Requirements Document, Issue 4 Rev.2, 13 October 1997, doc. no EPS/MIS/REQ/93001

#### 1.3.2 Reference Documents

- [RD-1] Ocean & Sea Ice SAF Science Plan, Version 2.0, July 1998
- [RD-2] R. van Westrhenen, The APL+ programme, KNMI Technical Report 153

### **1.4 Document Overview**

The document is organised in a way similar to the O&SI SAF Science Plan [RD-1]. For each product or sub-product, its general specification is given as a reminder (see the O&SI SAF Science Plan [RD-1] for more details). Then, the methodology followed for the algorithm development is described (use of data sets, models etc.....). In a third section, the selected algorithm is specified in detail. In a fourth section, an outlook of the processing chain organisation is given, together with an estimate of the computing resources (CPU, memory, disk) required. At last, the plan for the product validation is given, together with first validation results when available.

## 2. ATLANTIC LOW AND MID LATITUDE PRODUCTS WP21100

### 2.1 SST WP21121

#### 2.1.1 General Product Specification

See an example on figure 1.

**Input satellite data:**

Hourly GOES-East (0.6 , 3.9, 11 and 12  $\mu\text{m}$  for cloud mask, 3.9, 11 and 12  $\mu\text{m}$  for SST) and MSG data acquired at CMS.

**Time resolution:**

3-hourly means centered on 1, 4, 7UT,... 12-hourly means centered on 0UT and 12UT (in principle to meet the NWP models needs).

**Space resolution and projection:**

0.1 degrees, cylindrical equidistant projection.

**Coverage :**

From 60 North to 60 South and from 100 West to 45 East. The standard fields include 1451\*1201 pixels.

**Content:**

SST fields in hundredth of K, quality flags, mean time. At present the quality flag is a 3 bit parameter: all bits are set to 0 if quality is optimum. The first bit is set to 1 if the calculated SST is significantly lower than the minimum climatological value. The second and the third are set to 1 if the pixel is in the vicinity of cloud or land, respectively.

**Delivery time:**

SST fields are available for distribution 30 minutes after the data reception.

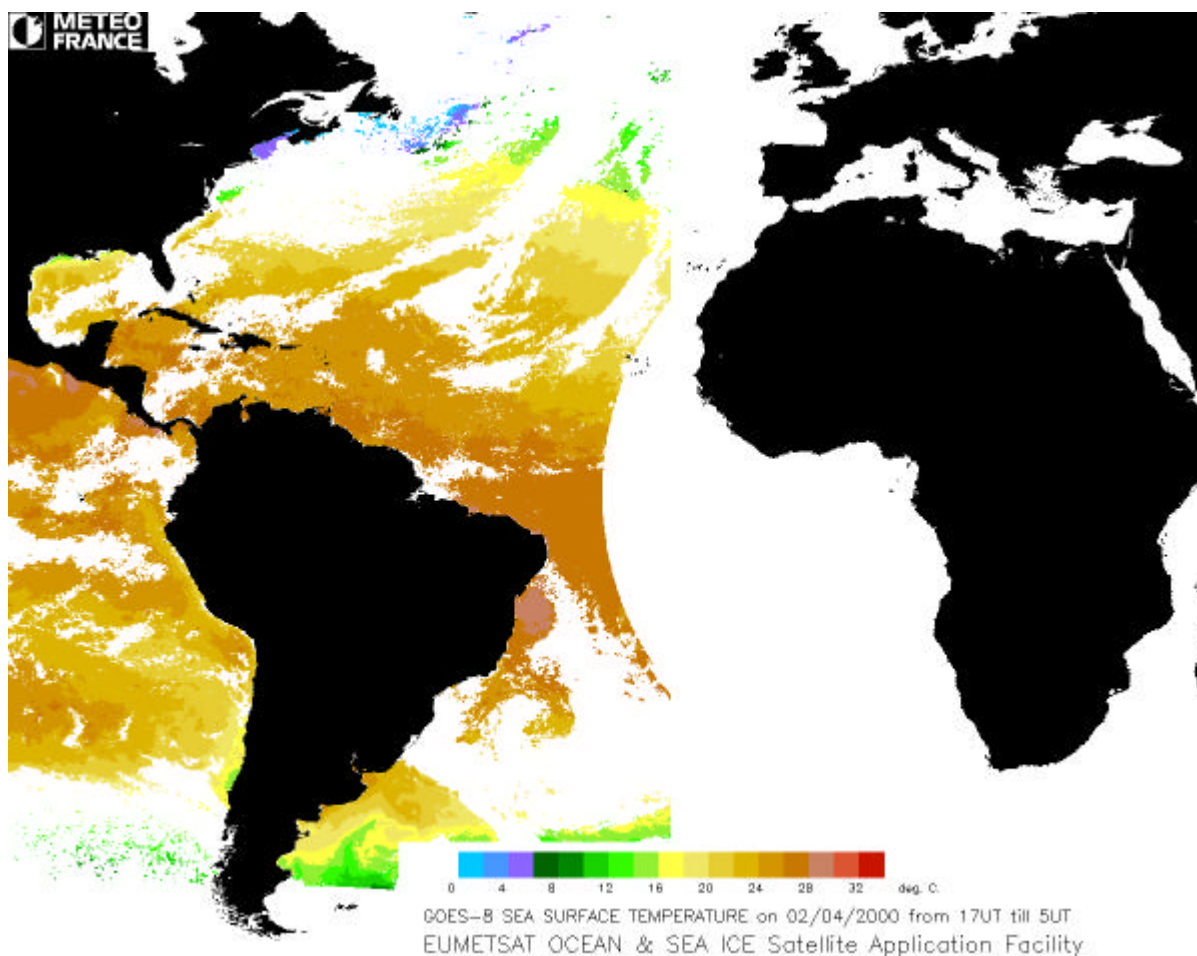


Figure 1 : Example of GOES-8 derived SST product in the LML area (60S - 60N). The remaining part of the area will be covered by MSG data.

### 2.1.2 Scientific Approach for Algorithm Development

#### *a) SST Algorithm*

The SST algorithm development within the O&SI SAF has been described in Andersen et al 1998 and more recently in Brisson et al. 1999 and François 1999. It included: definition of algorithms on simulated brightness temperatures, validation against in situ measurements, selection of algorithms for pre-operational applications. This simulation based approach has been preferred to determining directly the algorithms by regressions on buoy measurements because of the need to produce SST fields as quickly as possible when a satellite is in service (for instance MSG) without waiting for a representative set of in situ measurements and collocated radiative temperatures be collected. Furthermore it allows the use of various skin to bulk temperature conversion methods.

The simulations have been performed on radio sounding data bases. In a first step, TIGR (Tovs Initial Guess Retrieval database) made at LMD Paris and a set of Nordic maritime radio soundings collected at DNMI were used to determine the basic algorithms which are in use at present. MODTRAN has been used to compute the

brightness temperatures in function of the humidity and temperature profiles of each radio-sounding and various values of the viewing angle, surface temperature and emissivity. The coefficients corresponding to NOAA-14 NOAA-15 and GOES-8 have been determined for most of the formalisms available in the literature by regressions between the simulated brightness temperatures and the surface temperatures.

The resulting algorithms have been then applied on various Match-up Data Bases (MDBs) to check the validity of the approach, select the best formalisms and determine correction biases when needed.

Several problems were identified during the first algorithm development phase:

- the maritime part of TIGR is unbalanced towards mid latitude cases,
- the determination of the algorithms should account for the instrumental noise of the radiometers.
- no aerosols were considered in the simulations,
- etc..

C. François recently revisited the algorithm determination problem (François 1999). In particular, he completed the TIGR database with low and high latitude radio soundings and demonstrated the efficiency of eliminating cloudy radio soundings before determining the SST algorithms. This study confirmed the choice of formalisms made previously, but proposed a new set of coefficients which will be tested under operational conditions before replacing those presently used.

Different sets of SST algorithms have been developed for low/mid latitudes (LML) and high latitudes (HL). Distinct radiosounding databases were used for this purpose. The LML radiosoundings were collected at low/mid latitudes and the HL radiosoundings north of 50N. The performance of these algorithms on global and regional match-up data has been studied to investigate the regional differences. In Table 1 validation results for the temperature dependent NL algorithms on subsets of AVHRR Pathfinder Ocean Match-up Database (Podesta et al., 1997) is shown. Table 1 shows that there are only small differences between the LML and HL NL-algorithms in standard deviation. The LML-algorithm validates slightly better on the global data set, while the HL-algorithm validates slightly better on high latitudes. However, the validation results show no distinct benefit of using regional algorithms in spite of the different radiosounding that was used. One reason for this could be that the radiosounding databases used to develop the LML and HL-algorithms were biased against mid latitude conditions. Further investigations have been done on this topic (Eastwood, 1998) to see if there is a potential in improving the performance of the algorithms on a global scale by regional optimisation. The Pathfinder Match-up Database was then applied directly to define regional algorithms. The regions were defined both by dividing in latitude bands and SST bands (climatological values). Some improvements were found in areas with low and high SST using an optimisation in SST bands. Still the differences were not significant.

Validation files	Pathfinder global day/night		Pathfinder poleward 40N d/n		Pathfinder poleward 40N night	
no. Cases	9250		9795		4360	
	bias	st.dev.	bias	st.dev.	bias	st.dev.
NL-LML	0.22	0.67	0.14	0.57	0.16	0.61
NL-HL	-0.16	0.68	0.15	0.54	0.17	0.59

Table 1 : Validation results for the temperature dependent non-linear (NL) algorithms for low/mid latitudes (LML) and high latitudes (HL) developed for NOAA14. Three subsets of the AVHRR Pathfinder Oceans Match-up Database have been used.

### *b) Skin-to-Bulk temperature conversion*

A detailed analysis of the efficiency of using a parameterisation of the skin to bulk temperature difference has been made (Andersen et al., 1999). In the analysis three of the leading skin parameterisations were used and it was found consistently that the parameterisation of Fairall (1996) was best able to explain the observed variation in the difference between satellite (skin) and in-situ SST. The study furthermore indicated that the parameterisations could be driven by NWP data without impairing the performance. The amount of variance explained by the parameterisations was strongly affected by the quality of the SST retrieval algorithm, the quality of the in-situ measurements and presumably the magnitude of the skin effect for the region under consideration. Consequently it was not possible to show any correlation with drifting buoys and for the most favourable case of NDBC (National Data Buoy Center) moored buoys in the Atlantic off the American coast the amount of standard deviation explained by the skin parameterisations was at best very low, on the order of  $10^{-2}$  C. In the context of the O&SI SAF (i.e. using operational meteorological satellite presenting a significant radiometric noise level), applying mean night-time biases allows to correct for both effects without a significant loss of accuracy in comparison with using physical parameterisations. This means in practice that a few tenths of C bias is expected when a simulation derived algorithm is applied on a new satellite data and should be corrected after a few months of validation data are collected.

## 2.1.3 Selected Algorithm Specification and Tests Results

### *a) Cloud Mask*

For the low or mid latitude product, the cloud mask on GOES imagery is based on a threshold method developed at CMS (see Derrien and Le Gléau 1999). This cloud mask is mainly dedicated to nowcasting and this application is not very demanding for what concerns semi transparent or sub pixel cloudiness detection. Refinements specific to the marine conditions have thus been introduced to complement this cloud mask. They are based on the use of fine scale SST climatology, and on the temporal stability of the SST.

In view of processing GOES-East and MSG data, a world atlas of mean and minimum SST values has been made at CMS using the Pathfinder data from 1985 to 1995 (Faugere et al 1999). It has been built on a 10 day basis at a 9 km resolution. In permanently covered areas such as the Gulf Stream region, an Optimal Interpolation technique has been used to fill the gaps, using Reynolds climatology as a first guess

field. The local calculated SST value (TS) is compared to the climatological minimum temperature of the ten day period concerned (TSmin) : a too low SST is indicative of cloud contamination and if  $TS < TS_{min} + DTS$ , the pixel is considered as cloudy. DTS is a function of the distance of the considered pixel to the pre-calculated cloud mask :  $DTS = -1C$  about 20 km away from cloudiness and  $DTS = 0.5C$  in the immediate vicinity of a cloud.

The high temporal sampling of GOES (half-hourly) allows the analysis of rapid surface temperature variations. A cloud masking method, based on the assumption that the temporal variability of the SST is lower than the rapid temperature variations induced by cloud edges or sub-pixel cloudiness passing over a pixel, has been proposed by Wu et al., 1999. It has been successfully implemented in our processing scheme under the following form :

For a clear sky pixel, channel 11 temperatures at hour H (T11H) are compared to the maximum value of the corresponding temperatures at H+1/2 (T11H+) and H-1/2 (T11H-). If  $T11H - \text{Max}(T11H+, T11H-) < -0.5C$ , the pixel is considered as cloudy.

### *b) SST Algorithm*

The temperature dependent algorithms and the triple window algorithm (NL and TRI algorithms, see below) have been finally retained for testing during the prototyping and pre-operational phases. NL is used by day. By night, TRI is applied for GOES processing, since TRI performs better than NL under tropical conditions (Brisson et al 1999).

#### Temperature dependent algorithms (NL)

$$T_s = D T_{11} + (a_t T_{\text{guess}} + a_s S) (T_{11} - T_{12}) + C$$

In that case the climatological SST,  $T_{s_{\text{clim}}}$ , has been chosen as the first guess SST.

#### Simple triple window algorithms (TRI)

$$T_s = H T_{11} + J (T_{3.7} - T_{12}) + K$$

H, J and K may depend linearly on S

( $T_s$  is the calculated SST,  $T_{3.7}$ ,  $T_{11}$  and  $T_{12}$  are the brightness temperatures at 3.7, 11 and 12  $\mu$  respectively.  $S = \sec(\theta) - 1$  with  $\theta$ : satellite zenith angle ; all temperatures are in Celsius )

The coefficients used on an operational basis are given below:

	$D^*$	$A_t^*$	$A_s^*$	$C^*$	Bias correction term in use** (C)
GOES-08 (day)	0.981	0.063	1.143	1.085	0.11

\* derived from simulations \*\* deduced from preliminary results

Table 2 : Coefficients of the Non Linear algorithms selected for pre-operational applications (LML)

	H*	J*	K*	Bias correction term in use** (C)
GOES-08 (night)	1.005 + 0.0018 S	0.784 + 0.115 S	1.252 + 1.551 S	0.49

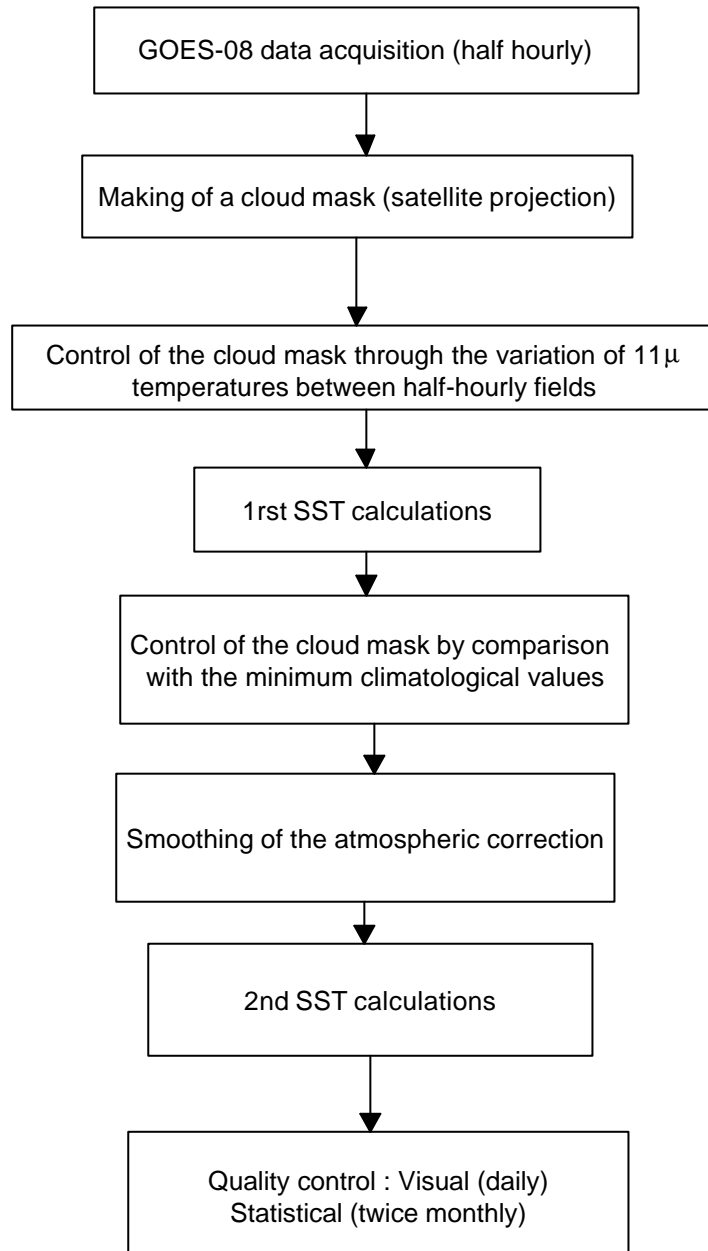
\* derived from simulations \*\* deduced from preliminary results

Table 3 : Coefficients of the Triple Window algorithms selected for pre-operational applications (LML)

#### 2.1.4 Processing Chain and Resources Requirements

These products are based on the combined use of GOES-East and MSG data. For obvious reasons, the East Atlantic will not be covered before the regular reception and processing of MSG data at CMS. The use of the GOES-East Extended Northern Hemisphere frame data has reached the pre-operational level at CMS since February 1999, and they are completed since recently by the Southern Hemisphere frame data.

The main steps of the present LML SST processing chain are given in figure 2 :

**ATLANTIC PRODUCT (LML) PROCESSING CHAIN**

The workstation supporting the prototype chain is :

SUN Enterprise 250 bi-processor  
392 Mb RAM  
2 bus wide SCSI (one fast)  
4 Gb internal disk + 2 x 9 Gb external disks

*a) cloud mask*

computer resources :

disk :            about 90 Mb for the climatologies and atlas.  
                  about 20 Mb for the ancillary data  
                  about 40 Mb for the input and output data  
memory :        180 Mb  
CPU :             9 minutes on line + 3 minutes off line

*b) SST computation*

computer resources :

disk :            about 610 Mb for the climatologies and atlas (uncompressed data).  
                  about 100 Mb for the auxiliary data  
                  about 200 Mb for the input/output data  
memory :        177 Mb  
CPU :             3 minutes up to the hourly LML SST production

*c) SST statistical quality control*

Since the in-situ measurements are not available before a 2 day delay, it is necessary to keep on line the data to put into the match-up data base. This match-up data base contains not only the calculated SST but also the radiative temperatures of the IR GOES and MSG channels involved in the calculation. So the disk resource needed for this component is about 1.4 Gb.

### 2.1.5 Product Validation Plan and First Results

The general principles of the quality control of O&SI SAF low and mid latitudes products are the following :

- 1) overall visual control: it is expected that all the basic ingredients of the calculations (ex: hourly SST or radiative flux fields over the Atlantic) will be controlled through movie loops.
- 2) detailed visual control: it will be made through a detailed analysis of samples through an operating mode which has been fully defined and implemented only for SST.
- 3) Statistical control: it will be made through the building of extensive Match-up Data Base (MDB) similar to those defined for algorithm development activities.

Statistics will be produced on a monthly basis and their results will be available on line, either under a graphic or a numerical form. Some delay ranging from a few days for SST to a few weeks for radiative fluxes should be expected, due to the availability of the in-situ measurements. The MDB themselves will be available on request.

*a) control and monitoring tool*

The quality of the SST products coming out of the CMS processing chains is controlled by two means:

- a visual monitoring of the consistency of the SST fields
- a statistical automatic control by comparison with in situ measurements

The corresponding tools will be referred to as QUALSST and STATSST respectively, and are based on the graphical PV-Wave commercial software.

**i) QUALSST :**

This tool allows the visualization of each SST fields of the chain and an appreciation of its quality by comparison with the following parameters :

- mean and minimum 10 day climatology
- preceding SST fields
- differences between the current SST field and each of the above mentioned references (actual minus climatology or actual minus preceding)
- multi-spectral color composite image (allowing a detailed analysis of the cloud cover).

Figure 3 shows the main window of the visual control interface for the Atlantic LML SST product :

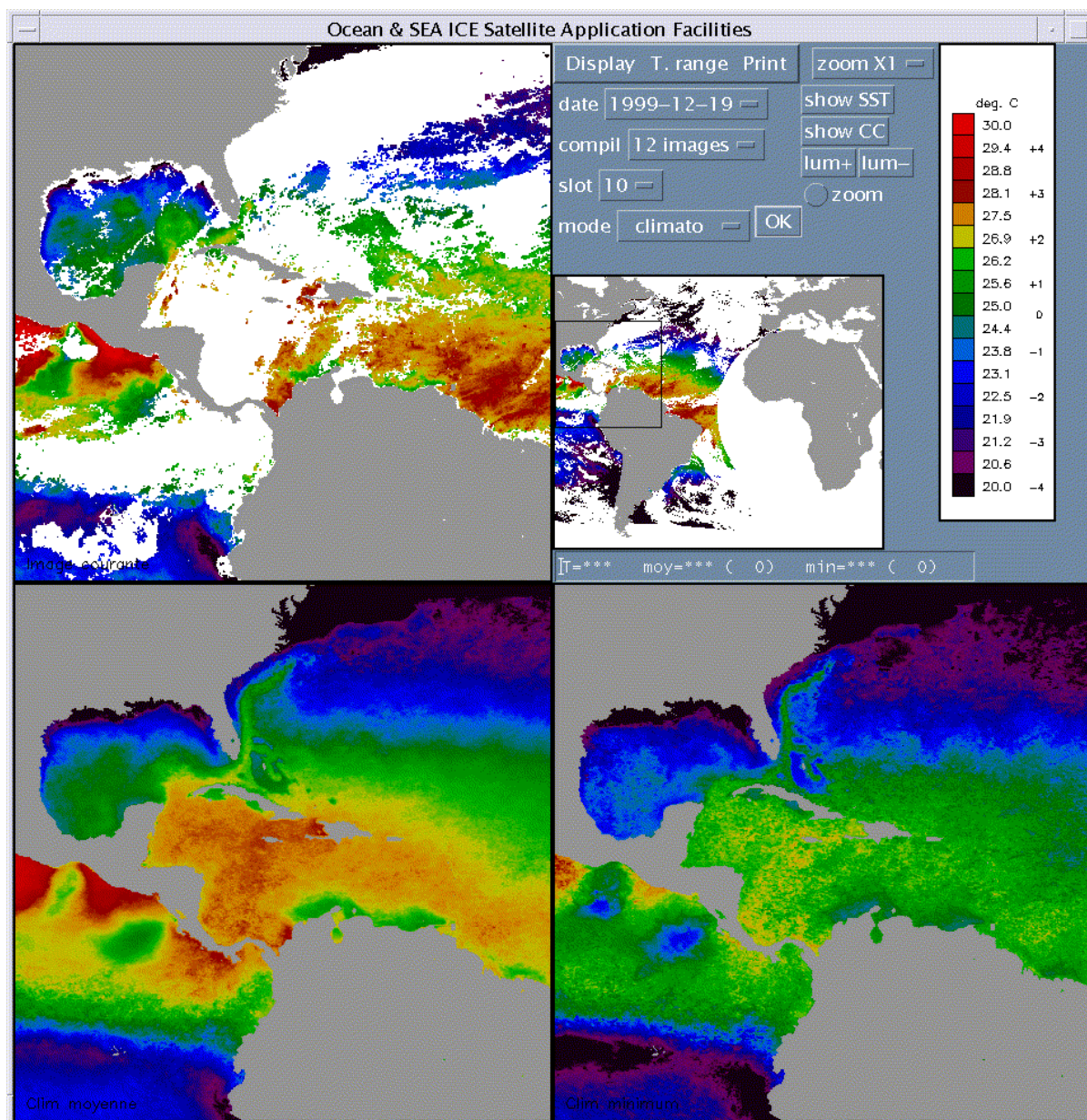


Figure 3 : visual quality control tool (QUALSST) over the Atlantic (GOES-08): main window

The operator has access to the following functions :

- display of numerical values at the location of the cursor
- zooming capacities
- changes in the color scale
- display of movie loops which provides a global view of the SST fields over several days
- printing capacities

## ii) STATSST :

This tool allows the monitoring of the quality of the GOES-East derived SST fields by comparison with simultaneous in situ measurements. Match-up data bases are built on a routine basis for GOES-East data . In situ data (buoy measurements) are collected daily through the GTS. The corresponding satellite data are collected in about 20\*20 km boxes (5\*5 pixel at IR resolution). The cloud coverage of a box must be below 60% The match-up time window is half an hour. To avoid dubious measurements, only buoy temperatures within 2C from the local fine scale climatological values have been used in the comparisons. GOES-08 data from 3 to 7h UT have been excluded to avoid the IR calibration anomaly that occurs around 5hUT. Three main tasks are made by this tool :

- match-ups generation and statistics computation
- display of statistics with various filtering options
- archiving of validation results, under graphical or numerical format

The error statistics can be displayed as a function of :

- measured SST
- latitude
- longitude
- integrated water vapor content
- satellite zenith angle
- T11-T12 temperature difference
- cloudiness
- time

Figure 4 shows an example of error map for the Atlantic LML SST product :

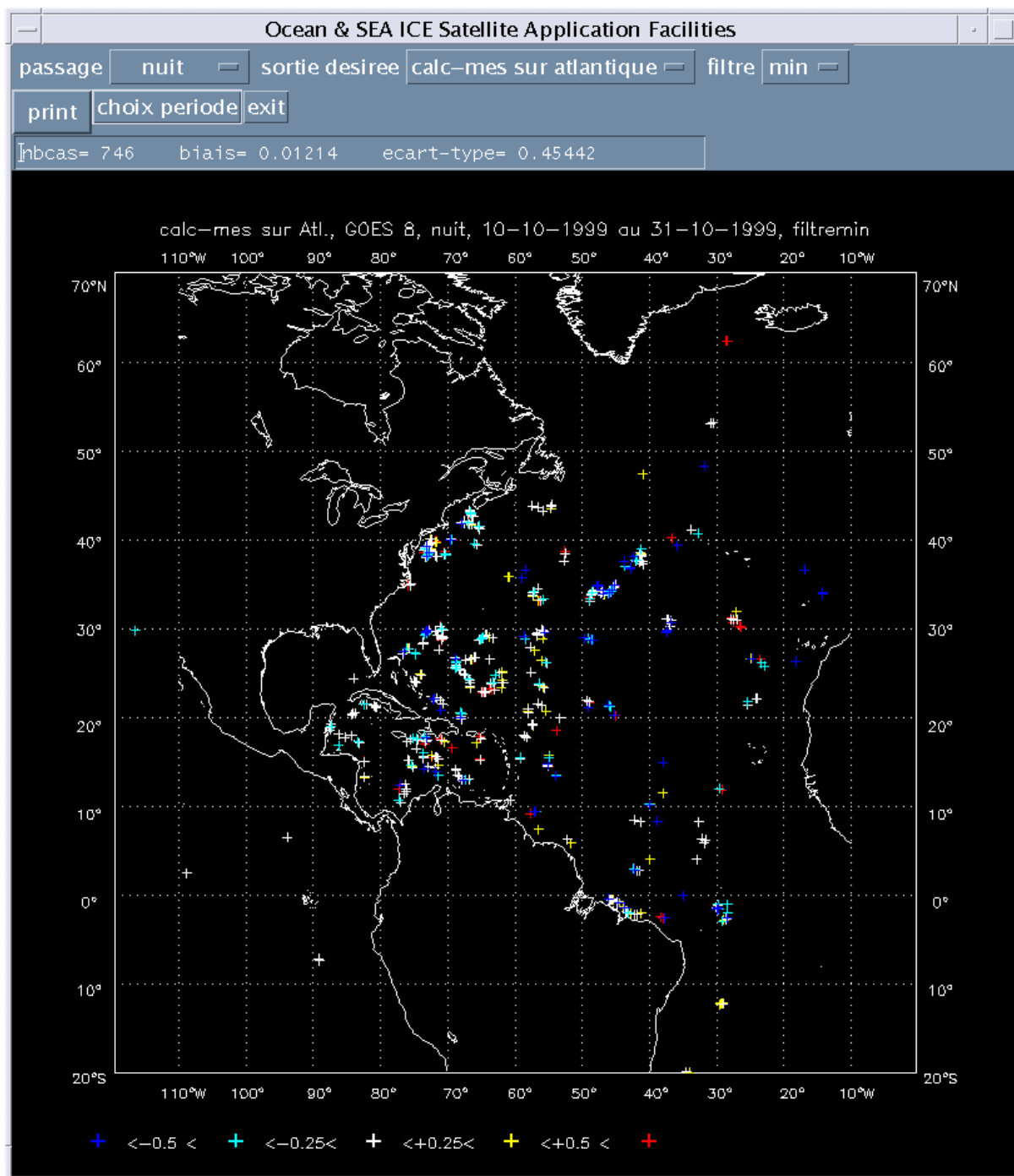


Figure 4 : statistical control tool (STATSST) over the Atlantic (GOES-08): error map

*b) control operating mode*

Quality controls are summarised on a monthly basis under the responsibility of the operation team at CMS. Each monthly control is reported in a detailed document.

**i) QUALSST :**

Once per day, an overall control through movie loops and then a detailed control of one daytime hourly field (17 UTC) and one nighttime field (2 UTC) are performed.

A warning is given to the CMS R&D team in case of persisting errors.

## ii) STATSST :

A visual examination of the statistics is made twice a month, monthly statistics are archived both as graphic documents and on files.

A warning is given to the CMS R&D team in following cases :

- for the daytime GOES-East statistics: if the bias  $|\delta|$  is  $> 0.3C$  or the standard deviation  $\sigma$  is  $> 0.6C$
- for the nighttime GOES-East statistics: if  $|\delta|$  is  $> 0.3C$  or  $\sigma$  is  $> 0.68C$

### c) statistical results

The results are shown in table 4 (correction biases deduced from preliminary results have been included in the algorithms). Two validation results are systematically presented : those obtained on all validation data and those obtained on data where the cloud coverage of the box is below 10% and the standard deviation of T11 in the validation box is below 0.4C. The all data results are representative of the raw accuracy of the products (including potential problems in the vicinity of the cloud mask) and the second are more representative of the algorithm performances. They have been compared, when possible, with results obtained using algorithms derived from regressions on in situ measurements and used in an operational context. The simulation derived GOES-08 algorithms perform better than the in situ data derived algorithms.

		GOES-08 night	GOES-08 day
	Number of cases	1988	2263
All data	Bias	-0.2	-0.37
	St. dev.	0.58	0.72
	Number of cases	714	799
Filtered data	Bias	-0.05	-0.19
	St. dev.	0.51	0.65
Navoceano algorithms on filtered data	Bias	0.00	-0.26
	St. dev.	0.64	0.85

Table 4 : Atlantic products (LML) validation results obtained using NL by day and TRI by night from 02/22/99 till 11/13/99. The 2 last lines represent the results obtained with the Navoceano algorithms applied on the filtered data (MCSST by day and TRI by night, see May and Osterman 1998)

## 2.1.6 References

Andersen, S., A. Brisson, S. Eastwood, P. Le Borgne and A. Marsouin, 1998, Developments on SST retrieval over the Atlantic using geostationary and polar orbiter satellite data in the frame of EUMETSAT O&SI SAF. Proceedings of the 9<sup>th</sup> conference on satellite meteorology and oceanography, Paris, France, pp.246-249.

Andersen, S., B. Candy and S. Eastwood, 1999, Regional optimizing of global SST algorithm and use of skin-to-bulk conversion. Proceedings of the 1999 EUMETSAT Meteorological Satellite Data Users' conference, Copenhagen, Denmark.

Brisson, A., Y. Faugere, P. Le Borgne and A. Marsouin, 1999, SST retrieval in the frame of the O&SI SAF: Mid and Low latitudes. Proceedings of the 1999 EUMETSAT Meteorological Satellite Data Users' conference, Copenhagen, Denmark.

Derrien, M. and H. Le Gléau, 1999, Cloud classification extracted from AVHRR and GOES imagery. . Proceedings of the 1999 EUMETSAT Meteorological Satellite Data Users' conference, Copenhagen, Denmark.

Eastwood, S., 1998: Regional optimization of SST algorithms, Report about Visiting Scientist stay at CMS, Météo-France. O&SI SAF Visiting Scientist Report to EUMETSAT.

Fairall, C.W., E.F. Bradley, G.S. Young, 1996, Cool-skin and warm-layer effects on Sea Surface Temperature. *J. Geophys. Res.*, **101**, 1295-1308.

Faugere, Y., P. Le Borgne, H. Roquet, 1999 A global fine scale SST climatology, O&SI SAF Report to EUMETSAT, in preparation.

Francois, C., 1999, SST retrieval (NOAA\_14 and GOES\_08) for the Ocean and Sea Ice SAF . Visiting Scientist Report to EUMETSAT.

May, D.A. and W. Osterman, 1998, Satellite-derived Sea surface Temperatures : Evaluation of GOES-8 and GOES-9 multispectral imager retrieval accuracy. *J. Atmos. Oceanic Technol.*, **15**, 788-797.

Podesta, G.P., S Sheno, J.W. Brown and R.W Evans, 1997: AVHRR Pathfinder Ocean Matchup Database 1985-1996 version 19.0. <http://www.rsmas.miami.edu/~gui/v19/matchupsv19.0..html>.

Wu, X., W.P. Menzel, G.S. Wade, 1999, Estimation of Sea Surface Temperatures using GOES-8/9 measurements. *Bull. Amer. Meteor. Soc.*, **80**, 6, 1127-1138.

## **2.2 Surface Solar Irradiance (SSI) WP21131**

### 2.2.1 General Product Specification

See an example on figure 5.

#### **Input satellite data:**

Hourly GOES-East (0.6 , 3.9, 11 and 12  $\mu\text{m}$  for cloud type, 0.6  $\mu\text{m}$  for SSI) and MSG data acquired at CMS.

**Time resolution:**

Products will exist at two temporal frequencies, 3 h and 24 h. The 3 h products will have a timing linked to the timing of LML Sea Surface Temperature (SST) products : a SSI field will be integrated over the 3h period between two consecutive SST fields. The timing choice is consistent with the use of these products by numerical models. The daily products will be integrated from 0 h to 24 h.

**Space resolution and projection:**

0.1 degrees, cylindrical equidistant projection.

**Coverage :**

From 60 North to 60 South and from 100 West to 45 East. The standard fields include 1451\*1201 pixels.

**Content:**

Solar irradiance in tenth of  $\text{W m}^{-2}$  reaching the Earth surface in the 0.3-3.  $\mu$  band, as usually measured by pyranometers. The products will be calculated as the energy integrated over a period of time divided by this time length. A quality flag field will be associated to each SSI field but this parameter is not precisely defined yet.

**Delivery time:**

The general requirement is to deliver each product 2 hours after the acquisition of the last satellite input to the product. However, this delay should be shorter for the 3h products since, for instance, SSI calculations with GOES data are available about 30mn after the last satellite data acquisition.

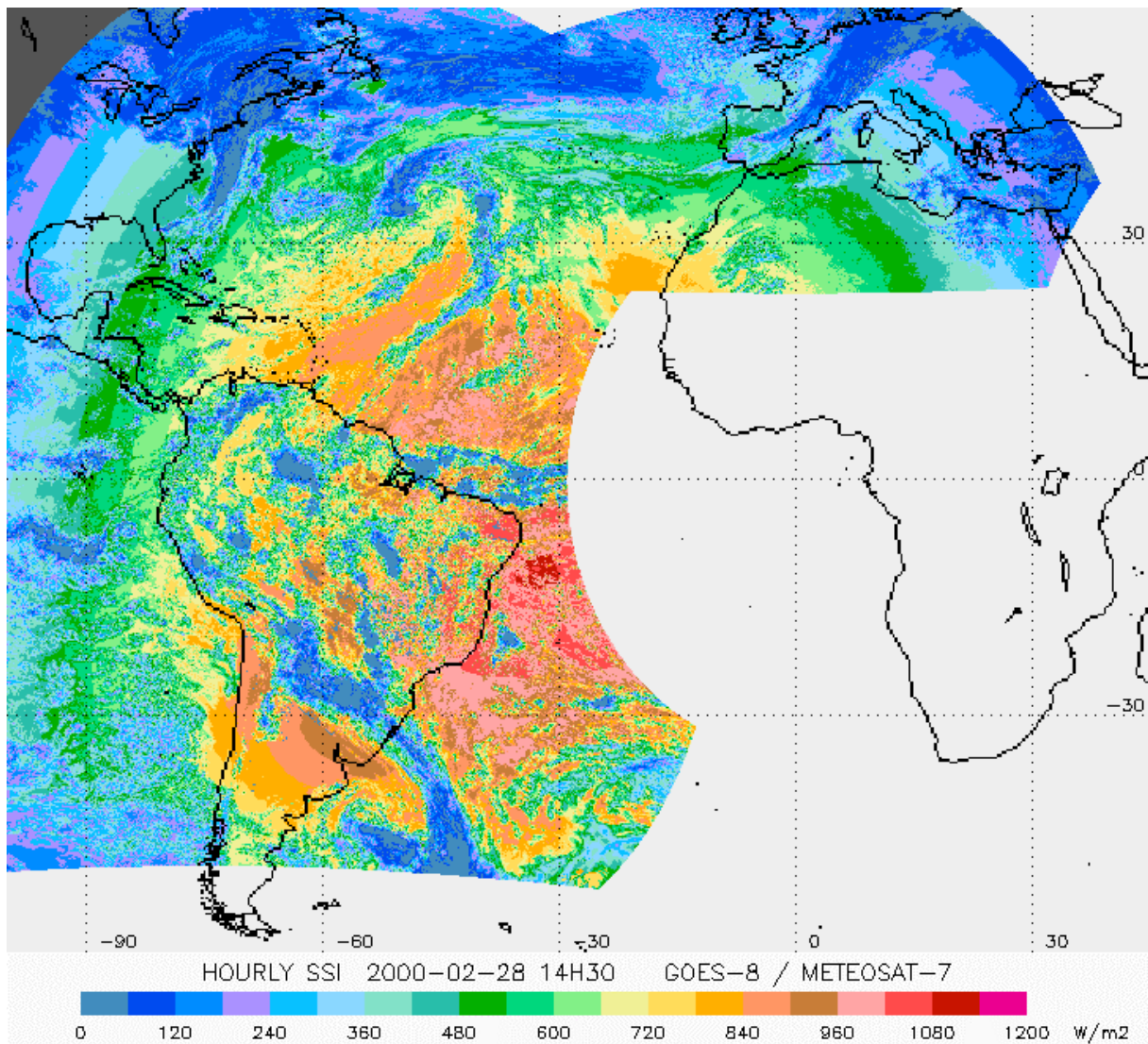


Figure 5 : Example of GOES-8 derived SSI product in the LML area (60S - 60N). For illustration purposes, the GOES-8 part is completed by the current operational CMS product, derived from Meteosat-7 over Europe. The remaining part of the area will be covered by MSG data.

### 2.2.2 Scientific Approach for Algorithm Development

A physical method based on the operational CMS scheme (Brisson et al., 1994) has been developed and tested on a comprehensive Match-up Data Base (MDB).

This MDB includes coincident pyranometer measurements and satellite data over North America, together with meteorological observations and NWP model output on the period January 97 to August 98. The main pyranometer measurement networks concerned are SURFRAD (4 stations), ISIS (9 stations) and ARIZONA (6 stations). The pyranometer measurements, which are 3 mn, 15 mn or 1 h averages depending on the network, have been integrated or interpolated over a 1 hour period centered on the time of the satellite measurement. Satellite data have been extracted over a 40 by 40 visible

pixel box centered on the pyranometer station, the resolution being degraded from 1 to 8 pixels by averaging. NWP model outputs have been derived from the ARPEGE global forecasts produced on a 1.5 degree grid.

### 2.2.3 Selected Algorithm Specification and Tests Results

This chapter outlines the SSI calculation method which has been fully described in Brisson et al., 1999a.

The main steps of the method are the following :

- re-mapping the satellite visible image (1km at GOES nadir) onto the 0.1 degree cylindrical equidistant grid of the final product, using a weighted average of the data corresponding to a grid point,
- calibration of the satellite visible count into a bi-directional reflectance (Eq. (1) to (3)),
- conversion from the narrow band of the radiometer spectral filter to the broadband of the solar spectrum, using Pinker and Lazlo, 1992 coefficients, which depend on the scene type (vegetation, desert, ocean, cloud) (Eq. (4)),
- conversion from the broadband bi-directional reflectance to the planetary albedo (independent of satellite viewing angles), using Manalo-Smith et al. 1998 formulas, which are also dependent on the scene type (Eq. 5),
- physical parameterization of the SSI as a function of the planetary albedo; the selected scheme combines a Frouin and Chertock, 1992, parameterization for clear sky and a CMS parameterization for cloudy sky (Eq. (6) to (10)). This parameterization leads to the theoretical minimum and maximum planetary albedo formulas given in equations (11) and (12).

$$L_{sc} = a [ 1 + b (t - t_0) ] (C - C_0) \quad (1)$$

$$R_{nb} = L_{sc} / [ v(j) \cos(\theta_0) ] \quad (2)$$

$$v(j) = 1 + 0.0334 \cos[ 2\pi (j-2) / 365.25 ] \quad (3)$$

$$R = M R_{nb} + B \quad (4)$$

$$A(\theta_0) = R / f_{aniso} \quad (5)$$

$$E = E_0 v(j) \cos(\theta_0) T_a \quad \text{in clear case} \quad (6)$$

$$E = E_0 v(j) \cos(\theta_0) T_1 T_{cl} \quad \text{in cloudy case} \quad (7)$$

$$T_{cl} = T_c / ( 1 - T_{bc} A_s \cdot A_c ) \quad (8)$$

$$T_c = 1 - A_c - A_c m \cos(\theta_0) \quad (9)$$

$$A = A_{ray} + T_{2top} A_c + A_s T_2 T_c^2 / ( 1 - T_{bc} A_s \cdot A_c ) \quad (10)$$

$$A_{min} = A_{ray} + A_s T_2 \quad (11)$$

$$A_{max} = A_{ray} + T_{2top} / ( 1 + m \cos(\theta_0) ) \quad (12)$$

with

C : radiometer count

C<sub>0</sub> : radiometer space count

$a$  : calibration coefficient valid at  $t_0$   
 $b$  : radiometer drift  
 $t_0$  : reference time (julian day)  
 $t$  : current time (julian day)  
 $\theta_0$  : sun zenith angle  
 $v(j)$  : corrective term accounting for the Earth-sun distance seasonal variation,  $j$  is the day of year  
 $L_{sc}$  : scaled radiance i.e. radiance divided by the effective solar spectral irradiance  
 $R$  : broadband reflectance  
 $R_{nb}$  : narrowband reflectance  
 $M, B$  : scene type dependent coefficients for narrow to broadband conversion  
 $f_{aniso}$  : anisotropic factor or bi-directional reflectance function (BDRF)  
 $A$  : Top Of Atmosphere (TOA) albedo or planetary albedo  
 $E$  : surface solar irradiance  
 $E_0$  : solar constant  
 $T_a$  : clear sky atmospheric transmittance (with multiple scattering)  
 $T_1$  : sun-surface atmospheric transmittance, without multiple scattering (consistent with  $T_a$ )  
 $T_2$  : sun-surface-satellite transmittance  
 $T_{2top}$  : sun-cloud-satellite transmittance  
 $T_{bc}$  : transmittance below cloud (to account for multiple scattering)  
 $A_{ray}$  : Rayleigh albedo  
 $A_s$  : surface albedo  
 $A_c$  : cloud albedo  
 $T_c$  : cloud transmittance  
 $T_{cl}$  : cloud factor  
 $m$  : cloud absorption factor  
 $A_{min}$  : minimum theoretical TOA albedo  
 $A_{max}$  : maximum theoretical TOA albedo

The method is based on already published parameterizations except for one parameter, the cloud absorption factor ( $m$ ), which has been tuned against GOES-8 data. It should be noted that the tuned value ( $m = 0.4$ ) is not fully independent from the satellite calibration. Generally speaking, the method needs a rigorous calibration of the visible channel, and in our case, a careful inter-calibration of the GOES and MSG visible channels.

The SSI calculation scheme uses auxiliary parameters (figure 6), some of them varying for each image and others deduced from monthly atlas already published. In both cases, they are re-mapped onto the cylindrical grid before any further use, this being done only once for the atlas. The list of auxiliary parameters and the options adopted in the pre-operational scheme are presented below :

#### **Surface albedo:**

It is obtained from a monthly atlas made by Gutman.

#### **Integrated water vapor content of the atmosphere:**

It is usually calculated from the predicted temperature and humidity profiles of the Météo-France Numerical Weather Predicting (NWP) model ARPEGE and, if model

outputs are not available, the Oort monthly climatology of specific humidity profile is used.

**Scene type:**

It is obtained by merging an atlas of surface scene type and a cloud mask derived from the SAF Nowcasting cloud classification (Derrien and Le Gléau, 1999), this classification is routinely applied at CMS on GOES half-hourly images both for three O&SI SAF products: SST, SSI and DLI .

**Ozone content:**

It is obtained from a monthly climatology made with Total Ozone Mapping Spectrometer data.

**Visibility:**

A latitude and month dependent value is used.

The method has been validated on the GOES-8 MDB, working in satellite coordinates at various spatial resolutions and not in the cylindrical grid presented above.

Various algorithm and auxiliary data options have been tested on two validation sets: a « whole set » of 14 stations, representative of land and ocean conditions, and a « restricted set » of four stations, rather homogeneous in terms of altitude and albedo, representative of maritime conditions. In the whole set, there are 8131 clear sky match-ups, with a mean measure of  $671.6 \text{ W/m}^2$ , and the selected clear sky algorithm gives a bias of  $-13.4 \text{ W/m}^2$  (i.e.  $-2.0\%$  of the mean measure) and a standard deviation of  $27.5 \text{ W/m}^2$  (i.e.  $4.1\%$ ). In the restricted set and for all cases (clear and cloudy), there are 34165 match-ups with a mean measure of  $435.9 \text{ W/m}^2$ , the selected algorithm gives a bias of 2.6 to  $11.4 \text{ W/m}^2$  (i.e. 0.6 to  $2.6\%$  of the mean measure) and a standard deviation of  $65.4$  to  $67.8 \text{ W/m}^2$  (i.e.  $15.0$  to  $17.6\%$ ), depending on which surface albedo and horizontal visibility are used as auxiliary data.

Specific tests on spatial resolution in the range 8 to 40 kms have shown that averaging reflectances before making the SSI calculations does not degrade significantly the result accuracy, as compared to averaging fine resolution SSI. This justifies the visible reflectance averaging made in the first step of the processing scheme. It also appeared that the spatial resolution choice for validation against hourly measurements may vary from 16 to 40 kms.

#### 2.2.4 Processing Chain and Resources Requirements

A pre-operational scheme using GOES data has been specified, the main components have been coded and they are routinely applied to the so-called GOES Northern Hemisphere images (limited to 20 S). Recently, the routine processing has been extended to GOES Southern Hemisphere images.

An overview of the hourly calculation scheme is shown in figure 6.

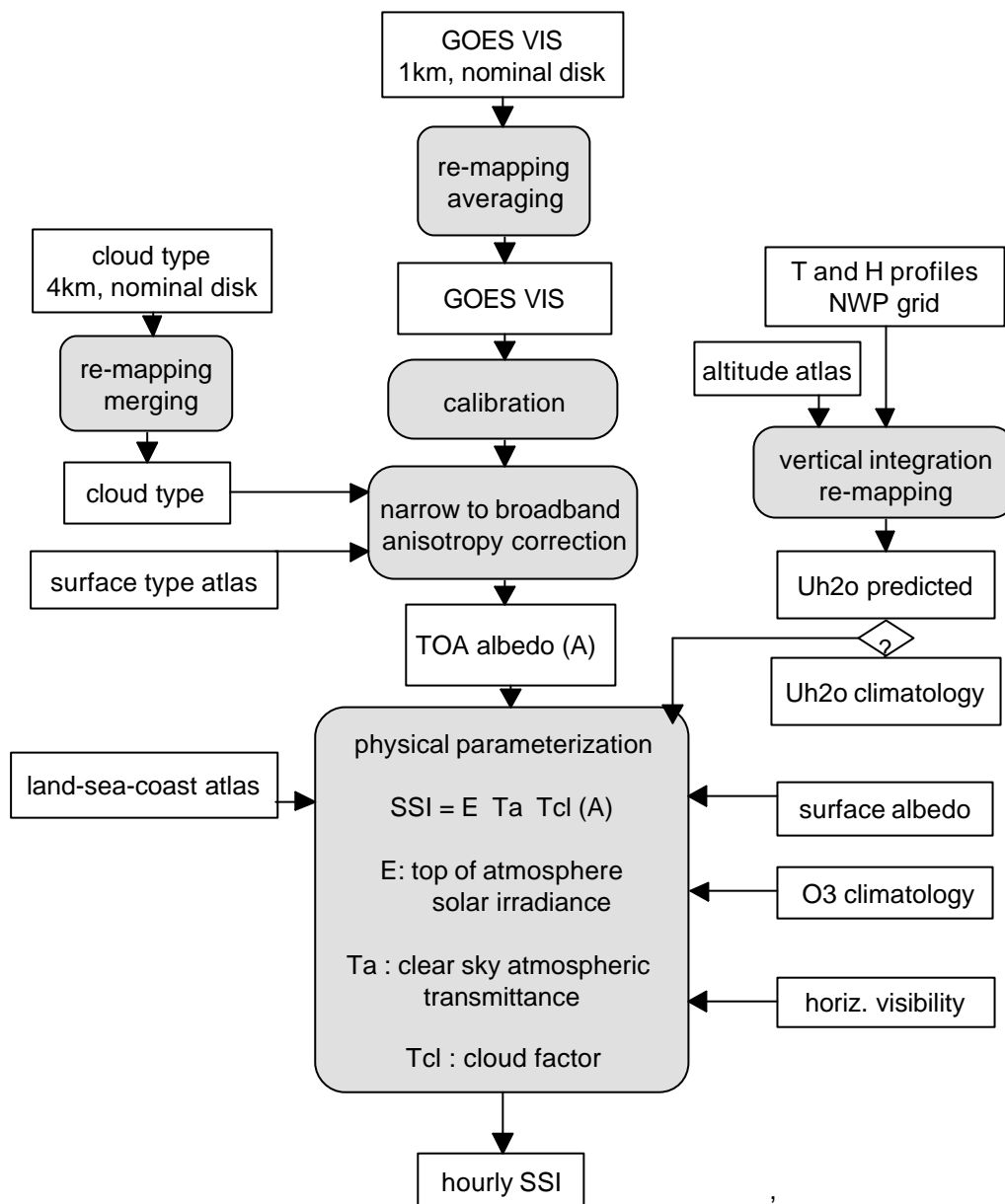


Figure 6 : Surface Solar Irradiance calculation scheme with GOES data

The workstation supporting the prototype chain is :

SUN Enterprise 250 bi-processor  
 392 Mb RAM  
 2 bus wide SCSI (one fast)  
 4 Gb internal disk + 2 x 9 Gb external disks

*a) cloud type*

computer resources :

disk :           about 90 Mb for the climatologies and atlas  
                   about 20 Mb for the ancillary data

memory : about 40 Mb for the input and output data  
175 Mb  
CPU : 3 minutes on line + 3 minutes off line

#### *b) SSI computation*

computer resources :

disk : about 175 Mb for the climatologies and atlas (uncompressed data)  
about 60 Mb for the auxiliary data  
about 150 Mb for the input/output data  
memory : 180 Mb  
CPU : 3 minutes up to the hourly LML SSI production

#### *c) SSI statistical quality control*

computer resources :

disk : about 50 Mb for the climatologies and atlas  
about 10 Mb for the auxiliary data  
about 20 Mb for the input/output data  
memory : 42 Mb  
CPU : 2 minutes

### 2.2.5 Product Validation Plan

Similarly to the quality control tool which has been defined and implemented for the SST fields, a set of visual and statistical control tools is in preparation for the SSI fields. Statistics will be based on the measurement stations available in the LML zone. In-situ data are abundant over land in the Northern Hemisphere Mid latitudes. To compensate the lack of routine measurements at sea, the O&SI SAF teams will try to collect experimental measurements made in the frame of oceanographic surveys during the preoperational experiment period. Similarly, a special care will have to be brought to collecting in-situ measurements under the low latitudes and in the Southern Hemisphere.

### 2.2.6 References

Brisson A., P. Le Borgne, A. Marsouin, T. Moreau, 1994, Surface irradiances calculated from Meteosat sensor data during SOFIA-ASTEX, International Journal of Remote Sensing, 15, 1, 197-203.

Brisson A., P. LeBorgne, A. Marsouin, 1999, Surface Solar Irradiance retrieval from GOES data in the framework of the Ocean and Sea Ice Satellite Application Facility, Proceedings of the 1999 EUMETSAT Meteorological Satellite Data Users' Conference, Copenhagen, 6-10 September 1999.

Derrien M. and H. Le Gléau, 1999, Cloud classification extracted from AVHRR and GOES imagery, Proceedings of the 1999 EUMETSAT Meteorological Satellite Data Users' Conference, Copenhagen, 6-10 September 1999.

Frouin R. and B. Chertock, 1992, A technique for global monitoring of net solar irradiance at the ocean surface. Part 1: Model, Journal of Applied Meteorology, 31,1056-1066.

Manalo-Smith N., G.L. Smith, S. N. Tiwari and W.F. Staylor, 1998, Analytic forms of bidirectional reflectance functions for application to Earth radiation budget studies, Journal of Geophysical Research, Vol. 103, D16, pp. 19,733-19,751, August 27, 1998.

Pinker, R.T., and Laszlo, I., 1992, Modeling surface solar irradiance for satellite applications on global scale, Journal of Applied Meteorology, 31, 194-211.

### **2.3 Downward Long wave Irradiance (DLI) WP21132**

#### 2.3.1 General Product Specification

**Input satellite data:**

Hourly GOES-East (0.6 , 3.9, 11 and 12  $\mu\text{m}$  for cloud type) and MSG data acquired at CMS.

**Time resolution:**

Products will exist at two temporal frequencies, 3 h and 24 h. The 3 h products will have a timing linked to the timing of LML Sea Surface Temperature (SST) products : a DLI field will be integrated over the 3h period between two consecutive SST fields. The timing choice is consistent with the use of these products by numerical models. The daily products will be integrated from 0 h to 24 h.

**Space resolution and projection:**

0.1 degrees, cylindrical equidistant projection.

**Coverage :**

From 60 North to 60 South and from 100 West to 45 East. The standard fields include 1451\*1201 pixels.

**Content:**

Downward long wave irradiance in tenth of  $\text{W m}^{-2}$  reaching the Earth surface in the 3.-50.  $\mu\text{m}$  band, as usually measured by pyrgeometers. The products will be calculated as the energy integrated over a period of time divided by this time length. A quality flag field will be associated to each DLI field but this parameter is not precisely defined yet.

**Delivery time:**

The general requirement is to deliver each product 2 hours after the acquisition of the last satellite input to the product.

#### 2.3.2 Scientific Approach for Algorithm Development

The algorithm development is based on the CMS hybrid method (bulk parameterization + satellite derived cloud information). This method, indeed, has been extensively validated during oceanographic campaigns with results comparing favorably with the other satellite methods (see table 5). Furthermore it is the only one suited for

hourly calculations over the Atlantic on a routine basis. In near real-time operational conditions, the bulk parameterization will use the outputs from the French NWP model ARPEGE, and cloud types will be obtained through the automatic cloud classification methods developed at CMS.

Author	campaign	method	inputs	nb cases	bias wm <sup>-2</sup>	std wm <sup>-2</sup>	correlation
Frouin et al. 88	Mildex daytime	full physical model (A)	TOVS + GOES cloud param.	16	-6.5	18.0	0.73
	"	simplified (D)	TOVS + GOES cloud cover	"	-1.0	21.7	0.53
		bulk (Anderson's)	conventional	"	-10.3	16.4	0.91
	Mildex night time	full phys. model (A)	TOVS + GOES cloud param.	104	-6.5	22.6	0.69
		simplified (D)	TOVS + GOES cloud cover	"	-1.2	24.9	0.58
		bulk (Anderson's)	conventional	"	-10.7	21.1	0.83
Breon et al. 91	Fasinex +Midex	full physical model (Morcrette)	RS profiles	43	10.5	25.3	-
		parameterization (Gupta's 89)	"	"	27.6	41.3	-
		bulk (Anderson's)	"	"	-2.8	18.4	-
Brisson et al. 96	Astex	bulk + Meteosat cloud types CMS	NWP outputs + Meteosat cloud types	289	-2.1	11.3	0.87
	Sema-phore	"	"	640	4.3	15.7	0.71
Schanz and Schlusser 1996	Coare	SSM/I	SSM/I brightness temperatures	47	-3.3	13.9	-
Francis 97	Cearex	RTM	TOVS	122	-3	21.0	0.78
	Leadex	"	"	98	9	26.0	0.74

Table 5: Summary of published results on DLI calculations from satellite data

The method has been developed and tested on a comprehensive Match-up Data Base (MDB).

This MDB includes coincident in situ pyrgeometer measurements, satellite (GOES-8) derived cloud types and ARPEGE model outputs (surface air temperature and humidity). The DLI measurements are made in 1 Baseline Surface Radiation Network (BSRN) station in Bermuda (Ohmura et al 1998) and 6 stations in the continental USA in the frame of the SURFRAD (or Integrated Surface Irradiance Study-ISIS level 2) network (Hicks et al 1996). The cloud types are determined at the IR pixel scale on a hourly basis from the GOES-08 imagery by the Derrien and LeGleau (1999) method. In situ measurements made at 3 minute intervals are integrated over 1 hour centered on the local time of the satellite measurement. Satellite cloud types are extracted over a 5\*5 IR pixel box centered on the pyrgeometer station. However, only a 3\*3 IR pixel box has been used for DLI calculations. NWP model outputs have been derived from the

ARPEGE global forecasts produced on a 1.5 degree grid. Aside this basic information, a range of complementary data were extracted when available: Surface Solar Irradiance measurements, in situ meteorological observations (surface air temperature humidity and pressure), satellite visible data.

This data base covers the July 1997 to June 1999 period. Two one year periods have been considered: July 1997-June 1998 and July 1998-June 1999. The Boulder data have been eliminated considering the elevation of the station. Among the remaining stations, only Fort-Peck, Bondville and Goodwin Creek have data included in the two time periods. The data from these three stations have been used to build two files, a learning file (from 13/07/97 to 30/06/98) and a validation file (from 01/07/98 to 30/06/99).

### 2.3.3 Selected Algorithm Specification and Tests Results

This chapter outlines the DLI calculation method which is fully described in Brisson et al., 2000. The new aspects of the method, compared to previous one developed at CMS and based on Meteosat data, are the use of a new clear sky parameterization (Prata, 1996), and the use of SSI calculations as input for cloud contribution instead of cloud type for daytime processing.

The main steps of the method are the following :

- clear sky emissivity calculation (Prata, 1996) (Eq. (1)),
- computation of cloud contribution from cloud type during nighttime (Eq. (3)) and from SSI during daytime (Eq. (4)),
- DLI calculation (Eq. (5)).

$$\varepsilon_0 = 1 - (1 + \xi) \exp\{-(1.2 + 3.0 \xi)^{1/2}\} - 0.05 (p_0 - p) / (p_0 - 710) \quad (1)$$

$$\xi = 46.5 (e_0 / T_a) \quad (2)$$

$$C = \sum (\eta_i C_i) \quad \text{for nighttime cases} \quad (3)$$

$$C = 1 - E / E_{\text{clear}} \quad \text{for daytime cases} \quad (4)$$

$$L = (\varepsilon_0 + (1 - \varepsilon_0) C) \sigma T_a^4 \quad (5)$$

with

- $\varepsilon_0$  : clear sky emissivity
- $e_0$  : surface water vapor pressure.
- $p_0$  : mean atmospheric pressure (1013.25 hPa)
- $C$  : infrared cloud amount
- $T_a$  : near surface air temperature (K)
- $\eta_i$  : fractional sky cover by cloud type i
- $E$  : surface solar irradiance (see 2.2.3)
- $E_{\text{clear}}$  : clear sky surface solar irradiance (see 2.2.3)
- $L$  : surface long wave irradiance
- $C_i$  : contribution coefficient of this cloud type
- $\sigma$  : Stefan-Boltzmann constant

For nighttime DLI computation, the cloud contribution coefficients have been adjusted on the pyrgeometer measurements and the observed air temperature and humidity of the learning file by a two-step procedure. A cloud contribution coefficient has been calculated for each cloud type of the detailed classification developed by the SAF NWC. Some cloud types have been merged according to the obtained coefficient values. Then, the final cloud contribution coefficients have been calculated for the new merged cloud types, corresponding to a simplified cloud classification.

Assuming that the same cloud type (i) covers the 3 by 3 IR pixel box centered on the station (i.e. “homogenous case”), a cloud contribution coefficient value for this cloud type can be obtained by (Eq. (6)) :

$$C_i = (L_M - \varepsilon_0 \sigma T_a^4) / [(1 - \varepsilon_0) \sigma T_a^4] \quad (6)$$

with :

$L_M$  : measured downward long wave irradiance

$\varepsilon_0$  : clear sky emissivity obtained with the Prata’s formula using the observed air temperature and humidity as input

The cloud types used for nighttime DLI computation are listed in table 6.

SAF NWC classification			simplified classification		
code	cloud type	abbrev	code	cloud type	abbrev
1	cloud free land	clr	1	clear	clr
2	cloud free sea	cls			
3	land contaminated by snow	clc			
4	sea contaminated by snow/ice	csc			
6	very low (stratiform) cloud	vlo	2	low cloud	low
8	low (stratiform) cloud	low			
10	medium (stratiform) cloud	med	3	medium cloud	med
11	very high opaque cloud	vho	4	high opaque cloud	hio
12	high opaque cloud	hio			
13	high semitransparent thin cloud	ci0	5	thin cirrus	cin
14	high semitransparent meanly thick cloud	ci1			
15	high semitransparent thick cloud	ci2	6	thick cirrus	cik
16	high semitransparent above other cloud	ci+			
17	fractional cloud	fra	7	fractional cloud	fra
19	sand cloud	san	8	sand cloud	san

Table 6: cloud types from SAF NWC classification and from simplified classification, used for nighttime DLI computation. Some cloud types, “very low cumuliform” (5), “low cumuliform” (7), “medium cumuliform” (9) are not used in the present version of the SAF NWC classification. The type “volcanic ashes” (18) has not been encountered in the data set.

For each cloud type, the mean value of the coefficients obtained by equation (6) over all homogeneous cases where this cloud type is encountered in the learning file gives an estimation of the corresponding cloud contribution coefficient. Daytime and nighttime cases have been processed separately. The study (Brisson et al., 2000) has shown that the nighttime cloud coefficients are of poorer quality than the daytime ones, due to probable mistakes of the cloud classification. The better results for nighttime DLI derivation were obtained when using cloud contribution coefficients computed with daytime cases of the learning file. It must be noted that we used a version of the cloud classification specific to off-line processing, which relies on the nearest in time (with no interpolation) air temperature, predicted from ARPEGE model outputs. This problem seems responsible for the numerous cases of misidentification of clear sky cases as low cloud cases that we observed, and which are not present in the operational (on-line) classification results.

Table 7 presents the calculated cloud contribution coefficients, together with similar values derived from a previous experiment based on a cloud classification applied to Meteosat data and pyrgeometer measurements over two French meteorological stations (Brisson 91, IGARS ou 94, IJRS). The Meteosat cloud types are not strictly identical to those of the present GOES classification but the correspondence is reasonable.

present study						Meteosat study	
code	cloud type	abrev	nbp	$C_i$	$\sigma C_i$	cloud type	$C_i$
2	low cloud	low	414	0.82	0.16	low stratiform cloud	0.70
						low cumuliform cloud	0.58
3	medium cloud	med	208	0.78	0.19	medium cloud	0.74
4	high opaque cloud	hio	197	0.72	0.24	high thick cloud	0.69
5	thin cirrus	cin	112	0.11	0.27	thin cirrus	0.41
6	thick cirrus	cik	240	0.49	0.32	thick cirrus	0.53
7	fractional cloud	fra	69	0.15	0.37	cloud edges	0.26
8	sand cloud	san	24	0.52	0.39		
	all clouds		1264	0.63	0.34	all clouds	0.57

Table 7: cloud contribution coefficients in the present study and from earlier Meteosat results.  $C_i$  and  $\sigma C_i$  are the mean and standard deviation of the cloud contribution coefficient obtained on the nbp homogeneous cases of the learning file (i.e. same cloud type on the 3 by 3 GOES IR pixel box centred on the pyrgeometer station).

The global performances of the selected DLI algorithm on the validation file considering all cases, clear and cloudy, and using predicted air temperature and humidity at 2m from ARPEGE outputs, are a bias of  $2.8 \text{ W/m}^2$  (0.9 %), a RMS error of  $26.5 \text{ W/m}^2$  (8.4 %) and a correlation coefficient of 0.92 (table 8). As predictable from earlier results, the daytime and nighttime performances are different. The daytime results are better with a bias of 0.2% and a RMS. error of  $20.0 \text{ W/m}^2$  (6.0 %). The nighttime performances are worse, with a bias of 1.6 % and a RMS error of  $30.9 \text{ W/m}^2$  (10.2 %).

data set	bias		$\sigma$		RMS		cor	nbp	M	$\sigma M$	
	W/m <sup>2</sup>	%	W/m <sup>2</sup>	%	W/m <sup>2</sup>	%				W/m <sup>2</sup>	W/m <sup>2</sup>
all cases	2.8	0.9	26.4	8.4	26.5	8.4	0.920	18155	315.3	65.6	20.8
daytime	0.5	0.2	20.0	6.0	20.0	6.0	0.951	8212	331.0	63.9	19.3
nighttime	4.8	1.6	30.5	10.1	30.9	10.2	0.891	9943	302.4	64.1	21.2

Table 8: DLI performances on the validation file with the selected algorithm. The DLI error bias, standard deviation,  $\sigma$ , and RMS are expressed in W/m<sup>2</sup> and in percentage of the mean measure M, cor is the correlation coefficient between calculated DLI and measured DLI,  $\sigma M$  is the standard deviation of the measured DLI and nbp the number of cases used to calculate the statistics.

### 2.3.4 Resources Requirements

The prototype processing chain for DLI products has not been developed yet, and this information is not available. However, the resources requirements for the DLI processing chain should be very similar to the ones for SSI.

### 2.3.5 Product Validation Plan

The validation plan for DLI products is similar to the one for SSI products. The pyrgeometer stations are however much less numerous than the pyranometer stations.

### 2.3.6 References

Brisson A., P. Le Borgne, A. Marsouin, T. Moreau, 1994, Surface irradiances calculated from Meteosat sensor data during SOFIA-ASTEX, International Journal of Remote Sensing, **15**, 1, 197-203.

Brisson, A., P. LeBorgne, A. Marsouin, 1996, Retrieval of air-sea interface parameters from Meteosat data, Proceedings of the 1996 Meteorological satellite data users' conference, Vienna, Austria, 16-20 September 1996.

Brisson, A., P. LeBorgne, A. Marsouin, 2000, Development of algorithms for Downward Long wave Irradiance retrieval at O&SI SAF Low and Mid Latitudes, O&SI SAF Report to EUMETSAT.

Bréon F.-M., Frouin, R., and Gautier, C., 1991, Downwelling long wave irradiance at the ocean surface: an assessment of in situ measurements and parameterizations, Journal of Applied Meteorology, 30, 17-31.

Derrien and LeGleau 1999, Cloud classification extracted from AVHRR and GOES imagery, Proceedings of the 1999 meteorological satellite data user's conference, Copenhagen, Denmark.

Francis, J.A., 1997, A method to derive downwelling long wave fluxes at the Arctic surface from TIROS operational vertical sounder data, Journal of Geophysical Research 102, 1795-1806.

Frouin, R., Gautier, C., and Morcrette, J.J., 1988, Downward long wave irradiance at the ocean surface from satellite data: methodology and in situ validation, Journal of Geophysical research, 93, 597-619.

Hicks, B.B., Deluisi, J.J. and D.R. Matt, The NOAA Integrated Surface Irradiance Study (ISIS)- A new surface radiation monitoring program, Bulletin of the American Meteorological Society, 77, 2857-2864.

Ohmura et al., 1998, Baseline Surface Radiation Network (BSRN/WCRP): New precision radiometry for climate research, Bulletin of the American Meteorological Society, 79, 2115-2136.

Prata, A.J., 1996, A new long-wave formula for estimating downward clear-sky radiation at the surface, Quarterly Journal of the Royal Meteorological Society, 122, 1127-1151.

Schanz and Schluessel, 1996, Atmospheric back radiation in the Tropical Pacific: Intercomparison of in-situ measurements, simulations and satellite retrievals, Meteorol. Atmos. Phys., 63, 217-226.

### 3. ATLANTIC HIGH LATITUDE PRODUCTS WP21200

#### 3.1 SST WP21221

##### 3.1.1 General Product Specification

See an example on figure 7.

**Input satellite data:**

All AVHRR passes acquired at DNMI.

**Time resolution:**

12-hourly means centered on 0 UT and 12 UT.

**Space resolution and projection:**

10km polar stereographic projection, true at 60N.

**Coverage:**

From 50 North to 90 North, 70 West to 60 East (those parts that are within the acquisition area of the DNMI receiving station).

**Content:**

SST fields in hundredth of K, quality flags (will be the same as for LML product), mean time.

**Delivery time:**

The SST fields should be available for distribution within 1 hour after the last data reception.

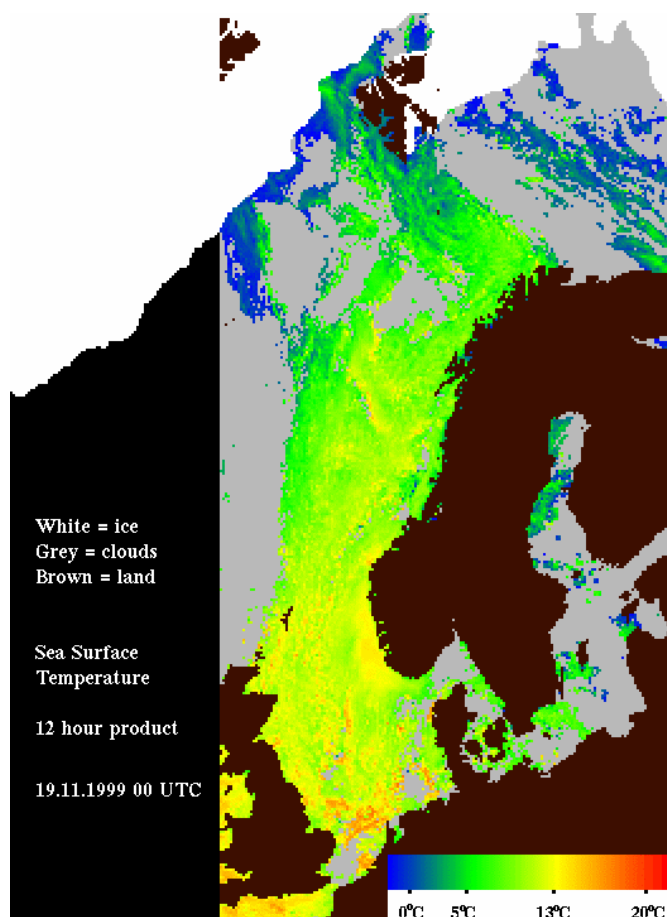


Figure 7 : 12-hourly (night time ) SST produced at DNMI on 11/19/99 using a provisional cloud mask over a subset of the final Atlantic High Latitude zone.

### 3.1.2 Scientific Approach for Algorithm Development

The algorithm development at high latitudes has used the same approach as for the low/mid latitudes. See 2.1.2.

### 3.1.3 Selected Algorithm Specification and Tests Results

#### *a) Cloud Mask*

For the high latitude products a method adapted to Nordic conditions has been developed by the Swedish Meteorological Office SMHI (Dybbroe et al 1999).

The central aim of the high latitude Cloud Mask is to identify absolutely cloud free pixels in a satellite scene with a high confidence. However, ocean and sea ice applications on one side and nowcasting applications on the other, impose different requirements on the Cloud Mask.

In order to try to meet the very strong requirements of ocean applications on a reliable detection of sub pixel and semi-transparent clouds, the method makes use of local texture information derived from the visible reflectance (0.6  $\mu$ ), the brightness temperature at 11 $\mu$ , and the brightness temperature difference at 3.7 and 12  $\mu$ . In order not to misinterpret ocean thermal fronts as clouds the texture in the 11  $\mu$  brightness temperature is always combined with one of the two other texture measures.

In addition a climatological quality check will be done on the calculated SSTs using a minimum SST climatology to detect remaining cloud contaminated pixels.

#### *b) SST Algorithm*

For the high latitudes a non linear temperature dependent (NL) algorithm formalism has been chosen for the pre-operational applications. The NL-algorithm will be used both night-time and daytime. A TRI-algorithm formalism using all three AVHRR infrared channels has been tested, but gave no better performance at high latitudes compared to the NL-algorithm.

#### Temperature dependent algorithms (NL)

$$T_s = (A_0 + A_1 * S) * T_{11} + (B_0 + B_1 * S + B_2 * T_{guess}) * (T_{11} - T_{12}) + C_0 + C_1 * S ,$$

where  $A_0$ ,  $A_1$ ,  $B_0$ ,  $B_1$ ,  $B_2$ ,  $C_0$  and  $C_1$  are constants and the climatological SST could be used as  $T_{guess}$ .

( $T_s$  is the calculated SST,  $T_{11}$  and  $T_{12}$  are the brightness temperatures at 11 and 12  $\mu$  respectively.  $S = \sec(\theta) - 1$  with  $\theta$ : satellite zenith angle ; all temperatures are in Celsius )

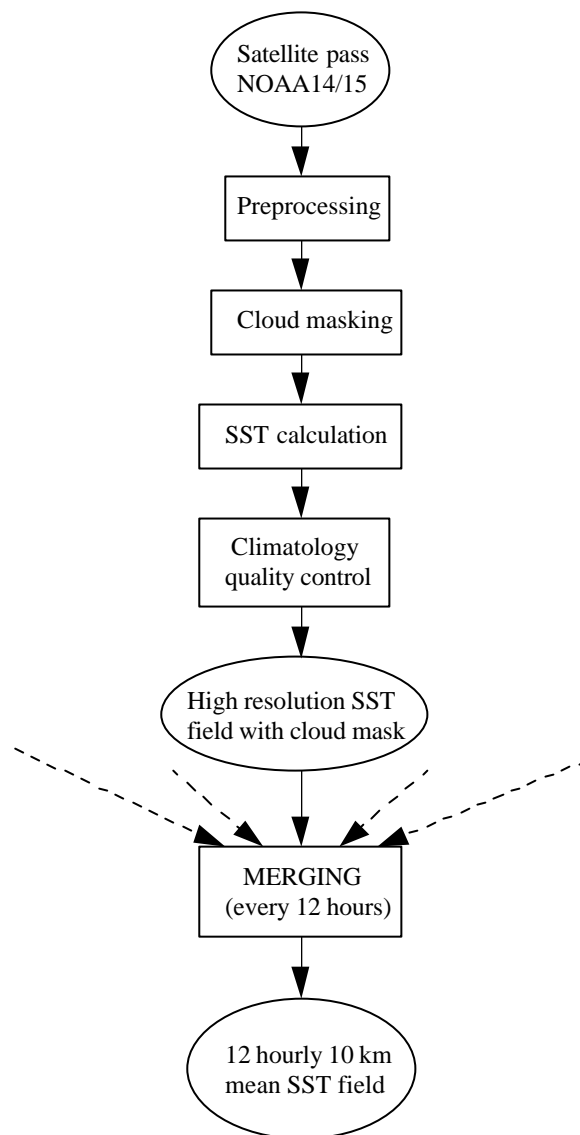
	$A_0$	$A_1$	$B_0$	$B_1$	$B_2$	$C_0$	$C_1$
NOAA-14	0.9879	0.0041	1.1067	0.4892	0.0305	0.4216	0.5270
NOAA-15	0.9886	-0.0024	1.1267	0.2754	0.0535	0.2280	0.4228

Table 9: Coefficients of the Non Linear temperature dependent algorithms selected for pre-operational applications at High Latitudes.

#### 3.1.4 Processing Chain and Resources Requirements

A first version of the pre-operational chain is running on DNMI. The SMHI cloud mask has been implemented and tested. It will be adapted to the DNMI internal file formats and data flow in the pre-operational chain. At present a local cloud mask is being used on parts of the area to be covered. This product is disseminated to Météo-France by ftp on a test basis.

The main steps of the present High Latitudes SST processing chain are given in figure 8 :



The workstation supporting the prototype chain is :

SGI Origin 200, 2 R10000 processors  
256 Mb RAM

computer resources (to process a selected 3600 km x 3600 km area in the Northern Atlantic every 12 hour using NOAA-14 and NOAA-15) :

disk :            about 50 Mb for the climatologies and atlas (uncompressed data).  
                  about 50 Mb for the input/output data  
memory :        about 50 Mb  
CPU :            about 15 minutes

### 3.1.5 Product Validation Plan and First Results

For the high latitudes no real-time validation has yet been performed. The validation results shown in Table 10 is therefore based on a Pathfinder match-up database . This match-up database was mainly used for comparing different algorithms, but it gives an idea of the performance that can be expected.

		Pathfinder night	Pathfinder day
	Number of cases	906	1682
High latitude NL SST algorithm	Bias	0.15	0.08
	Standard deviation	0.48	0.48
Operational NOAA NL SST algorithms	Bias	0.02	0.03
	Standard deviation	0.46	0.49
SAF regional NL SST algorithm	Bias	0.03	-0.01
	Standard deviation	0.47	0.50

Table 10: Atlantic products (HL) algorithm validation results obtained using the NL algorithms on the AVHRR Pathfinder Oceans Match-up Database. Match-ups from NOAA14 north of 50N and south of 50S from 1995 and 1996 have been used. The operational NOAA NL SST algorithms are different for night-time and daytime cases.

During the pre-operational experiment the High Latitude SAF SST product will be provided to DNMI's Sea Ice Service, which is also responsible for the DNMI's operational SST products. The High Latitude SAF SST product will be evaluated by the on duty analyst, and feedback reports will be provided on the quality and usefulness of the product.

Similarly the High Latitude SAF SST product will be provided to the NWP and ocean modelling departments, as well as the operational ice service of DMI. Their use of the products will provide feedback on the quality of the products. In addition the High Latitude SAF SST product will be collocated against available in situ measurements from buoys and the weather ship Mike (situated at 66N 2E). This will form a Match-up Data Base, which will be used to evaluate the performance of the algorithms in terms of standard statistical parameters.

### 3.1.6 References

Dybbroe, A., K.G. Karlsson and A. Thoss, 1999, The AVHRR cloud mask scheme of the SAFNWC, Proceedings of the 1999 EUMETSAT Meteorological Satellite Data Users' conference, Copenhagen, Denmark.

## **3.2 Surface Solar (SSI) and Downward Long wave Irradiance (DLI) WP21231**

### 3.2.1 General Product Specification

**Input satellite data:**

All AVHRR passes acquired at DNMI.

**Time resolution:**

Daily products integrated from 0 h to 24 h.

**Space resolution and projection:**

10km polar stereographic projection, true at 60N.

**Coverage:**

From 50 North to 90 North, 70 West to 60 East (those parts that are within the acquisition area of the DNMI receiving station).

**Content:**

Solar (respectively downward long wave) irradiance in tenth of  $W\ m^2$  reaching the Earth surface in the 0.3-4.  $\mu$  (respectively 4.-100.  $\mu$ ) band, as usually measured by pyranometers (respectively pyrgeometers). The products will be calculated as the energy integrated over a period of time divided by this time length. A quality flag field will be associated to each SSI (respectively DLI) field but this parameter is not precisely defined yet.

**Delivery time:**

The SSI and DLI fields should be available for distribution within 1 hour after the last data reception.

### 3.2.2 Scientific Approach for Algorithm Development

A Match-up Data Base including collocated AVHRR and pyranometer measurements has been built. Various steps of the method have been developed and tested on this data base. Validations are still in progress to determine the cloud factor algorithm.

Building of Match-up Data Base for NOAA data and pyrgeometer measurements has not started yet, but will be started in February 2000.

### 3.2.3 Selected Algorithm Specification and Tests Results

The SSI calculation from AVHRR data is not fully defined yet. The main steps used to estimate SSI from each AVHRR passage are the following :

- Bi-directional reflectances in channel 1 and 2 are used as input on a polar stereographic map projection at maximum spatial resolution. Calibration of counts to reflectances are performed using NOAA POES calibration procedures.
- A narrow band to broad band conversion of the channel 1 and/or 2 reflectances. Several versions are implemented, one set of coefficients has been developed by simulations using MODTRAN 3.5, another set has been received from McGill University, Canada (Feng Jian personal comm.), yet another set is described in Hucek and

Jacobowitz (1995). All methods are currently being tested along with the other elements of the method.

- Application of an Angular Dependence Model (ADM) to the broadband reflectivity. The model chosen is described by Manalo-Smith et al. 1998.
- Physical parameterization of the SSI as a function of the planetary albedo. The clear sky parameterization used will be the one defined by Darnell et al 1988 and Darnell et al. 1992, but other schemes are implemented in the processing software and can be used in different geographical regions. The cloudy scheme is not defined yet.

The SSI scheme needs auxiliary data as input, some of these parameters are static data (e.g. surface scene type, ozone content) and some are dynamic, AVHRR cloud classification or outputs from NWP models (e.g. precipitable water). These data are all re-mapped onto the polar stereographic map. The daily product is generated by application of a weighting factor to each individual AVHRR scene.

The methods for estimating the clear sky insolation at the surface has been validated against a data set containing cloud free pyranometer measurements from Bergen for the period 1965 to 1996. Various algorithms have been tested giving a bias from -2.5 to 7.3 W/m<sup>2</sup>, i.e. -1.5 to 4.5% of the mean measure, the best result achieved (figure 9) being 0.9 W/m<sup>2</sup>, i.e. 0.55%. The standard deviation varies from 13 to 17 W/m<sup>2</sup>, i.e. 8.0 to 10.5 %.

For cloudy conditions, the match up data base (MDB) consists of on AVHRR data locally received at DNMI station in Oslo and pyranometer measurements performed at different locations in Norway. The pyranometer measurements are one-hour averages. The AVHRR data are averages in boxes of 9x9 pixels at 1.5 km spatial resolution. At present, the MDB contain two stations, Bergen and Ås (south of Oslo) during two years, 1998 and 1999. In the future, more stations will be added: those from the Norwegian Crop Research Center and the Swedish meteorological station of Norrköping that should be better representative of the Baltic Sea conditions. The methods to use in cloudy conditions are currently being validated and thus the algorithm to use in the pre-operational phase is not determined yet.

## Staylor

Tested on positively cloudfree data from Bergen, Norway.  
The cloudfree data cover 1965-1996.  
Monthly mean climatological values are used for Precipitable water and Ozone.  
Bias: 0.8894212 (W/m<sup>2</sup>)  
Standard Deviation: 12.74809 (W/m<sup>2</sup>)  
Standard Deviation: 7.831458 (% of mean observed)

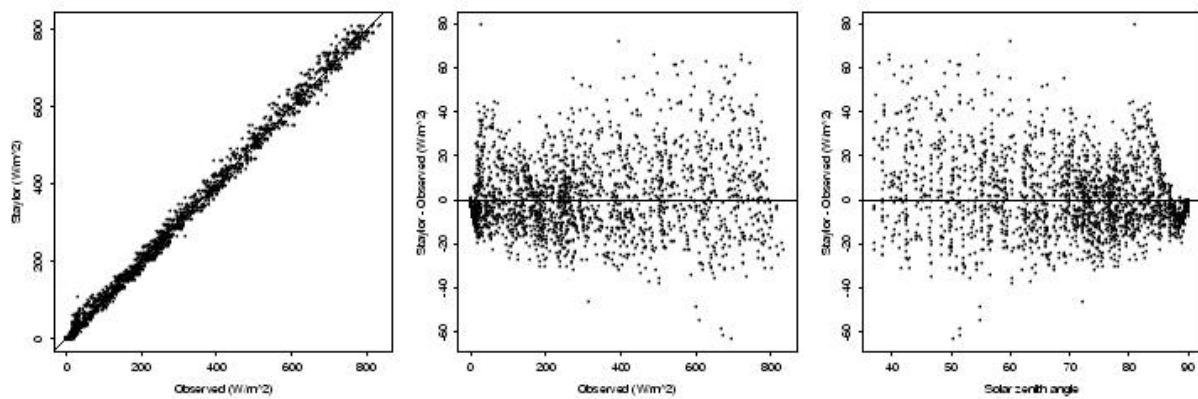


Figure 9: Clear sky insolation at surface tested at data from Bergen, Norway.

### 3.2.4 Resources Requirements

The software structure of a pre-operational scheme for SSI retrieval based on NOAA AVHRR data has been defined and implemented, but this scheme is not fully defined in cloudy conditions. This will be done quite soon and a routine processing of AVHRR data will be initiated early in 2000.

The main steps of the present High Latitudes SSI processing chain are given in figures 10 and 11 :

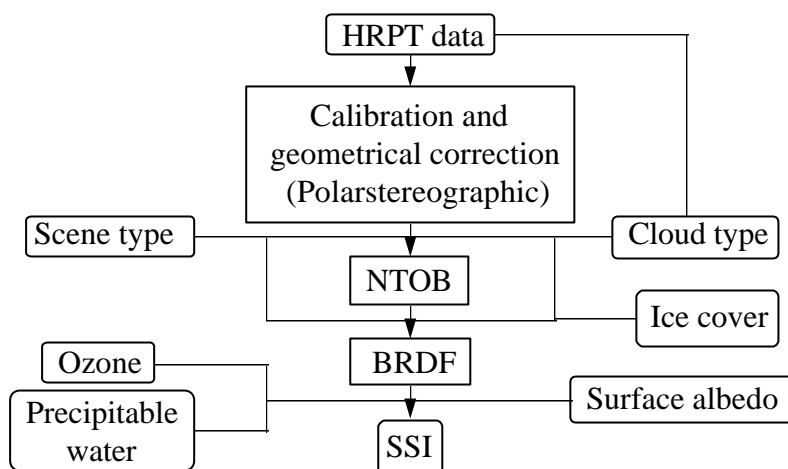


Figure 10 : Flowchart of the SSI processing for each AVHRR passage.

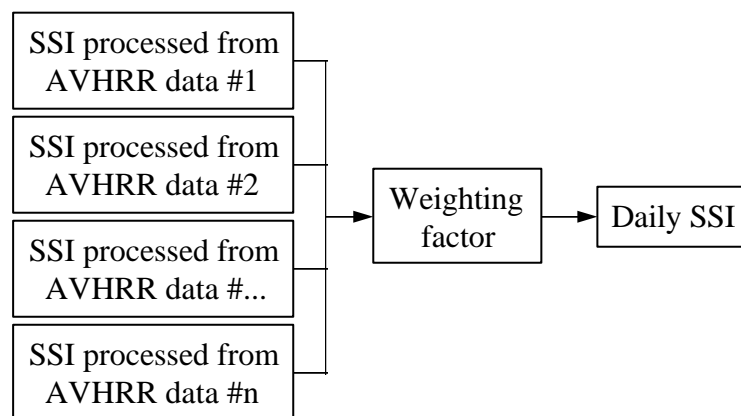


Figure 11 : Flowchart of daily SSI processing from AVHRR data. Each AVHRR passage is weighted in the resulting daily product.

### 3.2.5 Product Validation Plan

During the pre-operational experiment the SAF HL flux products will be evaluated against available flux measurements at Norwegian coastal stations. In addition DNMI is

partner in an EU proposal on direct use of Atmospheric model fluxes for driving Ocean models, IRIS. As a part of this it is proposed to set up radiative flux measurements on the Operational Weather ship Mike in the Norwegian Sea, and on the oil production platform Ekkofisk in the North Sea. This will be used in an inter comparison study involving radiative fluxes from the HL SAF, atmospheric models and the measurements. If accepted, the validation experiment will be performed in 2001 in parallel with the pre-operational experiment.

### 3.2.6 References

Darnell, W.L., F. Staylor, S.K. Gupta and F.M. Denn, 1988: Estimation of surface insolation using sun-synchronous satellite data, J. Clim., No. 1, pp. 820-835.

Darnell, W.F., F. Staylor, S.K. Gupta, N.A. Ritchey and A.C. Wilbur, 1992: Seasonal variation of surface radiation budget derived from international satellite cloud climatology project C1 data, J.G.R., Vol. 97, pp. 15741-15760.

Hucek, R., and H. Jacobowitz, 1995: Impact of Scene Dependence on AVHRR Albedo Models, J. Atm. Oce. Tech., Vol. 12, No. 4, pp. 697-711.

Manalo-Smith N., G.L. Smith, S. N. Tiwari and W.F. Staylor, 1998, Analytic forms of bidirectional reflectance functions for application to Earth radiation budget studies, Journal of Geophysical Research, Vol. 103, D16, pp. 19,733-19,751, August 27, 1998.

## 4. REGIONAL SEA SURFACE TEMPERAURES & STRUCTURES WP22000

### 4.1 *General Product Specification*

See the zone definition on figure 12 and an example on figure 13.

#### **Input satellite data:**

All AVHRR passes (0.6 , 1.6 when available, 3.9, 11 and 12  $\mu\text{m}$  for cloud mask, 11 and 12  $\mu\text{m}$  for SST) acquired at CMS.

#### **Time resolution:**

4 times a day, every 6 hours (times corresponding to each mosaic of consecutive passes acquired at CMS).

#### **Space resolution and projection:**

2 kms on a stereo polar grid. The space resolution is a compromise between the amount of data to be processed over the complete CMS potential acquisition area (12.6 Mega pixels see figure 13) and the maximum resolution (1 km at nadir) of the original satellite data

#### **Coverage:**

6 predetermined zones (see figure 12) of 1024\* 1024 pixels. These zones were defined to allow the drawing of the fronts interactively on a workstation, and to offer the users (presumably interested by local problems) the possibility of ordering (desarchiving, transmitting) only a subset of the whole area .

#### **Content and precision:**

Sea Surface temperatures in tenth of C (all zones), surface thermal fronts in units of Celsius per 5 km (all zones but North Sea, nighttime NOAA-14 passes only), time, quality flag (still to be defined).

#### **Delivery time:**

$\frac{1}{2}$  hour after the last data acquisition for all mosaics but the nighttime NOAA-14 mosaics. Front drawing induces a few hours delay, but the product is ready by noon the same day of the data acquisition.

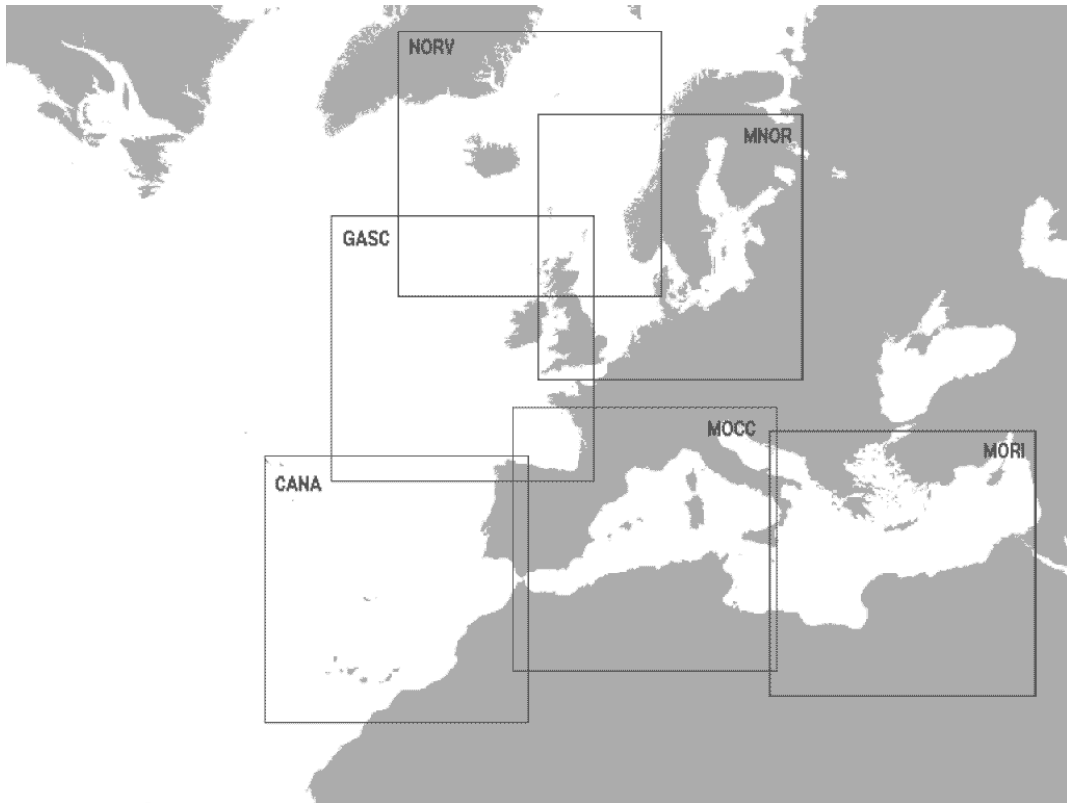


Figure 12: The 6 pre-defined zones of the regional SST products

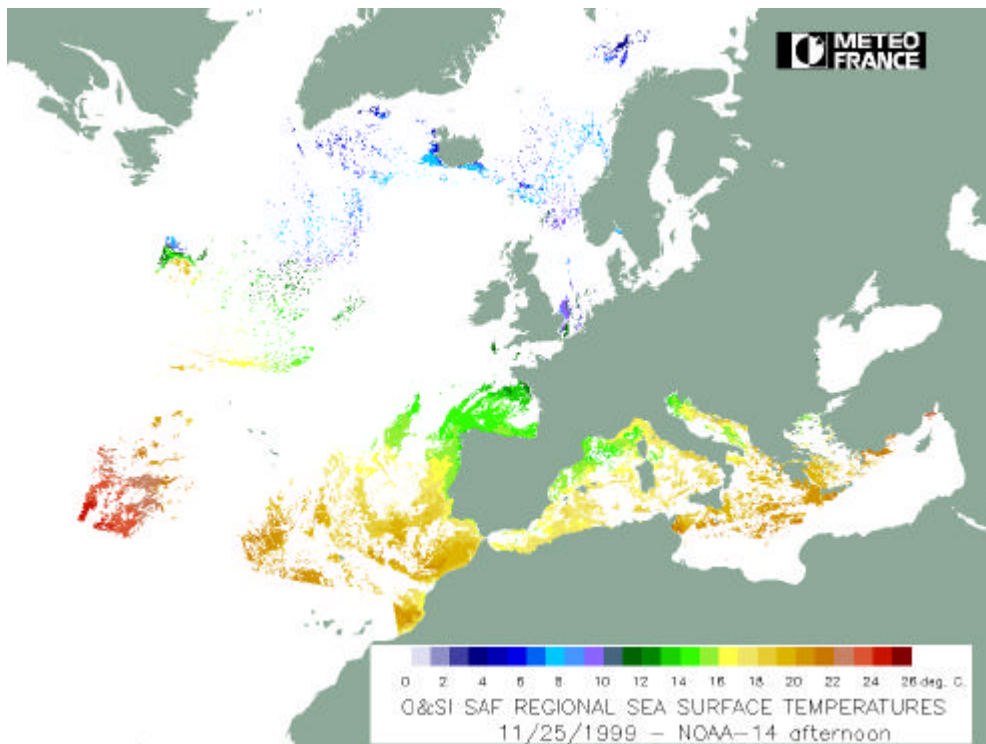


Figure 13: Example of the regional SST product on 11/25/1999, mosaic of NOAA-14 afternoon orbits.

## **4.2 Scientific Approach for Algorithm Development**

See 2.1.2.

## **4.3 Selected Algorithm Specification and Tests Results**

### 4.3.1 Cloud Mask

For the Regional products, the cloud mask on AVHRR imagery is based on a threshold method developed at CMS (see Derrien and Le Gléau 1999). This cloud mask is mainly dedicated to nowcasting and this application is not very demanding for what concerns semi transparent or sub pixel cloudiness detection. Refinements specific to the marine conditions have thus been introduced to complement this cloud mask. They are based on the use of fine scale thermal fronts and SST climatology.

Over this area, two types of 2 km resolution atlas have been built, mainly from AVHRR data routinely processed at CMS between 1989 and 1994 : A thermal front atlas (monthly mean and maximum intensity values ) and a SST atlas (monthly mean and minimum values ).

For each AVHRR pass the local calculated SST value (TS) is compared to the climatological minimum temperature of the ten day period concerned (TSmin) : a too low SST is indicative of cloud contamination and if  $TS < TS_{min} + DTS$ , the pixel is considered as cloudy. DTS is a function of the distance of the considered pixel to the pre-calculated cloud mask :  $DTS = -1C$  about 20 km away from cloudiness and  $DTS = 0.5C$  in the immediate vicinity of a cloud.

By night, a high value of the  $11\mu$  temperature gradient (GRT11) can be indicative of cloud edges or scattered cloudiness if not induced by surface thermal fronts. The local gradient is compared to the local climatological maximum gradient (GRT11max) deduced from the front atlas. If  $GRT11 > GRT11_{max} + DGR$ , the pixel is considered as cloudy. DGR is also a function of the distance to clouds : typical values are :  $DGR = 0.5 C/5km$  away from cloudiness and  $DGR = -0.5 C/5km$  in the vicinity of a cloud. In other words, near a cloud, the local  $11 \mu$  gradient should be lower than the maximum climatology whereas it can be slightly higher elsewhere. By day, diurnal warming creates warm patches which may induce strong temperature gradients randomly in any location and makes this test inapplicable.

### 4.3.2 SST Algorithm

The temperature dependent algorithms and the triple window algorithm (NL and TRI algorithms, see below) have been finally retained for testing during the prototyping and pre-operational phases. NL is used by day and by night, since TRI does not perform significantly better than NL under mid and high latitudes conditions (Brisson et al 1999).

#### Temperature dependent algorithms (NL)

$$T_s = D T_{11} + (a_t T_{\text{guess}} + a_s S) (T_{11} - T_{12}) + C$$

In that case the climatological SST,  $T_{s_{\text{clim}}}$ , has been chosen as the first guess SST.

( $T_s$  is the calculated SST,  $T_{11}$  and  $T_{12}$  are the brightness temperatures at 11 and 12  $\mu$  respectively.  $S = \sec(\theta) - 1$  with  $\theta$ : satellite zenith angle ; all temperatures are in Celsius )

The coefficients used on an operational basis are given below:

	D*	At*	As*	C*	Bias correction term in use** (C)
NOAA-14	0.979	0.064	1.227	1.097	0
NOAA-15	0.984	0.076	1.373	1.044	0.46

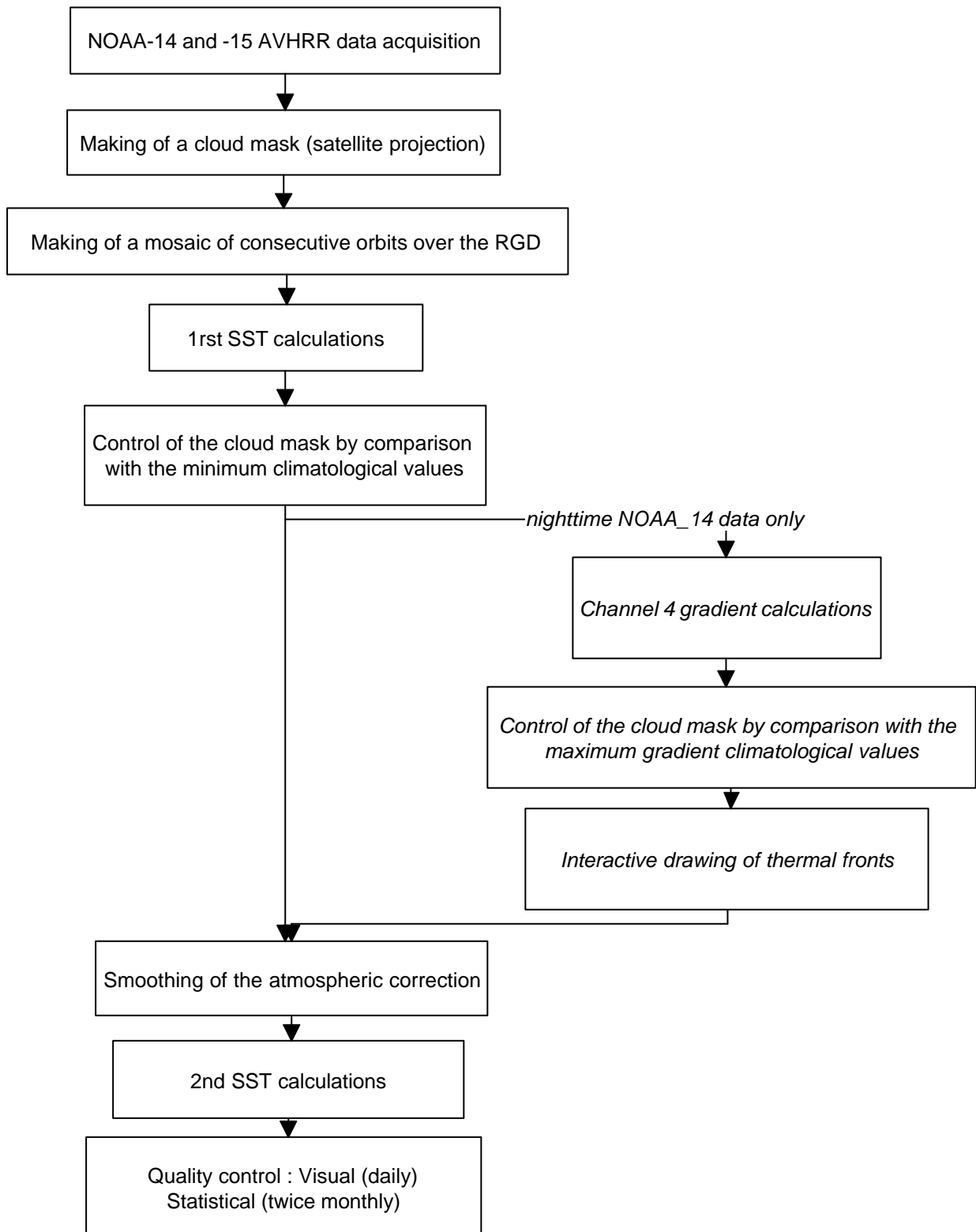
\* derived from simulations \*\* deduced from preliminary results

Table 11: Coefficients of the Non Linear algorithms selected for pre-operational applications (Regional products)

#### **4.4 Processing Chain and Resources Requirements**

These products have reached the pre-operational level: They have been produced on a routine basis under their present form since February 1999 and they have been recently integrated into the CMS operational chain.

The main steps of the present Regional SST processing chain are given in figure 14 :

**REGIONAL PRODUCT PROCESSING CHAIN**

*a) cloud mask*

computer resources (the area to be processed contains 12 MPixels) :

disk : at least 650 Mb for the several climatologies needed in this package.  
(without compression)  
at least 360 Mb for the intermediate files  
memory : 80 Mb  
CPU : 10 minutes

*b) SST computation*

computer resources (the area to be processed contains 12 MPixels) :

disk : at least 290 Mb for the several climatologies needed in this package.  
(without compression) ). They are already taken into account in the cloud  
mask package.  
at least 360 Mb for the intermediate files  
memory : 120 Mb  
CPU : 2 minutes

*c) Drawing of thermal fronts*

For this interactive part of the processing, the night time regional SST product is divided into 6 areas of 1024\*1024 each (see figure 12).

For each area, the operator displays the SST field and the corresponding cloud mask on a same image. The gradients field is coded into thermal fronts intensity using a scale from 1 (1°C/km) to 5 (5°C/km), which is laid over the SST image.

At first, the operator refines the cloud mask, interactively extending or reducing the cloud mask where needed. In the ideal case, the cloud mask is perfect and this step is not necessary. Then the operator draws the main thermal fronts on top of the gradients field. Finally, these thermal fronts are read from the image and written on a disk file.

*d) SST statistical quality control*

Since the in-situ measurements are not available before a 2 day delay, it is necessary to keep on line the data to put into the match-up data base. For 4 daily SST calculation, a disk space of about 1.3 Gb is needed.

**4.5 Product Validation Plan and First Results**

The general principles of the O&SI SAF Regional SST products validation are similar to the ones of the O&SI SAF low and mid latitudes SST products (section 2.1.5). However, due to the constraints of polar orbiting satellites, no visual control through movie loops can be performed.

#### 4.5.1 Control and monitoring tool

The quality of the SST products coming out of the CMS processing chains is controlled by the QUALSST and STATSST tools, described in section 2.1.5.

##### i) QUALSST :

Figure 15 shows the main window of the visual control interface for the Regional SST product :

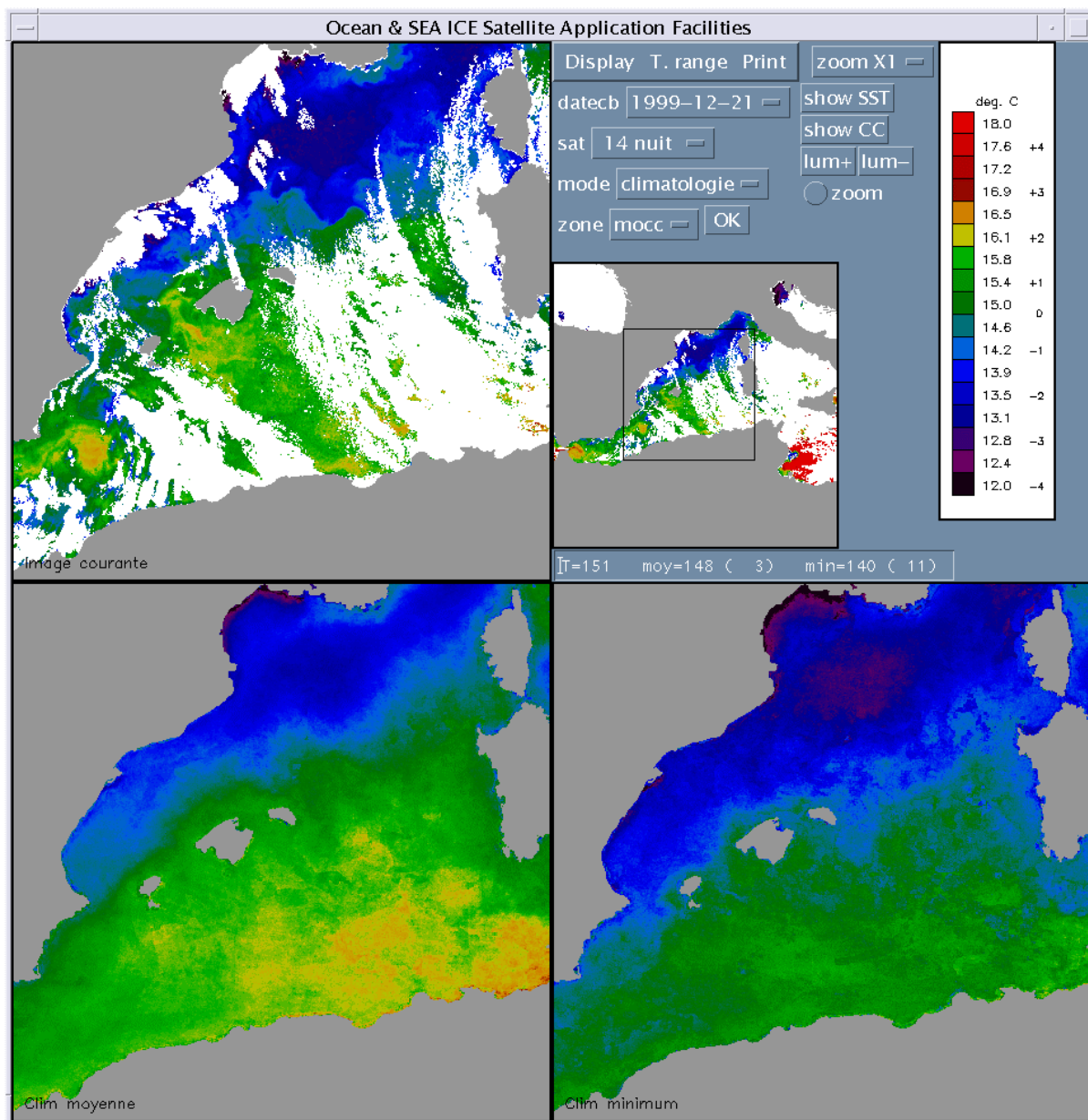


Figure 15 : visual quality control tool (QUALSST) of the Regional SST product over the Mediterranean Sea (NOAA/AVHRR): main window

##### ii) STATSST :

Match-up data bases are built on a routine basis for NOAA/AVHRR data . In situ data (buoy measurements) are collected daily through the GTS. The corresponding satellite data are collected in about 20\*20 km boxes (11\*11 pixels at 2 km resolution). The cloud coverage of a box must be below 60% The match-up time window is 3 hours. To avoid dubious measurements, only buoy temperatures within 2C from the local fine scale climatological values have been used in the comparisons.

Figure 16 shows an example of errors display for the Regional SST product as a function of measured SST :

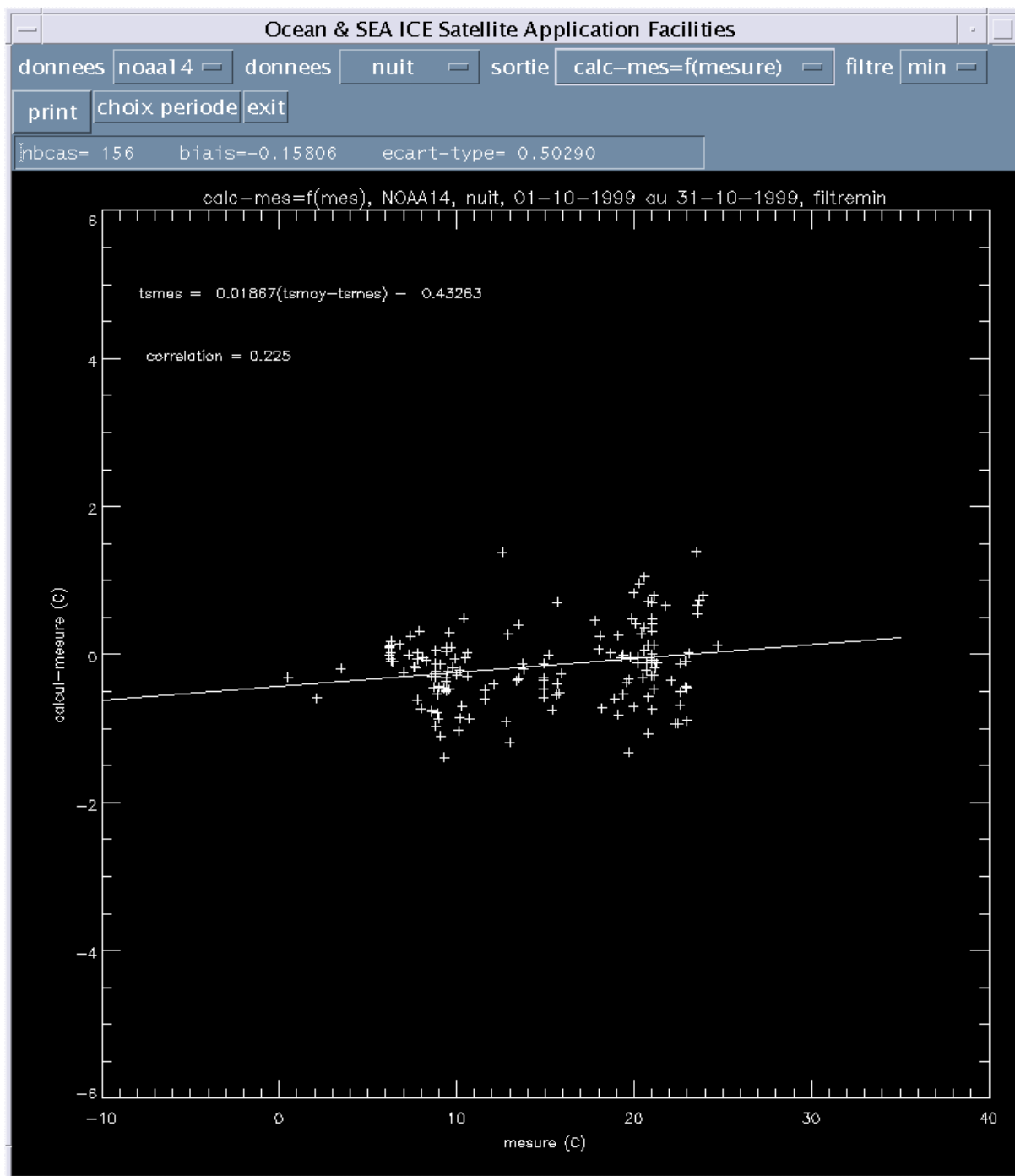


Figure 16: statistical control tool (STATSST) over the European Seas (NOAA/AVHRR): errors as a function of measured SST

#### 4.5.2 Control operating mode

Quality controls are summarised on a monthly basis under the responsibility of the operation team at CMS. Each monthly control is reported in a detailed document.

**i) QUALSST :**

Once per day and per mosaic, a control of a 1024\*1024 sub-area is performed. Every sub-area has to be controlled at least once per month.

A warning is given to the CMS R&D team in case of persisting errors.

**ii) STATSST :**

A visual examination of the statistics is made twice a month, monthly statistics are archived both as graphic documents and on files.

A warning is given to the CMS R&D team if the absolute value of the bias  $|\beta|$  is over 0.3C or if the standard deviation  $\sigma$  is over 0.6C.

4.5.3 Statistical results

The results are shown in table 12 (correction biases deduced from preliminary results have been included in the algorithms). Two validation results are systematically presented : those obtained on all validation data and those obtained on data where the cloud coverage of the box is below 10% and the standard deviation of T11 in the validation box is below 0.4C. The all data results are representative of the raw accuracy of the products (including potential problems in the vicinity of the cloud mask) and the second are more representative of the algorithm performances. They have been compared, when possible, with results obtained using algorithms derived from regressions on in situ measurements and used in an operational context. The simulation derived algorithms perform as well as the in situ data derived algorithms.

		NOAA-14 night	NOAA-14 day	NOAA-15 night	NOAA-15 day
	Number of cases	1321	2203	611	2062
All data	Bias	-0.16	-0.24	-0.36	-0.34
	St. Dev.	0.56	0.60	0.68	0.63
	Number of cases	492	1009	289	904
Filtered data	Bias	0.04	-0.11	-0.22	-0.15
	St. Dev.	0.50	0.56	0.61	0.55
NOAA operat. Algorithms on filtered data	Bias	-0.11	0.00		
	St. Dev.	0.50	0.54		

Table 12 : Regional product validation results obtained using the NL algorithms from 01/29/1999 till 11/13/1999. The 2 last lines represents the results obtained with the NOAA operational algorithms applied on the filtered data (NL by day and NL triple by night, see Walton et al 1998).

#### **4.6 References**

Brisson, A., Y. Faugere, P. Le Borgne and A. Marsouin, 1999, SST retrieval in the frame of the O&SI SAF: Mid and Low latitudes. Proceedings of the 1999 EUMETSAT Meteorological Satellite Data Users' conference, Copenhagen, Denmark.

Derrien, M. and H. Le Gléau, 1999, Cloud classification extracted from AVHRR and GOES imagery. . Proceedings of the 1999 EUMETSAT Meteorological Satellite Data Users' conference, Copenhagen, Denmark.

Walton, C.C., W.G. Pichel, J.F. Sapper and D.A. May, 1998, The development and operational application of nonlinear algorithms for the measurement of sea surface temperatures with the NOAA polar-orbiting environmental satellites, *J. Geophys. Res.*, **103** (C12), 27,999-28,012.

## 5. SEA ICE PRODUCTS WP23000

### 5.1 Introduction

Deriving sea ice parameters from satellite observations is a well established tradition. Objective algorithms for classifications of sea ice extension and types based on both passive and active satellite measurements in the microwave parts of the spectrum are in widely use. In combination with satellite information in the infrared and visible channels from meteorological satellites these data are used by operational ice services in routine production of sea ice maps. The final data fusion and the production of ice maps are mainly based on manual interpretations. In the O&SI SAF the aim is to develop an objective analysis system for sea ice parameters combining satellite data of different types, and to implement this system for operational retrieval of sea ice products. The products are meant to be input to numerical weather, ocean and sea ice models as well as information supporting operational sea ice services. The development of the analysis system is a co-operation between DNMI and DMI. Three main products are defined: ice edge, estimations of ice cover and ice type that distinguish between multi-year and first year ice. The products will be derived once daily and be provided on a 10 km resolution grid covering the North Atlantic and adjacent polar oceans.

This chapter review the development of the sea ice analysis in the framework of the O&SI SAF. The characteristics of the Sea Ice products are given, and the algorithms and methods are described. The remaining development to be done before the pre-operational phase starting in April 2001 is outlined.

### 5.2 General Products Specification

The sea ice products will be derived once daily and will be provided on a 10 km resolution grid covering the Atlantic high latitudes shown on Fig. 17.

#### **Input satellite data:**

The input data will be from polar orbiting satellites obtained from local receiving stations, trough available international networks, or through the EPS ground segment. The EPS ground segment is at present not fully defined, and additional adjustments and development of the Ocean & Sea Ice SAF data interfaces will therefore be necessary after pre-operational phase.

#### **AVHRR:**

- Pre-operationally: NOAA, received locally in near real time.
- Operationally: NOAA and EPS, Received locally and through EPS ground segment with up to 3 hours delay from observation time.

#### **Scatterometer data:**

- Pre-operationally: ERS received through GTS with up to 3 hours delay from observation time.
- Operationally: EPS received through GTS or through EPS ground segment with up to 3 hours delay from observation time.

**SSM/I:**

DMSP received through FTP or another international network with up to 4 hours delay from observation time.

**Time resolution and delivery time:**

Daily products, provided once daily at 0600 UTC valid for the previous day.

**Space resolution and projection:**

10 km polar stereographic projection, true at 60N (see Fig. 17).

**Coverage:**

North Atlantic and adjacent polar seas as shown on Fig. 17. Use of AVHRR will in the pre-operational phase be restricted to areas that are within the acquisition area of local receiving stations.

**Content:**

Sea Ice edge: probability of ice (%), Sea Ice cover: concentration (%), Sea Ice type: probability of multi-year/ first-year (%).

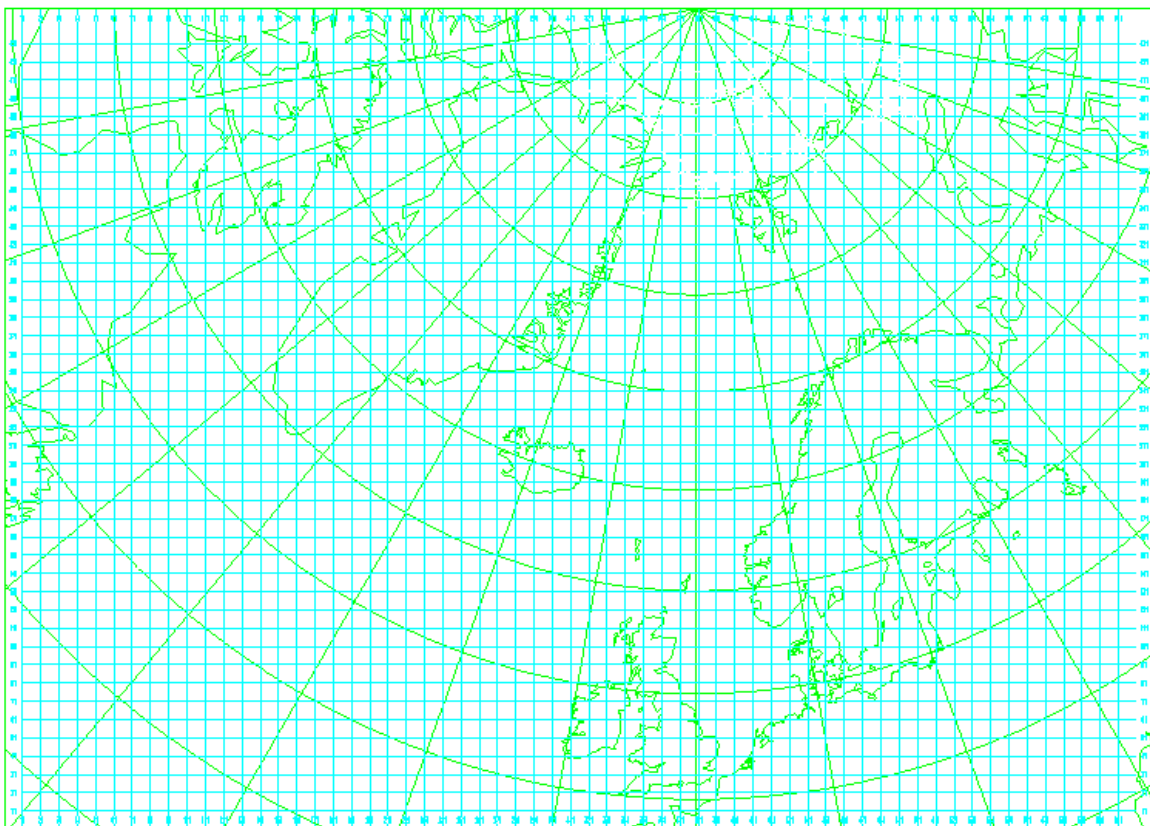


Figure 17: The SAF O&SI High Latitude Grid. Every tenth grid point is plotted.

### **5.3 Multi-sensor Sea Ice Analysis WP23410**

The development of the multi-sensor sea ice product is based ideas and work initially done to combine several parameters derived from ERS wind scatterometer for sea ice detection (Breivik and Schyberg 1998). This method was implemented for operational use at DNMI's Sea Ice Service in November 1998. Within the framework of the Ocean & Sea Ice SAF development project the method has been refined and further developed to take into account data from SSM/I and AVHRR. The project work packages defined for AVHRR and scatterometer are therefore to be seen as subsets of the work packages defined for the multi-sensor algorithm development.

The multi-sensor algorithm works well on distinguish between specific ice properties by use of information from different sensors. In the Ocean & Sea Ice SAF the method will be applied using SSM/I, scatterometer and AVHRR data to distinguish between ice and open water, between open ice and close ice and between first year and multi year ice.

#### 5.3.1 Multi-sensor Scientific Approach

The basic principles of the multi-sensor approach have been presented at several occasions, e.g. at the EUMETSAT data users conference in Copenhagen in September 1999 (Breivik et al 1999). In the following chapters we will present the main ideas of the multi-sensor method and the application on sea ice edge and type detection.

The idea of the multi-sensor Sea Ice algorithm is to develop a tool for combined use of information from different sea ice parameters from different sensors. The starting point is well-known sea ice parameters based on both physical knowledge and established empirical relations. This means that the main objective is not development of new sea ice algorithms, but development of an analysis tool to combine information from various remote sensing sources. The scientific challenge in making a combined product from the available sensors, AVHRR, SSM/I and scatterometer, is to obtain a single reliable ice product from the various observations involving different and possibly contradicting information. For doing this, it is necessary to use an algorithm that takes into account the uncertainties in the ice classification of the various instruments. It is therefore essential not only with an ice estimate, but also with knowledge of the uncertainty or degree of accuracy involved. A general tool for combining various data sources containing uncertain information is given by the Bayesian (inverse method) approach. Using this approach, several measured parameters can be combined to yield an optimal estimate. Combining independent information in this way will enable production of ice maps with improved temporal and spatial resolution.

The approach is based on knowledge of the averaged relationship between ice properties and the measured quantity together with knowledge of the scatter of the expected measurement value for a given ice class. This knowledge can be expressed

as a probability distribution of the measurement variable given the ice class. Assume e.g. that the satellite has measured a parameter  $A$ . From calibration data sets we can find the response of this parameter on an ice class  $I_k$  in terms of the probability distribution  $p(A|I_k)$ , the probability of doing an observation near  $A$  given that the ice class is  $I_k$ . This can be used to obtain an estimate of the probability of the ice class being  $I_k$  given the measurement,  $p(I_k|A)$ . Using Bayes theorem, we have :

$$p(I_k|A) = \frac{p(A|I_k)}{\sum_j p(A|I_j)p(I_j)} p(I_k) \quad . \quad (1)$$

The summation is performed over all possible, mutually exclusive ice classes  $I_j$ . Thus, knowing the probability distribution for a measured parameter  $p(A|I_j)$  for all possible ice classes  $I_j$  we have a powerful tool for estimating the probability of each ice class. An estimate of the prior probability for the ice class,  $p(I_j)$ , is also needed. A simple algorithm for ice edge detection can be made by allowing  $I$  to have two values, “ice” and “water”. The equation then gives a probability estimate for ice given the measurements. Setting both the prior probabilities for ice and water,  $p(\text{ice})$  and  $p(\text{water})$  equal to 50%, we get :

$$p(\text{ice}|A) = \frac{p(A|\text{ice})}{p(A|\text{ice}) + p(A|\text{water})} \quad . \quad (2)$$

This framework can be generalised to a method for combining several satellite-measured parameters to an optimal ice property estimate. It must be stressed that the method requires more than just thresholds on the measured parameter indicating an ice class. Such thresholds just give information on the relation between  $I$  and the most probable value of  $A$ . Here we use the full probability distribution of the measurement given the ice property. The method works in such a way that the measured parameters that the statistics shows to be most secure in distinguishing between ice properties are the ones that alter the probability. Another advantage is that we not only obtain estimates of the most probable value of the ice parameters, but also the uncertainty of the estimate.

### 5.3.2 The Analysis System

Using the above described framework an objective analysis scheme has been developed to calculate probability for ice classes. The analysis scheme has been implemented to operate on a 10 km resolution polar stereographic grid covering the Arctic and North Atlantic as shown on Fig. 17.

The final analysis is a two-step procedure as illustrated on Fig.18.

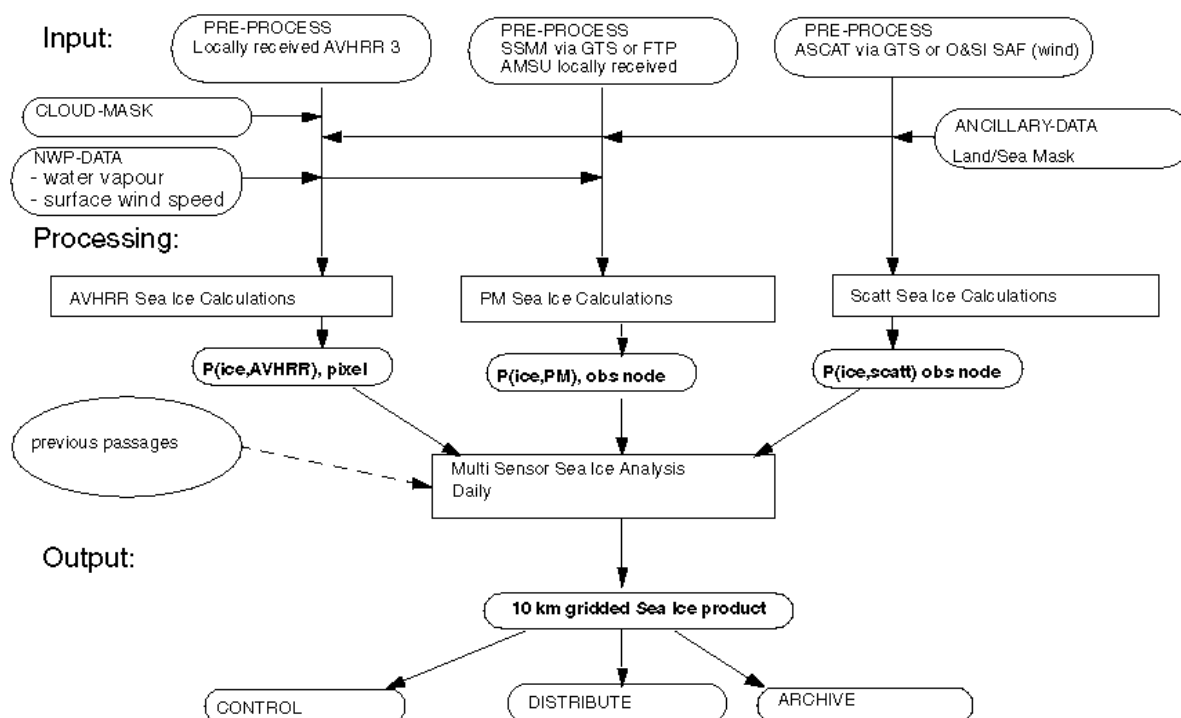


Figure 18: Flow chart for multi-sensor ice product.

In the first step each file of input data, from AVHRR, SSM/I and Scatterometer, is treated separately. Using the pre-estimated probability distributions for each ice class and the Bayesian approach described above, a probability for each ice class is calculated at each observation node. In the second step the final analysis is performed using the multi-sensor algorithm to derive the final probability values on the grid. The combined results from step one is used to calculate the probability of the ice class for each grid point. The coverage, or influence of each individual observation depends on the actual observation resolution. In addition to the estimate of most probable ice class, the associated probabilities for the ice class are stored and used as an estimate of the uncertainty of the analysis in each grid-point.

### 5.3.3 Sea Ice edge detection

In this section we will present the system applied on ice edge analysis. For this we might divide the ocean surface into two classes, sea ice and open water. However we found that the number of classes could well be extended to give even more useful information. Using SSM/I data, where the measured radiation clearly depend on ice concentration, one could easily divide into a set of ice-classes representing ice concentration intervals. This was tested and found to give a product very similar to a traditional ice concentration product. The scatterometer measurements over ice do not have the same clear dependency on ice concentration. However it was found that the

use of scatterometer data could be refined to distinguish between open water, open ice and closed ice.

The first step in building the analysis system is to derive statistics of the relationship between the classes and the measured quantity. This includes knowledge of the average as well as the scatter of the expected measurement values over ice and water. To obtain this statistical knowledge large sets of SSM/I, scatterometer and AVHRR data have been collocated with background information on sea ice obtained from the operational sea ice analysis produced by the Ice Service at DNMI Tromsø. These operational ice analysis are produced daily and are based on manual subjective interpretation of in-situ observations, AVHRR images, SSM/I data and ERS scatterometer data as well as previous analysis. To account for seasonal variations data have been collocated and statistics derived for 10-days periods in January, April, May/June, July, September and November. The operational Ice analysis deals with five classes: open water, very open drift ice, open drift ice, close drift ice, very close drift ice and fast ice. For the SAF sea ice edge analysis we operate with 3 classes, 1: water/very open drift ice, 2:open drift ice and 3: close/very close drift ice. The limits between water and open drift ice is defined to be as between very open and open drift ice which means around 35% ice concentration. The limits between open drift ice and close drift/very close drift ice is defined around 70 % ice concentration.

Some of the results of these collocations in terms of mean values and standard deviations of the sea ice related parameters compared to the Ice Service analysis are shown in the next sections in Table 13, 14, 15 and 16. Based on this statistics and assuming Gaussian error distributions the probability distribution functions necessary for the multi-sensor approach have been derived.

#### *a) Scatterometer Ice edge analysis WP23310*

Currently scatterometer data from the European Remote Sensing satellite ERS-2 are available. By the launch of EPS ASCAT data will be available giving more than twice the data coverage compared to ERS. Over sea ice, following Cavanie et al. 1994, two properties of the backscattering can be utilized. Firstly, backscattering is relatively isotropic over sea ice compared to the strong anisotropic behaviour, which is the basis for scatterometer wind direction retrieval, over water. Secondly, the change of backscatter with incidence angle shows larger variation over water than over sea ice. In alignments with this, two parameters are derived from the scatterometer measurements:

- The anisotropy coefficient,  $A$
- The change of backscatter with incidence angle,  $D$ .

In addition we use the distance of the observation from the scatterometer wind model result (Stoffelen, 1997) :

- Distance to wind model "cone",  $C$ .

Mean values and standard deviation from January 1999 of  $A$ ,  $D$  and  $C$  for 5 different incidence angles across the ERS scatterometer ground swath are given in Table 13, 14 and 15. Assuming Gaussian error distributions the probability distribution functions have been derived. Then, using the scatterometer measurements, a 'multi parameter' sea ice

analysis can be performed. As seen from the tables the classification capability of the parameters vary across the swath. However, the multi-sensor method will work in such a way that the parameters that the statistics shows to be most secure in distinguishing between ice properties are the ones that alter the probability.

Results from an analysis 15 February 2000 are presented on Fig. 19. The ERS scatterometer, which is single sided and which cannot be operated continuously due to shared resources with the ERS SAR, gives about one third of the amount of observations compared to what will be available from ASCAT. To give a useful number of scatterometer data three days of ERS data are used for testing the method.

Cell nb	Mean water	Std water	Mean open ice	Std open ice	Mean close ice	Std close ice
1	0	21.8	0	19.7	0	6.2
5	0	30.4	0	19.8	0	5.6
10	0	36.4	0	20.2	0	5.3
15	0	35.8	0	17.3	0	5.3
19	0	36.7	0	17.5	0	5.0

Table 13: Mean values and standard deviations of anisotropy coefficient,  $A$ , for 5 different cell numbers across the ERS scatterometer swath based on collocated data in January 1999

Cell nb	Mean water	Std water	Mean open ice	Std open ice	Mean close ice	Std close ice
1	0.87	0.15	0.59	0.21	0.30	0.07
5	0.58	0.15	0.34	0.14	0.19	0.05
10	0.37	0.15	0.22	0.08	0.17	0.04
15	0.23	0.16	0.16	0.04	0.15	0.03
19	0.19	0.17	0.15	0.04	0.16	0.03

Table 14: Mean values and standard deviations of the change of backscatter with incidence angle,  $D$ , for 5 different cell numbers across the ERS scatterometer swath based on collocated data in January 1999

Cell nb	Mean water	Std water	Mean open ice	Std open ice	Mean close ice	Std close ice
1	2.3	2.8	20.6	14.8	35.8	8.3
5	2.5	2.4	10.0	7.4	27.5	8.1
10	2.5	1.8	2.8	2.4	3.2	1.8
15	3.0	2.6	7.4	3.9	9.0	2.6
19	3.1	2.7	10.4	5.5	14.1	4.7

Table 15: Mean values and standard deviations of distance to wind model cone,  $C$ , for 5 different cell numbers across the ERS scatterometer swath based on collocated data in January 1999

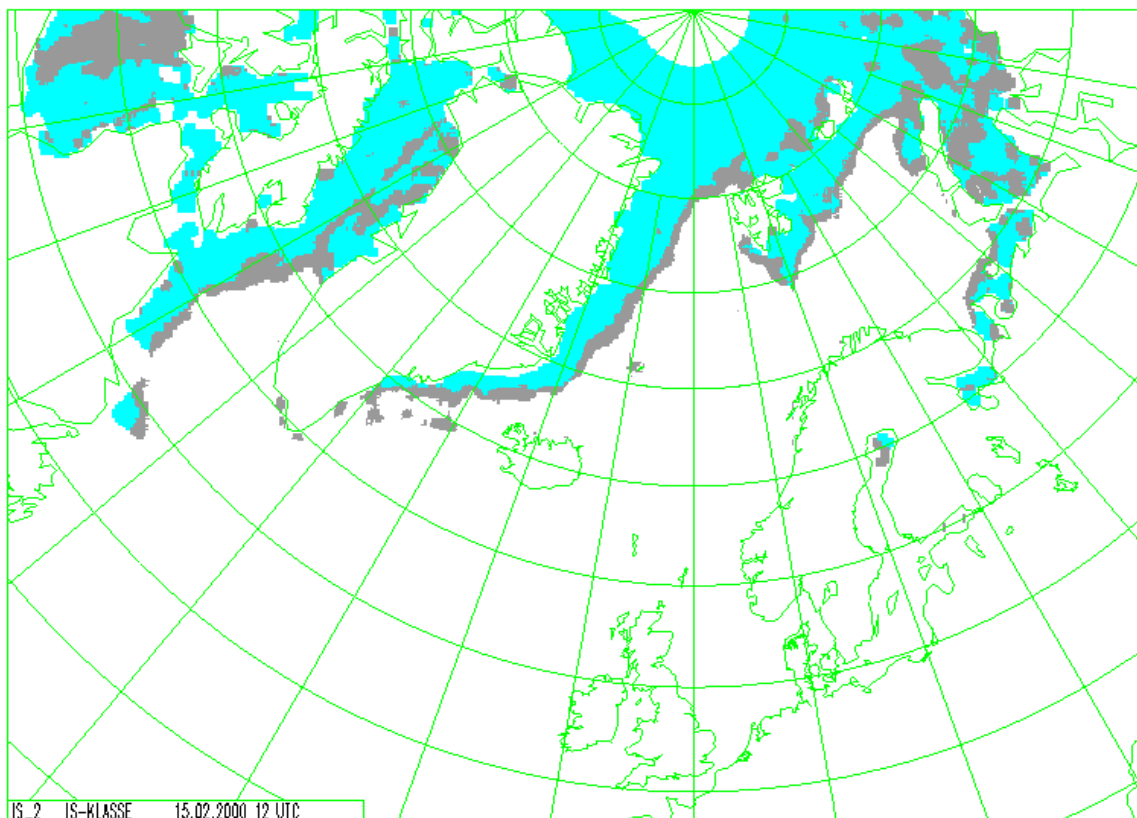


Figure 19: Sea Ice analyses using 3 days of scatterometer data, 13, 14 and 15 February 2000. Blue represent close drift ice while grey represent open drift ice.

On figure 19, areas classified as sea ice are seen also in areas where we expect open water. This is partly due to the anisotropy parameter in cases where the sea surface wind blows parallel to the scatterometer ground track. In these cases the ocean surface will seem isotropic and be misinterpreted as sea ice. Work is on going to check the possibility of including background information on surface wind direction into the statistics, to give less weight to cases with these wind directions.

#### *b) SSM/I and the multi-sensor product WP23410*

There are long traditions in utilising SSM/I data for sea ice information retrieval. Based on the established knowledge in the field some key parameters have been picked for utilisation in the multi-sensor analysis (Steffen et al, 1992). These are the difference between horizontal and vertical polarised radiation, commonly termed polarisation ratio, in the 37 and 85 GHz channels:

$$PR(37) = (Tb_{37v} - Tb_{37h}) / (Tb_{37v} + Tb_{37h})$$

$$PR(85) = (Tb_{85v} - Tb_{85h}) / (Tb_{85v} + Tb_{85h}),$$

and the change of radiation as a function of frequency expressed by the difference in radiation between the 37 GHz and the 19 GHz channels, commonly termed gradient ratio:

$$GR(19,37,V) = (Tb_{37V} - Tb_{19V}) / (Tb_{37V} + Tb_{19V}).$$

As for scatterometer data the SSM/I data have been collocated with DNMI's operational Ice Service analysis and statistics have been derived. Examples of mean values and standard deviations, based on data sets from January, April and July 1999, are given in Table 16 below.

Parameter	Mean water	Std water	Mean open ice	Std open ice	Mean close ice	Std close ice
PR(37) Jan.	16.6	2.7	9.5	4.3	3.2	1.9
PR(37) April	16.4	2.6	12.1	3.8	4.3	2.4
PR(37) July	16.1	2.8	11.3	2.9	5.1	2.1
PR(85) Jan.	11.1	2.6	6.7	3.4	2.4	1.0
PR(85) April	10.8	2.4	9.0	3.1	2.8	1.0
PR(85) July	7.9	2.3	6.6	2.0	3.8	1.5
GR(19,37) Jan.	-5.8	0.9	-2.1	1.9	1.8	2.0
GR(19,37) April	-6.0	0.7	-3.2	1.3	1.9	2.0
GR(19,37) July	-5.8	0.8	-3.4	1.1	-0.5	1.6

Table 16: Mean values and standard deviations of SSM/I parameters based on a data set from January, April and July 1999.

Assuming Gaussian error distributions probability distribution functions have been derived and applied in the multi-sensor algorithm. An example of analysis from 15 February 2000 are given on Fig. 20 and 21.

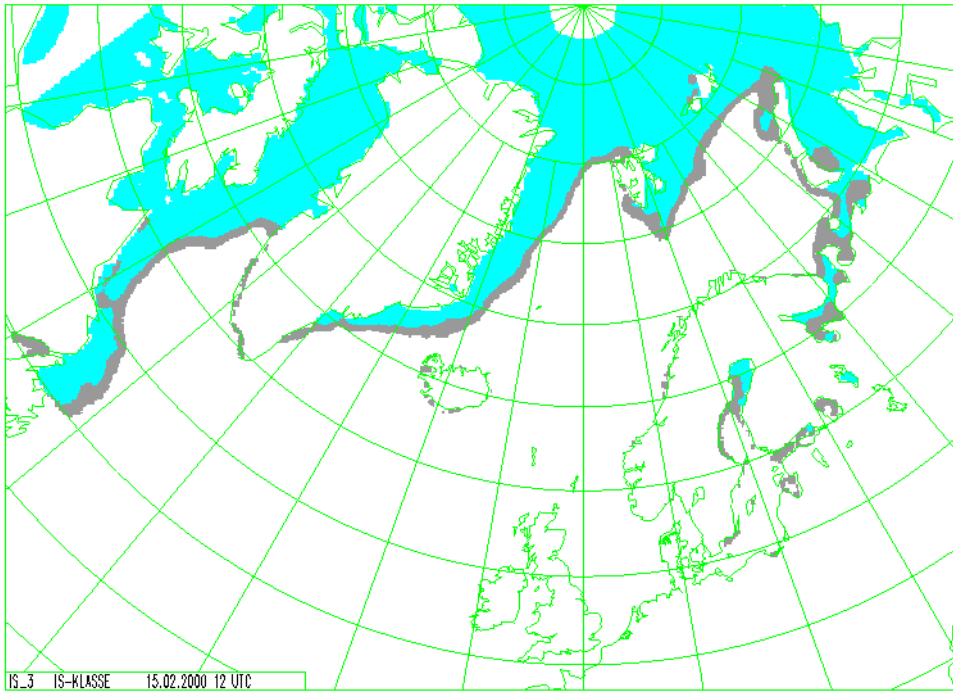


Figure 20: Sea Ice analyses using SSM/I data, PR(37) and GR(19,37), 15 February 2000. Blue represent close drift ice while grey represent open drift ice.

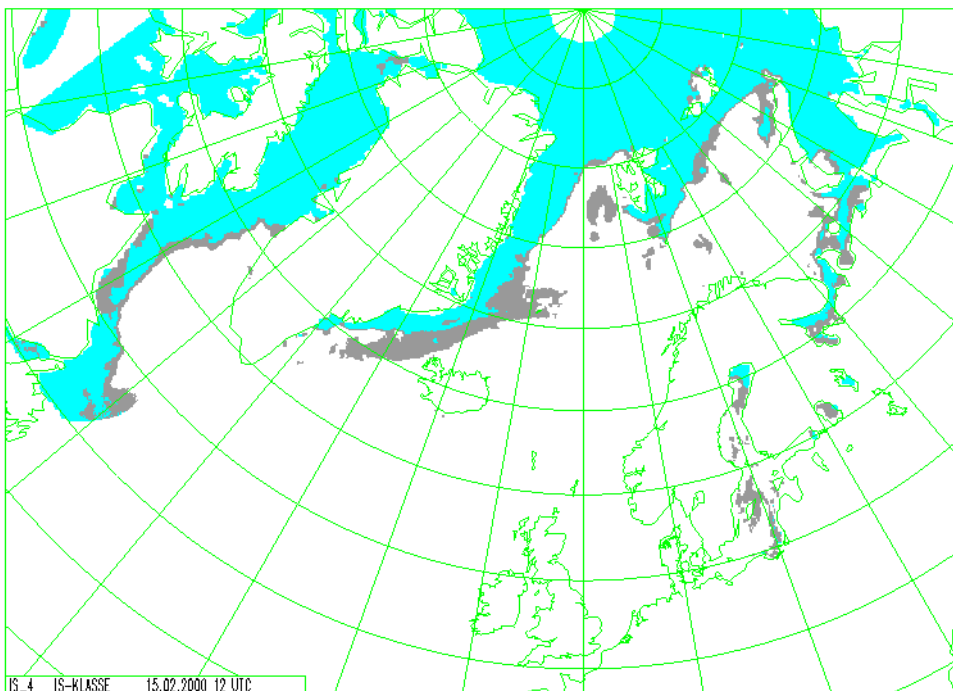


Figure 21: Sea Ice analyses using SSM/I data, PR(85), 15 February 2000. Blue represent close drift ice while grey represent open drift ice.

In the presented examples some areas where we would expect open water, but which are obviously wrong classified as sea ice, have been corrected. This is done by use of a

background filter of SST information from the operational weather forecast model HIRLAM. A grid-point where SST exceeds 4° C is classified as open water. However, this simple filter is not useful close to the ice edge. As can be seen both from Fig. 20 and 21 there are areas miss-classified as sea ice. These are in many cases due to atmospheric humidity. A method to correct for this has been tested and implemented for the SSM/I ice concentration algorithm as will be described below (WP23110). A similar approach will be introduced for multi-sensor sea ice edge product.

The results of combining scatterometer and SSM/I in the final analysis for 15 February 2000 are shown on Fig. 22.

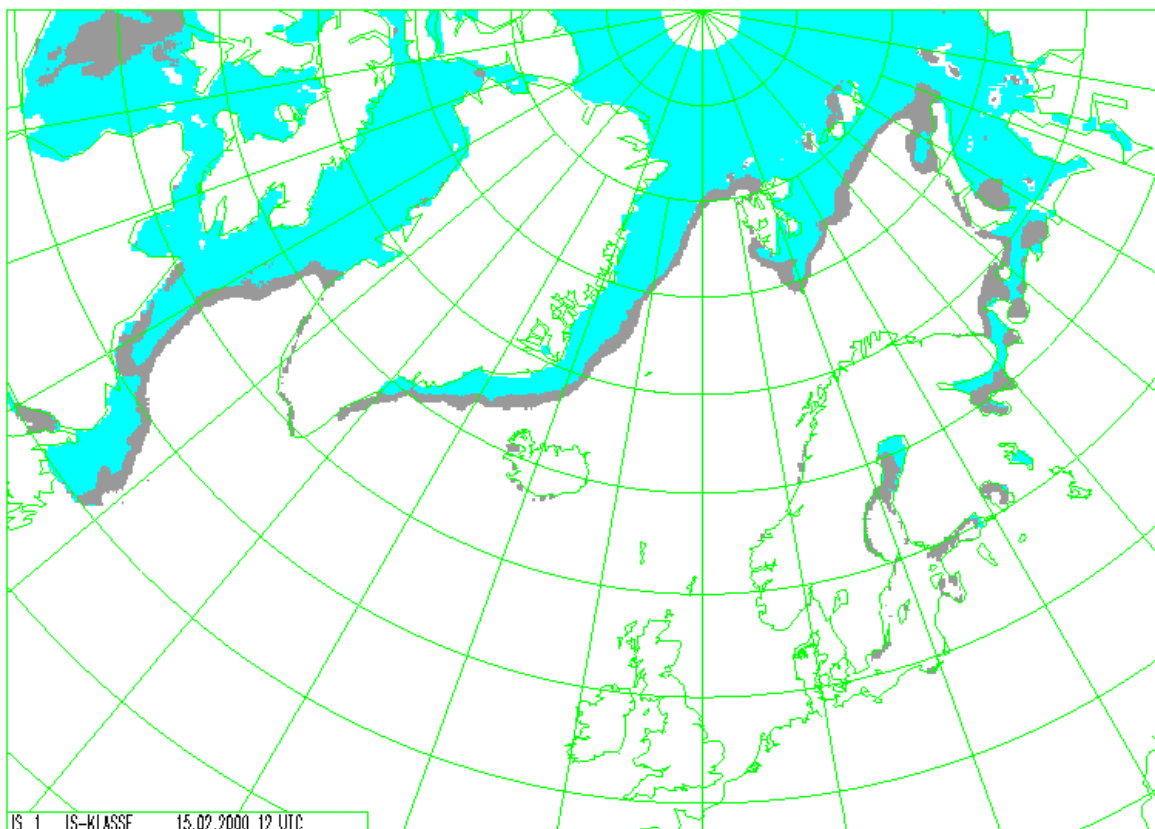


Figure 22: Multi-sensor Sea Ice analyses using available scatterometer and SSM/I 15 February 2000. Blue represent close drift ice while grey represent open drift ice.

### *c) AVHRR WP23210*

Data from the AVHRR instrument flown on the NOAA POES system have been used by operational ice services for a long time. Most services have interpreted these data subjectively while the aim of the O&SI SAF is to develop an automatic interpretation of the data. A prototype of the AVHRR Sea Ice Edge product, based on the multi-sensor approach, has been developed using a training data set from February and March 1998, covering most of the Barents, Greenland, and Norwegian Seas. The spectral features examined were the bi-directional reflectance of channel 2 and the estimated bi-directional reflectance of channel 3. The reflectance of channel 3 was

estimated using the difference between channels 3 and 4. Usually, geophysical parameters are assumed to have a Gaussian distribution. Examination of the training data using QQ plots revealed that the assumption of Gaussian distributions were inadequate. Further investigation led to the selection of two-parameter Gamma distributions for both the parameters examined.

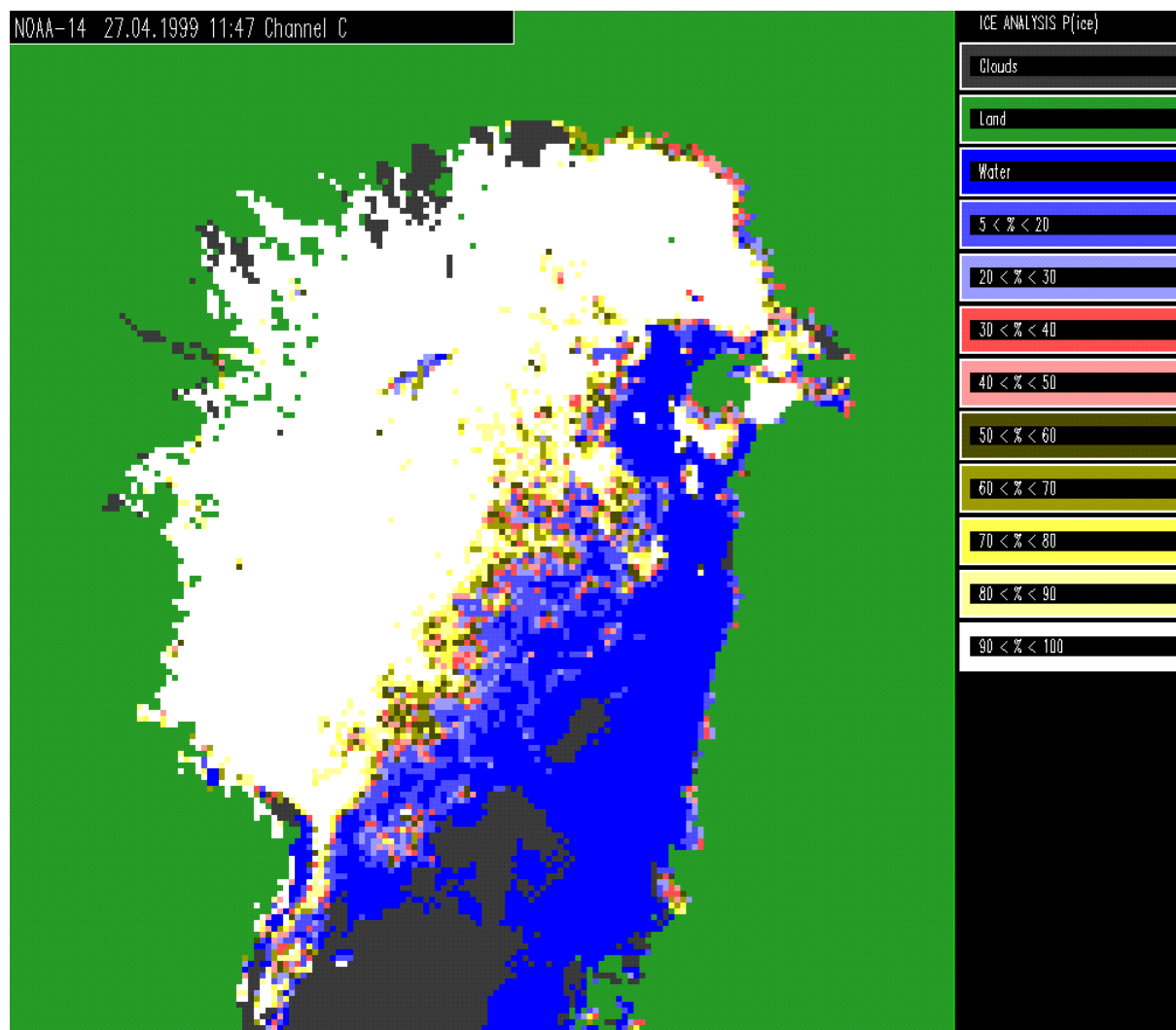


Figure 23: AVHRR Ice probabilities 27 April 1999.

Prototype software for automatic detection of sea ice in AVHRR imagery has been developed and tested on data from April and May 1999. As the AVHRR channels are dedicated to cloud observation a cloud mask has to be integrated in the SAF processing chain. In the present prototype this cloud mask is not the final one and further improvement is expected. An example of the AVHRR product from the Bothnic Bay is given in Fig. 23 for 27 April 1999, 11:47 UTC. The interior of the ice sheet has very large probabilities of ice, while probabilities are dropping as expected towards the ice edge. It is also possible to detect some leads in the ice sheet. In Fig. 24 the analysis on the 10 km SAF grid based on two high resolutions AVHRR products are shown in the upper left

panel. The figure also shows the results using SSM/I and the combined analysis using both AVHRR and SSM/I.

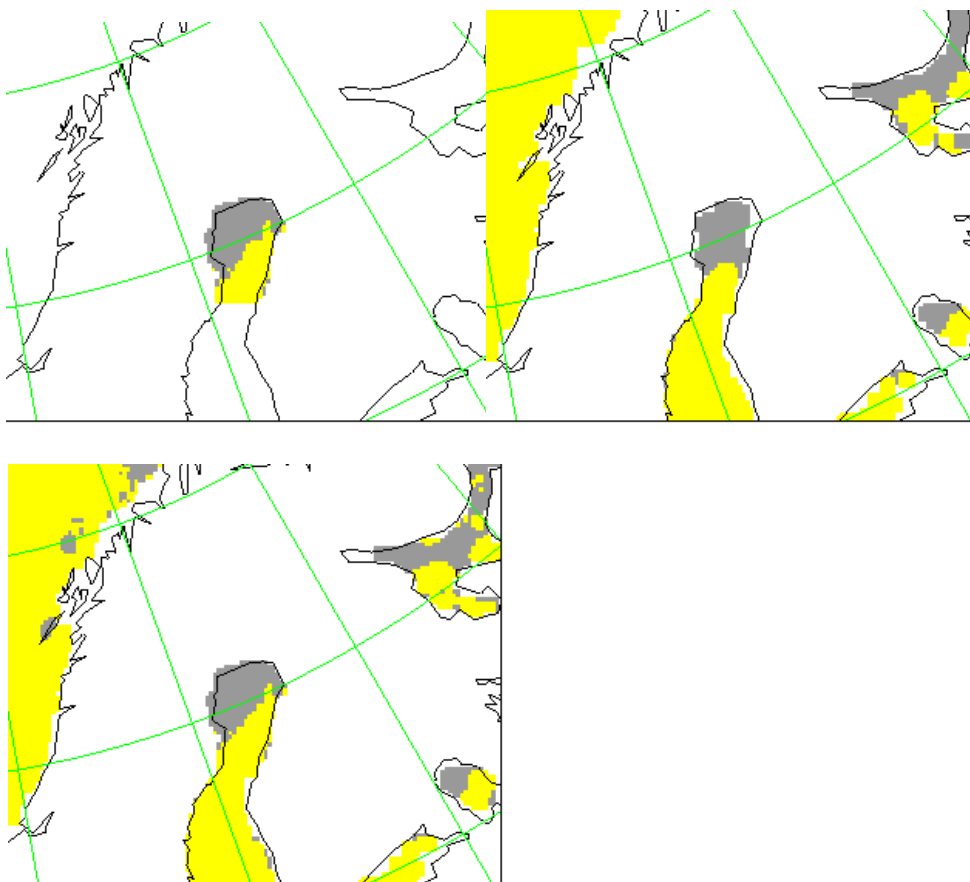


Figure 24: Sea ice analysis 27 April 1999. Upper left panel: AVHRR results, upper right: SSM/I results. Lower panel: multi-sensor analysis. Grey: Ice, yellow: water, white: unclassified (for AVHRR due to clouds)

#### 5.3.4 Sea Ice type

The multi-sensor ice analysis system as described in the previous section can in principle be applied on any set of independent measured parameters related to any set of mutually exclusive ice classes. To apply the method one first need knowledge, preferably based on a physical understanding, about the relation between the measurements and the ice classes. Then statistics have to be derived to model the probability of doing the measurements given the known ice class. In the O&SI SAF we attempt to use this approach to classify between first-year and multi-year sea ice.

##### *a) Scatterometer Sea Ice type analysis WP23310*

The normalised scatterometer backscatter  $\sigma^0$  from sea ice is dependent on ice type (Cavanie et. al. 1994). Multi-year ice is rougher than first-year, and hence the backscatter is larger. In addition the change of backscatter with incidence angle,  $D$ , is

larger for first-year ice compared to multi-year ice. Mean values and standard deviation of  $B=100 * \sigma^0$  (linear) for 5 different incidence angles, cell numbers, are given in Table 17 based on data from April 1999.

Cell number	Mean first-year	Std first-year	Mean multi-year	Std multi-year
1	7.0	3.9	8.8	3.9
5	4.2	1.4	6.1	2.3
10	2.9	1.1	4.7	2.0
15	2.2	0.8	4.0	1.5
19	1.6	0.7	3.1	1.4

Table 17: Mean values and standard deviations of the averaged backscatter  $B$  for 5 different cell numbers across the ERS scatterometer swath

The data used to derive the statistics given in Table 17 are based on measurements in areas where the ice type is known. In April we know that sea ice in the Barents Sea is new-ice while sea ice north of 85 degrees latitude is multi-year ice.

#### *b) SSM/I and multi-sensor Sea Ice type analysis WP23410*

Due to increased internal scattering in multi-year ice the change in radiation as a function of frequency might be used to distinguish between ice types. For SSM/I the gradient ratio of the 19 and 37 GHz vertically polarised channels :

$$GR(19,37,V) = (Tb_{37V} - Tb_{19V}) / (Tb_{37V} + Tb_{19V})$$

has proved particularly useful (Steffen et. al. 1992). Mean values and standard deviations of this parameter are given in Table 18.

Parameter	Mean first-year	Std first-year	Mean multi-year	Std multi-year
<b>GR(19,37,V)</b>	-1.8	1.5	- 4.5	1.4

Table 18: Mean values and standard deviations of the SSM/I parameter  $Td$  based on a dataset from April 1998.

The data used to derive the statistics in Table 18 are similar as for scatterometer data described above, based on measurements in areas where the ice type are known. For example in April we know that sea ice in the Barents Sea is new-ice while sea ice north of 85 degrees north is multi-year ice. In addition there will be areas with a mixture of multi-year and first-year ice. We do not have statistics for this "ice type". However in the present version of the analysis we have assumed a prior probability for having *mixed* to be 50%.

An example of multi-sensor Sea Ice type analysis is given in Fig. 25.

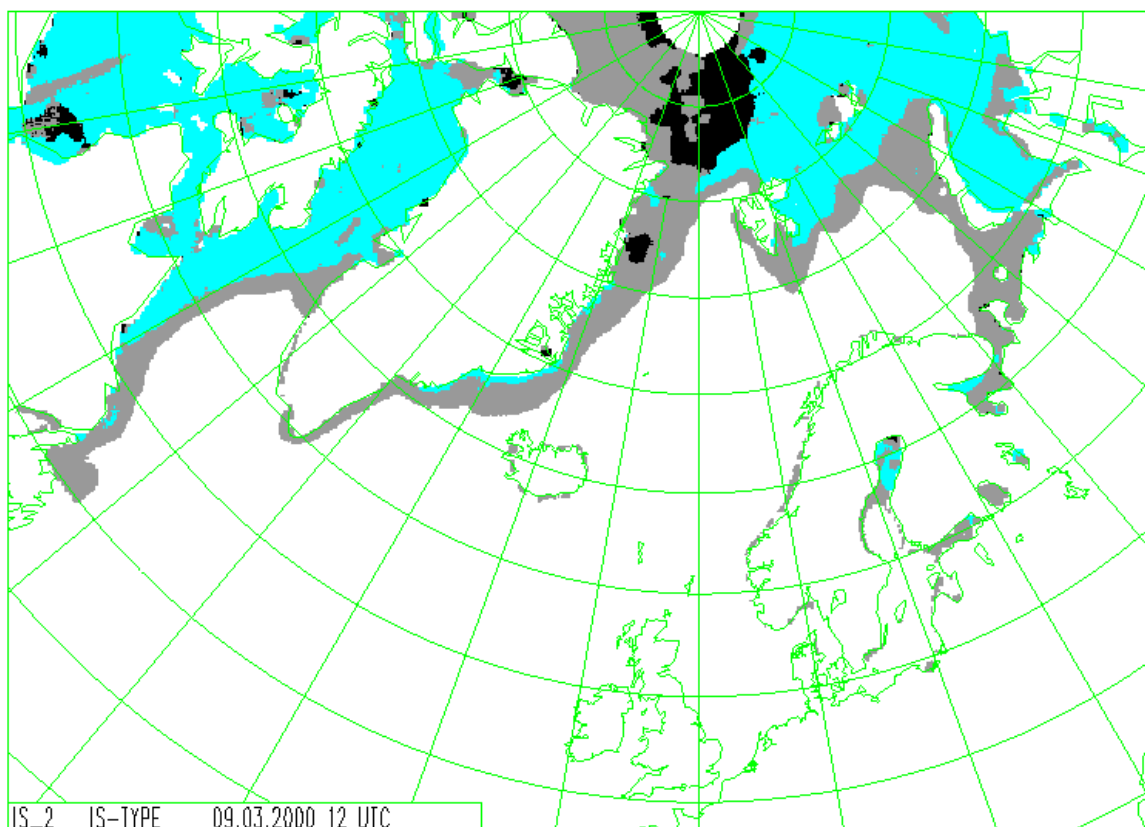


Figure 25: Ice type analysis valid 9 March 2000, blue: first-year, black: multi-year, grey: mixed.

This work package is not completed, and the final choice of parameters and updating and refining of the statistics are ongoing.

### 5.3.5 Resources Requirements

The multi-sensor sea ice analysis as described in the float chart of Fig. 18, but not including use of AVHRR data, is currently running pre-operational at DNMI. The analysis includes probability estimation of 3 ice classes (close ice, open ice and water) and two ice types. The data recourses in use for this purpose are:

SGI O2 workstation, R 5000, 180 MHz

128 Mb RAM

4 GB internal disk

The total analysis takes approximately 3 minutes

### 5.3.6 Validation Plan

At DNMI the multi-sensor sea ice analysis, as well as the individual results using only ERS scatterometer and SSM/I parameters are currently daily produced and stored together with the subjective Sea Ice analysis from the Operational Ice Service. These will

be collocated and a comparison in terms of standard statistical parameters will be performed.

The AVHRR Sea Ice Edge product will be collocated with and evaluated against the Sea Ice analysis from the Operational Ice Service. In addition a special data set will be collected during a campaign in Mars/April 2000 involving SAR data and measurements from the research vessel Lance operated by the Norwegian Polar Institute. These data will be made available for evaluation of SAF O&SI Ice products.

During the pre-operational experiment the SAF Sea Ice products will be provided to DNMI's and DMI's operational Sea Ice Services. The SAF products will be evaluated by the on duty Sea Ice analyst, and feed back reports will be provided on the quality and usefulness of the products. The products will also be provided to DNMI's and DMI's NWP and ocean modelling departments. Their use of the products will provide feedback on the quality of the products. In addition the SAF Sea Ice products will be evaluated against available in situ Sea Ice observations provided by e.g. the Norwegian Polar Institute.

#### **5.4 *Passive Microwave Sea Ice concentration WP23110***

##### **5.4.1 Scientific Approach for Algorithm Development**

The concentration product is based on passive microwave data from the SSM/I and, if useful, AVHRR. With SSM/I, the emphasis is on optimisation of existing algorithms, including the development of a set of monthly tiepoints and methods for removal/reduction of atmospheric contamination. A total of 8 concentration algorithms have been taken into account, including 2 algorithms that use the 85 GHz channels. The algorithms are 1) NASA/Team (Cavalieri et al., 1984), 2) Bootstrap (Comiso, 1986) in polarisation mode, 3) Bootstrap (Comiso, 1986) in frequency mode, 4) Cal-val (Ramseier et al., 1991), 5) Norsex (Svendsen et al., 1983), 6) Bristol (Smith, 1996), 7) Near 90 GHz algorithm (Svendsen et al., 1987) and 8) TUD improved resolution bootstrap algorithm.

As part of the algorithm selection, a sensitivity study has been performed using the MWMOD (Fuhrhop, 1997) radiative transfer model (RTM), that solves the complete radiative transfer equation with polarisation dependent Mie scattering. The sensitivities of the algorithms to the atmospheric parameters wind over water, total precipitable water (TPW), cloud liquid water (CLW) and surface temperature were established for different ice concentrations and types. The analysis shows that the actual differences between algorithms 3, 4 and 5 are very small indeed. Furthermore, it was evident that the use of the horizontally polarised channels (algorithms 1, 2, 6) raises the sensitivity to wind and CLW considerably over open water. Algorithm 2 is furthermore found not to perform better than most other algorithms over consolidated ice. The sensitivities experienced with algorithm 7 were found to be substantial and its use in an automatic concentration algorithm is therefore questionable. This finding is in line with recent literature (Lubin et al., 1997). Algorithm 8 by combining a concentration estimate from the 85 GHz channels with algorithm 3, was able to mitigate the shortcomings of

algorithm 7 to a high degree and is therefore kept under consideration. As for surface temperature, all algorithms except 1, 2 and 7 displayed substantial and approximately equal sensitivities. Finally, over consolidated multi-year ice algorithms 3, 4 and 5 showed a sensitivity to CLW approximately 5 times larger than that over first year ice. This is potentially a serious shortcoming since the distribution of CLW is poorly known and therefore difficult to explicitly correct for. Algorithm 6 also inherits this unfortunate shortcoming, although to a slightly milder extent.

To investigate the actual significance of the sensitivities found theoretically and to see if factors not accounted for in the model set-up, such as snow cover, might be significant, the behaviour of the algorithms with real satellite data was examined. The algorithms were tested using data from 1997 and 1998 over an open water area in the North Atlantic and areas known a-priori to contain pure ice types in high concentrations. The characteristics outlined above were found to apply well with the exception of algorithm 2 performing even worse than anticipated over consolidated ice. However, it is well known that the 37 GHz horizontally polarised channel is highly sensitive to changes in different vaguely known surface properties. Over multi-year ice the retrievals using algorithm 3 were noticeably depressed. This may partly confirm that the large sensitivity to CLW is significant.

Contamination arising from atmospheric water vapour content and wind roughening of the open water surface is a common problem as can be seen from Figure 26. There are several options for mitigating this shortcoming and the most common is by simple threshold filtering (e.g. Cavalieri et al., 1995). Due to some unfortunate aspects of threshold based weather filters, an alternative method has been developed based on radiative transfer modelling and NWP model information: Using the radiative transfer model by Wentz (1997) a correction based on the HIRLAM weather model fields of surface wind and atmospheric water content is computed and applied to the SSM/I brightness temperatures. Figure 26 shows a comparison of the ice concentration retrieval with and without use of the correction scheme. The uncorrected concentration field on the left displays a tongue of atmospheric contamination protruding South of Iceland and spurious ice is also observed around Spitsbergen. The right part of Figure 26 shows the concentration field computed using corrected brightness temperatures. It is evident that most of the contamination South of Iceland is eliminated and, more important, the spurious ice close to the ice edge at Spitsbergen is completely eliminated. As the method works in brightness temperature space, it is useful for reducing the scatter also in connection with the Bayesian technique adopted for the ice edge and -type analysis. Tables for correction of the 85 GHz channels, where the Wentz RTM is not valid, have been prepared (Kern, 1999). In comparisons with threshold based weather filtering, the NWP model based correction is found to be more accurate in the marginal ice zone at the expense of removing somewhat less weather related pixels. Since stable ice edge information can be obtained from the SAF multi-sensor ice edge product, the latter would not seem to be a serious shortcoming and the use of NWP model output has been preferred. It further retains the possibility of correcting brightness temperatures directly, allowing a larger range of passive microwave parameters to enter the multi-sensor products.

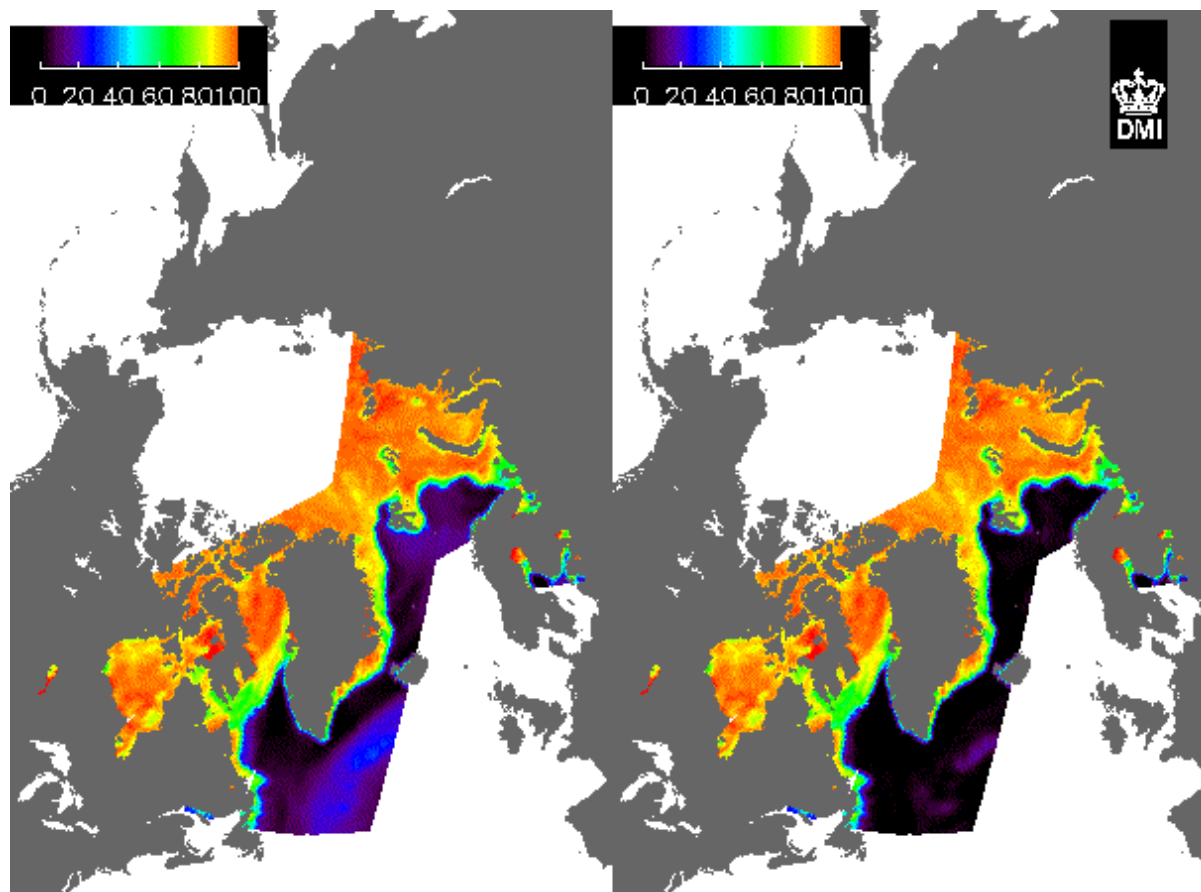


Figure 26 : Concentration retrievals of 3 SSM/I passes on 02 April 1999 using the NASA/TEAM algorithm based on unaltered brightness temperatures (left) and brightness temperatures corrected using output from the HIRLAM NWP model.

To further be able to directly correct for surface temperature as well as the annual variation in surface and atmospheric radiative characteristics to first order, a monthly set of tiepoint emissivities has been established. Figure 27 shows the effect of the new improved tiepoint set for a  $5 \times 5^\circ$  area of open water south of Spitsbergen during the months from January till June, 1999. The retrievals using the new tiepoint set (full line) shows a marked improvement in terms of both scatter and bias when compared to the retrieval using the latest NASA/Team tiepoints taken from Comiso et al. (1997). Over ice covered areas, analysis of the data set spanning 1997-1998 also shows that the new tiepoints improve the concentration retrievals giving monthly mean concentrations that are more uniform and closer to 100%.

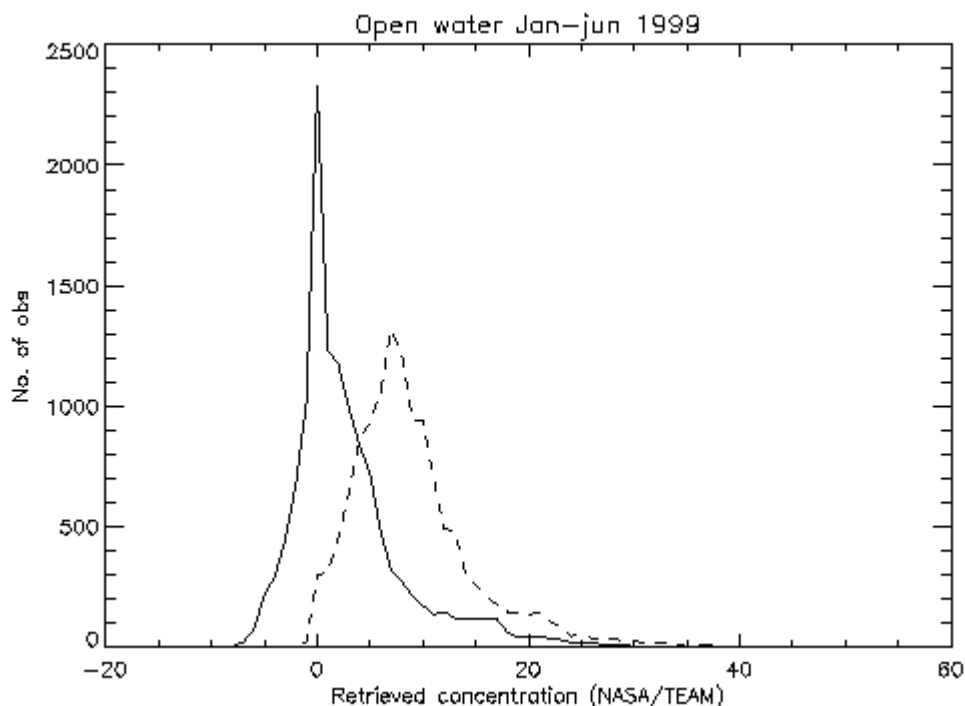


Figure 27 : Concentration retrievals of 3 SSM/I passes on 02 April 1999 using the NASA/TEAM algorithm based on unaltered brightness temperatures (left) and brightness temperatures corrected using output from the HIRLAM NWP model.

At last, it is planned to investigate the options for using information from AMSU. This is not yet finalised, however concentration algorithms developed at NESDIS (<http://orbit18i.nesdis.noaa.gov>) have been identified and will be evaluated to reveal if they can contribute with useful information.

#### 5.4.2 Selected Algorithm Specification and Tests Results

The criteria for selecting the final algorithm has included the following:

1. Accuracy of concentration estimate
2. Noise resistance
3. Resolution

Of these the last point is to a large extent in contradiction to the first two. However, as the SAF targets a wide community with differing knowledge of sea ice analysis and to a wide extent will be a source of data to automatic processing, it seems important to provide a robust product. Therefore the emphasis has been given to the first two points, ruling out algorithm 8 that provides higher resolution on the expense of higher noise levels and in the switching between high and low resolution modes introduces some unfortunate discontinuities. The selected algorithm has been established as a smooth combination of the NASA/TEAM algorithm and the Bootstrap frequency mode algorithm. This ensures an optimum performance over both marginal and consolidated ice. There are many options for combining the two algorithm estimates, however it is important that

the virtues of each algorithm be retained. This means that the NASA/TEAM algorithm should be given very little weight at low concentrations, while the opposite should be the case over high ice concentrations. The following equation is a union of these properties, gradually increasing the weighting of the NASA algorithm up to a concentration threshold  $T$ , from where it is given full weight:

$$C_T = (1 - W_c) \cdot C_{NASA} + W_c \cdot C_{Comiso}$$

$$W_c = \frac{|T - C_{T_0}| + T - C_{T_0}}{2T}$$

To avoid the need for an iterative solution,  $C_{T_0} = \sqrt{C_{NASA} \cdot C_{Comiso}}$  rather than the more accurate  $C_{T_0} = C_T$  can be used without incurring large errors. The algorithm is run on brightness temperatures corrected using the NWP based correction scheme and using the SAF monthly tiepoint set (Andersen, 1999). Based on archived data, the performance of the Comiso algorithm over open water has been assessed. The noise level is equivalent to standard deviations of 3.32% for the uncorrected case, using tiepoints supplied with the algorithm. This is reduced to 2.04% using the NWP model based correction and new tiepoints, while the bias is reduced from 2.0% to 0.6% (Andersen, 1999). Over consolidated ice, where on one hand the atmospheric noise level is much lower but the surface emissivity slowly varies, the new monthly tiepoint set has succeeded in reducing the variance of monthly mean concentration estimates. During the winter months (Jan-May and Oct-Dec) the standard deviation of a 2 year data series is lowered from 3.6% to 1.9% while including the summer months the improvement is from 5.3% to 3.6%.

#### 5.4.3 Resources Requirements

The SSM/I concentration products will be based on BUFR encoded, near real time SSM/I brightness temperatures from DMSP F13 and F14, relayed from NESDIS to UKMO from where it is fetched. The main steps of processing are given in Figure 28:

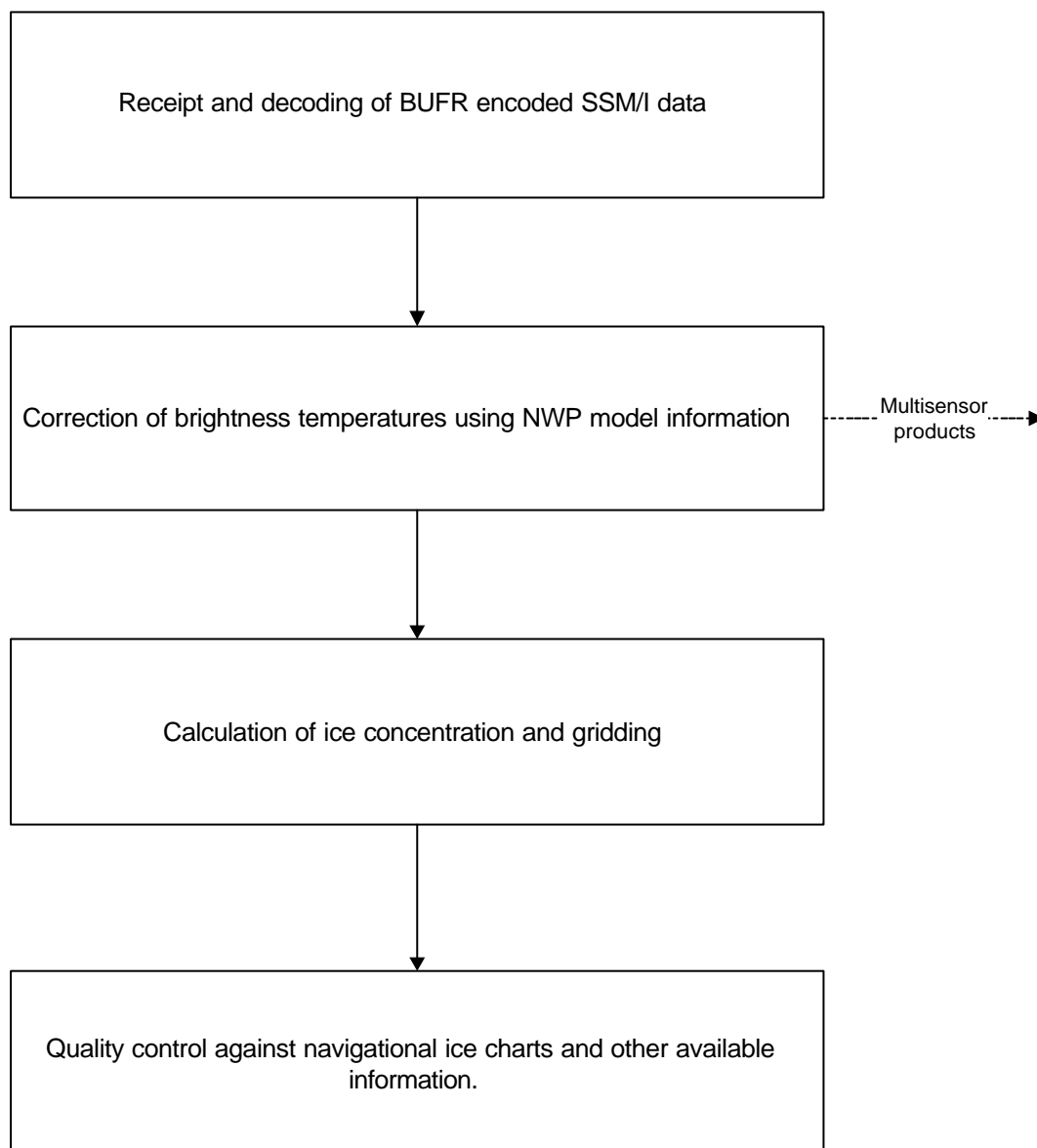


Figure 28: Main steps in the processing of SSM/I data to concentration grid. The first steps of processing are common to the multi-sensor ice edge and -type products.

The workstation supporting the prototype chain is:

SUN ULTRA 10, 300 MHz

256 Mb RAM

2 bus wide SCSI

4 Gb internal + 2x9Gb external disks

#### *NWP model based correction*

Computer resources to process one swath of SSM/I data (28 swaths total for F13 and F14 each day):

disk: 20 Mb for model data

15 Mb for SSM/I data  
Memory: ~200 Mb max.  
CPU: 40 seconds

#### *Concentration calculation*

Computer resources:  
disk: 10 Mb per swath for input output data  
50 Mb atlas data, etc.  
Memory: 50 Mb max.  
CPU: 10 seconds per swath

#### 5.4.4 Validation Plan

Storage of product validation follows a general approach applicable to all ice products: Upon availability of validation data (e.g. a weekly ice chart), all non-static information necessary for starting the processing chain is stored for at least 24 hours centred at the time of the validation observation. This database is regularly used for making statistics describing the performance of the product. At DMI, on availability of a weekly navigational ice analysis or for special events, the storage of product validation data is started and follows the outline of Figure 29. All data SSM/I, scatterometer, AMSU and AVHRR data received at DMI are archived as is and are therefore available even in the case that the validation information arrives late.

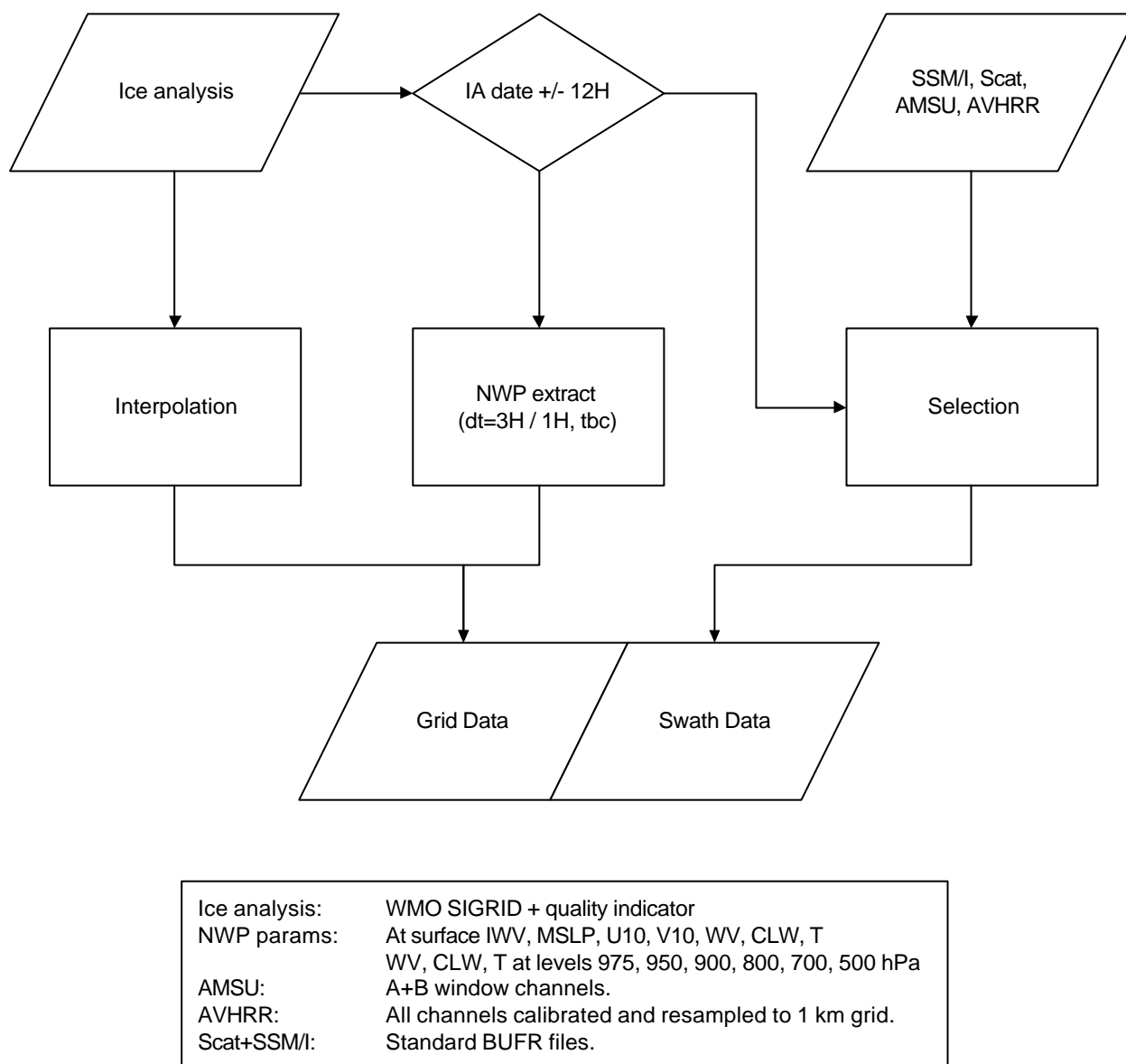


Figure 29 : Outline of the process of collecting validation data at DMI. (IWV=Integrated Water Vapour; MSLP=Mean Sea Level Pressure; U10/V10=wind speeds at 10 m; WV=Water Vapour; CLW=Cloud Liquid Water; T=Temperature)

## 5.5 References

Andersen, S.: Monthly arctic sea ice signatures for use in passive microwave algorithms. Proceedings to 1999 EUMETSAT Meteorological Satellite Data Users' Conference, Copenhagen, 6-10 September 1999, in press.

Breivik, L.A, Ø. Godøy, H. Schyberg and S. Andersen, 1999, Status of the development of a multi sensor ice product. Proceedings to 1999 EUMETSAT Meteorological Satellite Data Users' Conference, Copenhagen, 6-10 September 1999, in press.

Breivik, L-A and H. Schyberg, Scatterometer data for SAF Sea Ice Products. Emerging Scatterometer Applications, From Research to Operations, ESA SP-424, ESTEC, 5-7 October 1998,

Cavalieri D.J., P. Gloersen, W.J. Campbell: Determination of sea ice parameters with the Nimbus 7 SMMR, J. Geophys. Res., 89, D4, 5355-5369, 1984.

Cavalieri D.J., K.M. St. Germain, C.T. Swift: Reduction of weather effects in the calculation of sea ice concentration with the DMSP SSM/I. J. Glaciology, 41, 139, 455-464, 1995.

Cavanie, A., F. Gohin, Y. Quilfen and P. Lecomte, 1994, Identification of Sea Ice Zones using the AMI Wind: Physical Bases and Applications to the FDP and CERSAT Processing Chains. In: Proceedings Second ERS-1 Symposium, Hamburg 11 - 14 October 1993.

Comiso J.C.: Characteristics of arctic winter sea ice from satellite multispectral microwave observations. J. Geophys. Res., 91, C1, 975-994, 1986.

Comiso J.C., D.J. Cavalieri C.L. Parkinson, P. Gloersen: Passive microwave algorithms for sea ice concentration: A comparison of two techniques. Remote Sens. Environ., 60, pp. 357-384, 1997.

Fuhrhop R.: MWMOD user manual, Institut für Meereskunde, Christian-Albrechts Universität, Kiel, Germany, 82 pp, 1997.

Kern S.: Compensating for atmospheric effects on passive radiometry at 85.5 GHz using a radiative transfer model and NWP model data (Report on visiting scientist stay). Institute of Environmental Physics, University of Bremen, Germany, 9pp, 1999

Lubin D., Garrity C., Ramseier R.O., Whritner R.H.: Total sea ice concentration retrieval from the SSM/I 85.5 GHz channels during the arctic summer. Remote Sens. Environ., 62, 63-76, 1997.

Ramseier R.O., Section 10: Sea ice validation. in J.P. Hollinger (ed): DMSP special sensor microwave/imager calibration/validation - Final report volume II, Naval Research Laboratory, Washington, DC, 1991.

Smith D.M.: Extraction of winter sea-ice concentration in the Greenland and Barents Seas from SSM/I data. Int. J. Remote Sensing, vol.. 17, no. 13, 2625-2646, 1996.

Steffen, K., J. Key, D.J.Cavalieri, J.Cosimo, P.Gloersen, K.St.Germain, I.Rubenstein: The Estimation of Geophysical Parameters Using Passive Microwave Algorithms. Geophysical Monographs 68, Microwave Remote Sensing of Sea Ice, Frank D. Carsey, 1992.

Svendsen E., Kloster K.; Farelly B., Johannesen O.M., Johannesen J.A., Campbell W.J., Gloersen P., Cavalieri D.J., Mätzler C.: Norwegian remote sensing experiment:

## 6. SCATTEROMETER WIND WP24000

### 6.1 General Product Specification

#### Input satellite data:

Scatterometer data, pre-operationally: ERS, operationally ERS and EPS received through GTS with up to 3 hours delay from observation time.

#### Time resolution:

Determined by dissemination frequency of the ERS and EPS scatterometer data. Every useful input backscatter product should have a corresponding output wind product.

#### Coverage :

Global and regional seas (seas watering Eumetsat member states including a large part of northern Atlantic).

#### Content:

Input product (location, backscatter data and measurement geometry), unique wind solution (chosen) and its corresponding ambiguity, quality information (wind quality indicator, wind direction skill, ice screening information, recommendation for use).

#### Delivery time:

A wind product is available for distribution 10 minutes after the backscatter product reception.

### 6.2 Scientific Approach for Algorithm Development

#### 6.2.1 Ice Screening WP24200

At IFREMER much experience exists on the interpretation of backscatter measurements over ice. Several parameters are known to be correlated to ice parameters, and conversely some combinations of these parameter values are unlikely over ice. On the other hand, the distance to the cone is related to the likelihood of a node to be a water surface (Stoffelen and Anderson, 1997a) and ice surfaces often exhibit large distances to the cone. As such, from the triplet of backscatter measurements at each node some information may be derived on the ice or wind properties. Moreover, when past scatterometer data are used as well, then the combination of several azimuth and incidence angles in a certain area may reveal sufficient information for the exclusion of ice points, or the acceptance of ocean points in the wind product. IFREMER will use their experience to develop an ice screening subroutine along these lines.

Cross sections in the 3D measurement space reveal a distinction between ice and ocean points (figure 30). In fact, much of the distinction is lost when only an isotropy parameter, and/or a derivative of the backscatter with respect to incidence angle is computed. The distance to the wind cone provides the probability of a water surface. Similarly, a distance to the ice "line" could be computed that provides a measure of the ice probability. Cavanié et al (1998) derived an empirical ice model that may be representative for such an ice "line" in the 3D measurement space. Again, since ice surfaces are generally stationary, an ice parameter history could be kept on a map, in

order to constrain the ice likelihood to a very small sub-space of the 3D measurement space. As such, ice screening may be performed effectively. Of particular concern for the ice screening routine are melt and freeze processes, including percolation. In the context of the O&SI SAF, the effectiveness of the 3D measurement space approach is investigated, and, if effective, it will be included in the ice screening algorithm.

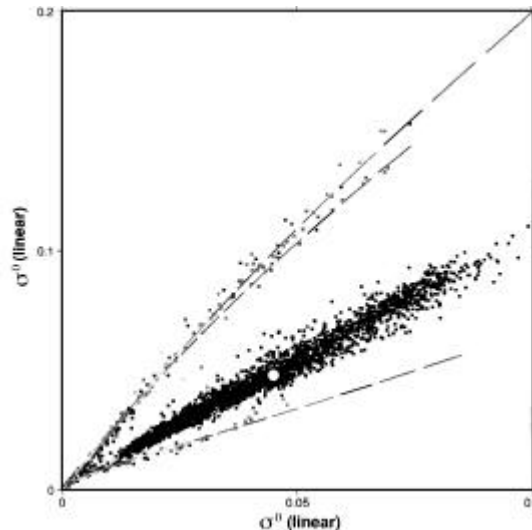


Figure 30 : Cross section in 3D measurement space for triplets over ice and open water for node 15 and south of 55S. Only triplets for which the ECMWF sea surface temperature is below 0 °C are black; other triplets are assumed to be over open water and grey-scales according to wind speed. The grey lines indicate the cross-section with the CMOD4 cone surface. The white dot depicts a particular local ice type inferred from recent data. Whereas wind triplets lie along the cone, ice triplets are located closely to a line, and locally, if stationary, close to a point.

### 6.2.2 Ambiguity Removal WP24300

Although ambiguity removal schemes work well in most cases, they fail in the most dynamic situations, where no good quality prior information is available on the direction of the wind. We note that extreme weather events like, e.g., hurricanes are most relevant and continued effort on improving algorithms is important. Figure 31 shows a case of large wind variability near the ice edge where ambiguity removal is a challenge, and is processed through 2D-VAR. The variational meteorological analysis methodology is being applied for ambiguity removal (de Vries and Stoffelen, 1998, Schyberg and Breivik, 1998), thereby relying on prior NWP model information. IFREMER is looking into the possibility of a variational ambiguity removal method that is more independent from such prior information.

De Vries and Stoffelen (2000) developed a new 2D-VAR procedure for the O&SI SAF that can be applied effectively in real time on bathes of (A)SCAT messages. the method uses the known spatial structure of the wind field, as used in meteorological analysis, to improve ambiguity removal skill. In 2D-VAR a cost function is minimised. The cost function is formulated in terms of wind increments and penalises deviations from both a

background wind field and the ambiguous scatterometer wind solutions obtained from ERS scatterometer wind retrieval. A main feature of 2D-VAR is the use of a discrete grid that extends beyond the scatterometer swath to incorporate wind increments generated outside the swath due to scatterometer observations at or near the edge of the swath. The wind increments contribute to the cost function and help obtain to obtain a realistic and meteorologically consistent solution. Another feature of 2D-VAR is observation grouping which exists in appointing a mean location to a group of neighbouring ambiguous winds. This has the effect of spatial smoothing that appears to have a beneficial effect in areas with large gradients (e.g., fronts), due to reduced overfitting effects.

Validation of its performance shows that 2D-VAR has both strengths and weaknesses. An objective comparison with PRESCAT (Stoffelen, 1998a) slightly favours PRESCAT. However, subjective analysis by meteorologists at KNMI favours 2D-VAR for cases where 2D-VAR and PRESCAT give substantially different solutions. 2D-VAR is now applied for QuikSCAT winds.

IFREMER is looking into the possibility of a variational ambiguity removal method that is more independent from NWP prior information (following Roquet and Ratier, 1991). Le Ru (1999) provided a first implementation at IFREMER. She solved the problem by the subsequent minimisation of two cost functions

$$J = \mathbf{a}J_{SIG} + \mathbf{g}J_{LIS} \quad (1)$$

$$J = \mathbf{a}J_{SIG} + \mathbf{b}J_{ANI} + \mathbf{d}J_{DIV} \quad (2)$$

where the global terms

- $J_{SIG}$  penalises the local differences between observed and control backscatter values weighted by the expected backscatter noise;
- $J_{ANI}$  penalises the local difference between observed and control values of  $(\mathbf{s}_1^0 - \mathbf{s}_3^0)/(\mathbf{s}_1^0 + \mathbf{s}_3^0)$ ;
- $J_{LIS}$  acts to smooth the wind direction field; and
- $J_{DIV}$  acts to constrain the divergence of the control wind vector field.

After some optimisation Le Ru found that in the first minimisation  $\mathbf{g} > \mathbf{a}$ , whereas in the second minimisation  $\mathbf{b} \gg \mathbf{a} \approx \mathbf{d}$ . IFREMER is further developing the method.

In a second stage of this development the relative merits of 2D-VAR and IFREMER's variational method will be assessed in order to provide visibility and a recommendation for the users on what method suits their application. Moreover, for the SAF operational phase a baseline algorithm for near real-time processing has to be established.

### 6.2.3 Quality Control and Monitoring WP24400

The ERS-2 geophysical validation strategy includes an "ocean" sigma naught calibration procedure as described by Stoffelen (1998a). Moreover, instrument monitoring, see Le Meur et al (1996), and backscatter QC (Stoffelen and Anderson, 1997a) results in a product with a well characterised quality. Moreover, the spatial error correlation

characteristics have been investigated (Stoffelen, 1996). It can not be stressed too often that a few low quality observations may destroy the beneficial impact of many good quality observations, and that Quality Control and monitoring are essential for NWP, but also for direct use by meteorologists in Nowcasting.

By comparing to NWP model winds the QC will be refined. The monitoring scheme implemented at ECMWF is being adopted (Le Meur et al, 1996), and developed for use in the SAF to allow monitoring over a smaller time window (6 hours).

#### 6.2.4 ASCAT study WP24600

Given the error characteristics of the ASCAT instrument, a model for the interpretation of C-band scatterometer data, and a realistic wind spectrum, one may predict the performance of the ASCAT scatterometer by Monte-Carlo simulation. It is useful to do this since the wind retrieval errors are non-linearly related to the ASCAT instrument backscatter errors. Moreover, the sensitivity to instrument errors depends on node position. At this point it is interesting to note that the increased backscatter noise, when going from a 50 km to a 25 km footprint is equivalent to the average wind variability on scales between 25 and 50 km. This means that over the ocean the higher resolution is only relevant in situations with above-average wind variability (Stoffelen, 1999a).

#### 6.2.5 Geophysical Model Function WP24700

ASCAT measures at larger incidence angles than ERS SCAT. The tuning software that was used to derive Cmod4 will be revised for use at these larger incidence angles, in case Cmod4 needs revision. The latter we do not expect since the behaviour of Cmod4 is rather smooth with incidence angle for these higher incidence angles, as one would physically anticipate.

While Cmod4 predict the coherence of the ERS backscatter triplets to great precision, one degree of freedom remains to scale the retrieved wind speed. After careful tuning against buoys and NWP model output in a triple collocation exercise, it turns out that ERS-retrieved wind speeds using Cmod4 are generally 5% too low with a small non-linear correction, giving rise to the formulation of a Cmod5 (Stoffelen, 1998a).

In addition, Carswell et al (1998) contains important measurements on the radar backscatter behaviour at extreme wind speeds. The sensitivity of Cmod4 to extreme winds turns out to be too high. The data measured by Carswell et al suggest the presence of more extreme wind speeds than retrieved by ERS, but at an accuracy that is clearly worse than for wind speeds below 25 m/s. These results are being implemented and tested to lead to Cmod5.

#### 6.2.6 Measurement Space visualisation WP24800

A crucial element in the validation and calibration of the ERS scatterometers is the coherence of the backscatter triplets in the 3D measurement space (Stoffelen and Anderson, 1997a). By making cross-sections through this space, the quality of the data can be subjectively verified. The existing visualisation software will be upgraded and extended to be ready to deal with ASCAT.

### **6.3 Selected Algorithm Specification and Tests Results**

An example of ERS wind scatterometer product is given in Fig. 31.

Algorithm development and selection is ongoing for the O&SI SAF wind product. The scientific approach for the IFREMER ice screening is well established, but the algorithm specification needs further testing. Moreover, the new KNMI ice screening methodology is conceptually clear, but its practical application much less so. In particular, the algorithms to deal with non-stationary ice conditions need further investigation.

Quality control and monitoring algorithms are based on those described in Stoffelen (1998) and Le Meur (1996) and are being re-tuned as described in section 6.2.

The development of Cmod5 is described in Stoffelen (1998) and in addition specified by the suggestions of Carswell at extreme wind speeds (1998).

Ambiguity removal procedures are described in detail in de Vries and Stoffelen (2000) and in Le Ru (1999). Further testing and tuning is being considered as described in section 6.2.

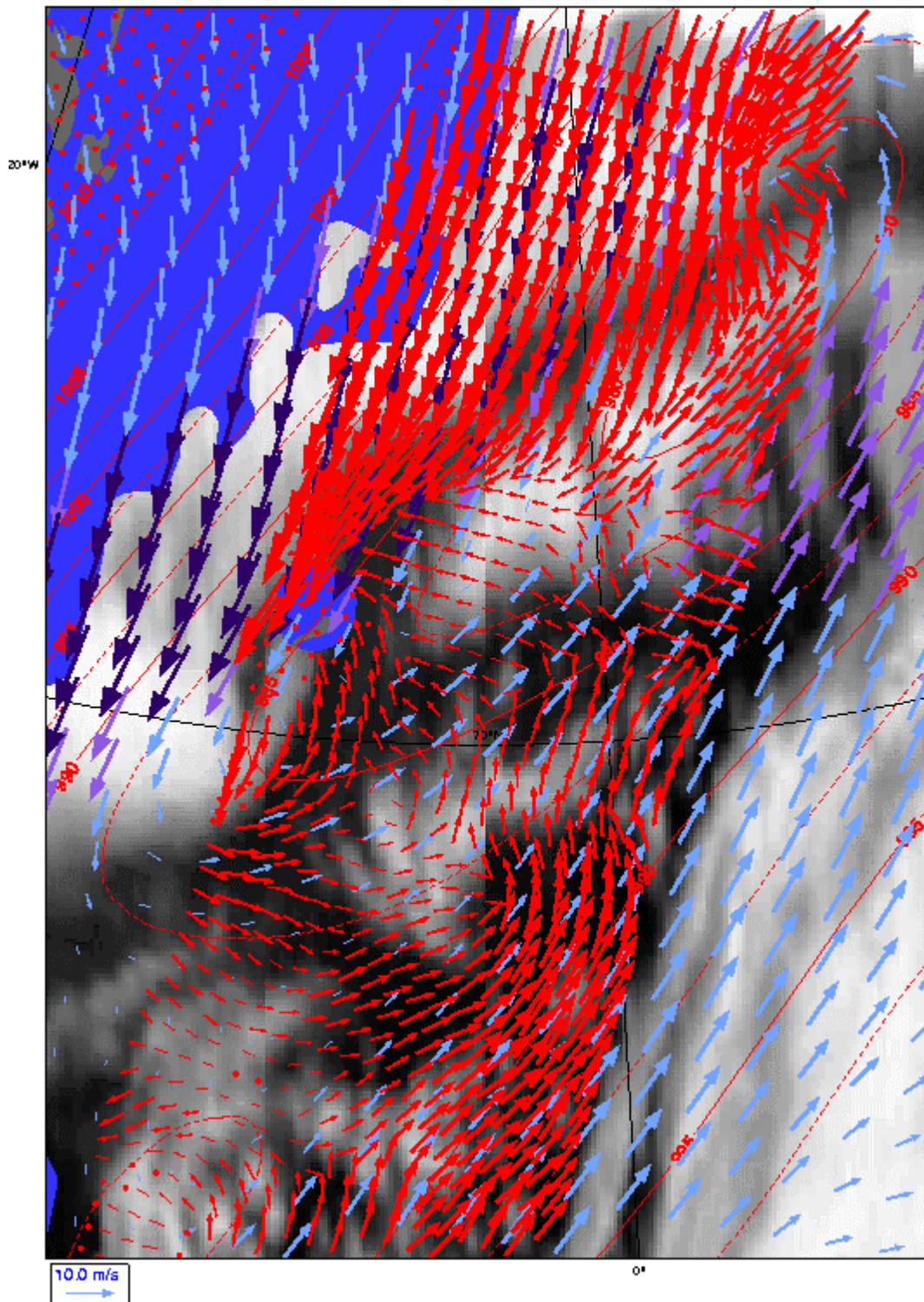


Figure 31 : Scatterometer winds from ERS-2 as processed by the O&SI SAF around 12 GMT on 24/11/99 at 70N and 0W. The following information is displayed : IR METEOSAT image. Blue mask for which the sea surface temperature is below zero degrees and where sea ice is probable. Grey mask for land presence at 80N and 20W (top is north). Red contours of surface pressure from the HIRLAM model at KNMI (3-hour forecast). Blue and purple wind vectors from HIRLAM (the amount of purple increases with wind speed). Red wind vectors depicting the ERS-2 winds as processed by the

SAF. At the red dots the winds were rejected because of a confused sea state (lower left) or the presence of sea ice (top left). The wind legend is at the lower right.

In the O&SI SAF the QC is being extended to include a measure of the local ocean surface anisotropy of radar backscattering. This is useful to allow further analysis of the backscatter geophysical relationship. For example, if anything, in the presence of steep ocean waves the backscattering from gravity-capillary waves may become more isotropic (Stoffelen, 1998a). Figure 32 depicts an observed triplet  $\mathbf{o}$ , a backscatter triplet  $\mathbf{s}$  corresponding to a wind vector solution, and the isotropy point  $\mathbf{m}$ , computed as the average of the solution triplets over all wind directions (the Lissajous curve). A distance to the cone with a sign is now defined by

$$D = \frac{(\mathbf{s} - \mathbf{m}) \bullet (\mathbf{s} - \mathbf{o})}{\|\mathbf{s} - \mathbf{m}\|} \quad (3)$$

where negative values of  $D$  correspond to more isotropy than in Cmod4 and positive values to less isotropy.

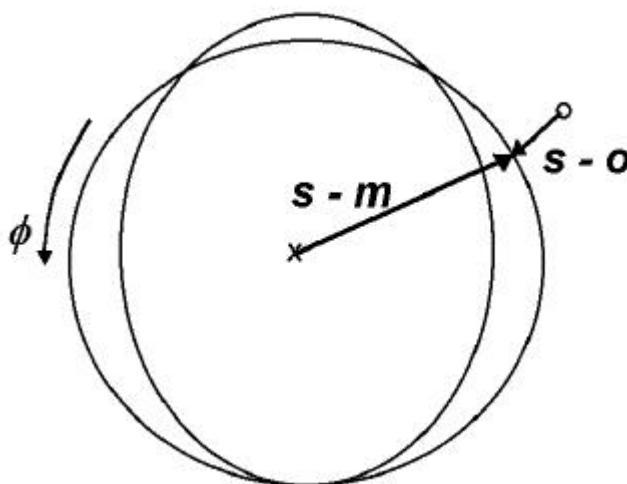


Figure 32: Projection across the cone of the solution backscatter triplets (Lissajous curve) for varying wind direction  $\phi$  that correspond to the observed triplet  $\mathbf{o}$ . The minimum distance solution  $\mathbf{s}$  lies in between the observation  $\mathbf{o}$  and the isotropy point  $\mathbf{m}$ , i.e., the centre of gravity of the curve.

#### 6.4 Processing Chain and Resources Requirements

KNMI has a prototype processing chain running in near real-time with ERS data for the north Atlantic and global areas. This prototype is based on PRESCAT. The processing is being extended with monitoring, visualisation on the WWW, and archiving functionalities.

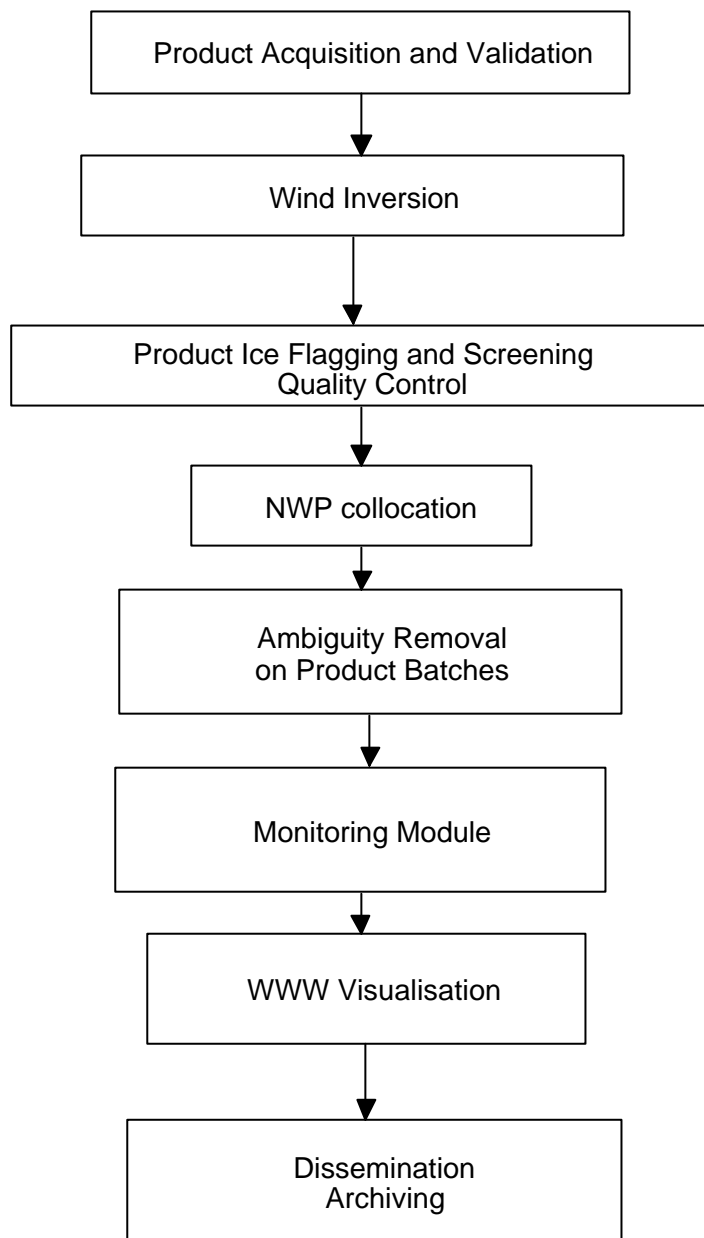
**GLOBAL (A)SCAT PROCESSING CHAIN**

Figure 33: Global (A)SCAT processing chain as being developed by the O&SI SAF

The ASCAT data flow amounts to about twice the ERS SCAT data volume, i.e., only 1.5 Mbyte per orbit or per 100 minutes. The output of the global processing chain is about 2 Mbyte per orbit. The prototype global processing chain is currently run on the KNMI computing service for application development (Silicon Graphics). Sufficiently large internal disks, RAM, and fast SCSI resources are accommodated. The operational

ASCAT data flow would be run on the operational Automatic Production Line, APL [RD-2], where the process would be scheduled and prioritised.

Where the data volume is relatively small, the look-up table used during the inversion is about 1 Mbyte and the NWP global or regional input requires about 4 Mbyte of memory storage. This may increase in the future as higher resolution NWP grids become available. The ice screening requires TBD memory for the storage of backscatter data on a 25-km grid around the poles, and the storage of ice edge climatologies. Processing CPU time for PRESCAT is less than one minute per orbit. Variational ambiguity removal and ice screening will an additional require TBD minutes per orbit.

Data volumes and processing time are thus limited. The global processing chain is written in such a way that product validation, inversion and ice screening are performed with minimum delay after receiving a (A)SCAT BUFR message on the KNMI Message Switching System (up to TBD minutes). A second process involving ambiguity removal and monitoring will then be started on a batch of time continuous BUFR messages as they become available from the first processing step. Batch length maximisation for SCAT and ASCAT is considered for trade-off against processing delay.

### **6.5 Product Validation Plan and First Results**

Each step in the processing is validated separately and also the product as a whole by a quality control and monitoring scheme. The product validation step is controlled by visual inspection, and a statistical analysis is performed to control the validation steps. The inversion step is controlled in the same way. The ice screening algorithm specification can be tested against the O&SI SAF ice edge product in those areas where the ice edge is well determined. For ambiguity removal schemes an objective scheme exists that relies on initialisation with a one-day lead NWP forecast and validation of the ambiguity selection against NWP analyses. Moreover, de Vries and Stoffelen (2000) describe subjective comparison of the 2D-VAR and PRESCAT schemes by routine operational meteorologists. The data quality and product monitoring software is tested on documented ERS SCAT anomalies that occurred due to orbit manoeuvres for example.

Ocean calibration and other data quality assessment and monitoring software is developed within the O&SI SAF to provide established analysis tools to manage instrument anomalies (see also Stoffelen, 1998a).

### **6.6 References**

Carswell, James, et al., 1998: "Scatterometer Geophysical Model Functions at C-band and Ku-band in extreme wind conditions", AMS conference, Paris, May, 1998.

Breivik, Lars-Anders, et al, 1998: "O&SI SAF Ice Product", (ESA, 1998).

Cavanié, Alain, et al, 1998: "An empirical C-band Ice Model", (ESA, 1998).

ESA, 1998, "Emerging Scatterometer Applications: From Research to Operations", Proc. of a workshop held at ESA/ESTEC, Noordwijk, the Netherlands, from 5-7 October 1998, ESA SP-424.

Figa, Julia, and Ad Stoffelen, 1998: "NSCAT Scatterometer Quality Control", (ESA, 1998).

Isaksen, L., D. Le Meur, and A. Stoffelen: "Tropical Cyclone forecasting at ECMWF", (ESA, 1998).

Le Meur, D., 1996: "Monitoring of ERS scatterometer winds", ECMWF Technical Note, available from ECMWF, Reading, UK.

Le Ru, Maria, 1999, "Inversion de mesures des radars diffusiométriques d'ERS-1 et ERS-2: Etude d'une nouvelle approche basée sur une methode variationelle stage de DESS, Rennes I at Dép. d'Océanographie Spatiale, IFREMER, Brest, France.

Stoffelen, Ad, 1999a, ASCAT performance simulation, report for the ASCAT Science Advisory Group, KNMI, de Bilt, the Netherlands.

Stoffelen, A., 1999b, "A simple method for calibration of a scatterometer over the ocean", *J. Atmos. Oceanic Technol.* 16, 275-282.

Stoffelen, Ad, 1998a, "Scatterometry", PhD thesis, ISBN 90-393-1708-9, <http://pablo.ubu.ruu.nl/~proefsch/01840669/inhoud.htm>.

Stoffelen, Ad, 1998b, "Error modeling and calibration; towards the true surface wind speed", *J. Geophys. Res.* 103 (C4), 7755-7766.

Stoffelen, Ad, 1996, "Error modeling of scatterometer, *in-situ*, and ECMWF model winds; A calibration refinement", Technical report 193, published by KNMI, Postbus 201, 3730 AE de Bilt, the Netherlands.

Stoffelen, Ad and David Anderson, 1997a, "Scatterometer Data Interpretation: Measurement Space and inversion", *J. Atmos. Oceanic Technol.*, 14(6), 1298-1313.

Stoffelen, A. C. M. and D. L. T. Anderson, 1997b, Scatterometer data interpretation: Estimation and validation of the transfer function CMOD4, *J. Geophys. Res.*, 102(C3) , 5767-5780.

Stoffelen, A. C. M. and D. L. T. Anderson, 1997c, Ambiguity removal and assimilation of scatterometer data, *Q. J. Roy. Meteorol. Soc.*, 123, 491-518.

Vries, de, John, and Ad Stoffelen, 2000, 2D variational ambiguity removal, Project report for the BCRS, KNMI, de Bilt, the Netherlands.

Wentz, Frank, and Mike Freilich, 1998: "The NSCAT-2 geophysical model function", submitted for publication.

